Path Following with Roll Constraints for Marine Surface Vessels in Wave Fields

by

Zhen Li

A dissertation submitted in partial fulfillment
of the requirements for the degree of
Doctor of Philosophy
(Naval Architecture and Marine Engineering)
in The University of Michigan
2009

Doctoral Committee:
Professor Jing Sun, Chair
Professor Robert F. Beck
Professor Michael G. Parsons
Professor Huei Peng

Dedicated to my father, Guofu Li, and to my mother, Meiya Song.

ACKNOWLEDGEMENTS

Many thanks are due to those who encouraged and helped me to finally finish this dissertation.

First, I would like to give my grateful and sincere thanks to my advisor, Professor Jing Sun. Her consistent encouragement and support enabled my substantial growth from knowing nothing about control theory, when I became her student four years ago, to finishing the dissertation with a focus on ship motion control today. Her rigorous training on analytical thinking and problem solving will benefit me for life. I am extremely thankful to Professor Robert Beck. His outstanding work in the wave load calculation is the most important foundation of the numerical test-bed developed in this dissertation. His constructive suggestions helped greatly in improving this dissertation and our co-authored paper. I want to thank Professor Michael Parsons for his great assistant in the model development, especially in the calculation of second-order wave loads. Particularly, I am so grateful for his attendance in my defense, coming back from faraway Oregon. I also want to thank Professor Huei Peng for his excellent teaching (digital control), which provided me with important fundamental knowledge related to this dissertation. I am also grateful for his agreement to be my committee member at the last minute notice. Furthermore, I want to thank Professors Armin Troesch and Robert Smith for their constructive comments and suggestions.

I would also like to give my grateful and sincere thanks to all my friends and colleagues in the RACE Lab at the University of Michigan for stimulating discussions

and enjoyable friendship. Particularly, I would like to thank Soryeok Oh, Yanhui Xie, Handa Xi, Gayathri Seenumani, Reza Ghaemi, Christopher Vermillion, Vasilios Tsourapas, Amey Karnik, Jian Chen, Zhao Lu and Irina Dolinskaya. I would also like to express my thanks to Mrs. Feifei Ren for her generous help in writing my dissertation.

I also like to acknowledge the U.S. Office of Naval Research for the financial support under grants N00014-05-1-0537 and N00014-06-1-0879.

Finally, the biggest thanks go to my family. My parents always have faith in me through the years and their constant encouragement gives me the strength to overcome the difficulties. I am especially grateful to my lovely wife, Junrui Wu. Her love and support keep my life joyful, which is the very reason for me to vigorously pursue my dream.

TABLE OF CONTENTS

LIST OF FIGURES

Figure

LIST OF TABLES

ABBREVIATION

DC-MPC	Disturbance Compensating Model Predictive Control
DGPS	Differential Global Positioning System
DoF	Degree of Freedom
FDBS	Feedback Dominance Back-Stepping
FRF	Frequency Response Function
GPS	Global Positioning System
LQR	Linear Quadratic Regulator
MPC	Model Predictive Control
PID	Proportional-Integral-Derivative
QP	Quadratic Programming
RAO	Response Amplitude Operator
RMS	Root Mean Square
RPM	Round Per Minute
RSS	Rudder Roll Stabilization
SF	Serret-Frenet
TV-MPC	Time Varying Model Predictive Control

ABSTRACT

Path Following with Roll Constraints for Marine Surface Vessels in Wave Fields

by

Zhen Li

Chair: Jing Sun

Ways to improve maneuverability of marine surface vessels through judicious application of advanced control theory are explored. Although for years the problem of marine vessel maneuvering has been addressed in many publications, the control design to achieve path following with roll constraints in wave fields remains to be an open problem. This is the exclusive focus of this research.

A ship dynamical model, together with path following error dynamics, is first introduced to facilitate the control design. A numerical test-bed combining the ship dynamics and wave effects on vessels is also developed to provide a platform for evaluating the performance of ship motion control systems in wave fields. A novel Feedback Dominance Back-Stepping (FDBS) controller is then designed and tuned to achieve path following without roll constraints. This controller is promising for industrial applications, in terms of easy implementation and robustness against model uncertainties and disturbances. The path following capability and robustness of the FDBS controller are demonstrated through theoretical analysis, numerical simulations, and experimental validations.

The need to enforce roll constraints and the fact that the rudder actuation is limited in both amplitude and rate make the Model Predictive Control (MPC) approach a natural choice for the design of the path following controller. The simulation results are presented to verify the effectiveness of the resulting controller and a simulation-based tuning process for the controller is also presented. Meanwhile, through simulations, issues associated with roll constraint violation and successive feasibility have been identified for the standard MPC path following controller in wave fields. Several mitigating strategies, such as constraint tightening and softening and gain re-tuning, are proposed to meet the state constraints of the path following for marine surface vessels in wave fields.

Motivated by the constraint violation and feasibility issues of the standard MPC in the presence of disturbances, a novel disturbance compensating MPC (DC-MPC) algorithm is developed to guarantee the state constraint satisfaction. The satisfactory performance of DC-MPC algorithm is validated by numerical simulations of ship heading control. The limitations of the DC-MPC scheme are discussed along with potential future work.

CHAPTER 1

Introduction

Marine transportation plays a critical role in modern society as 99 percent of the volume of overseas trade (62 percent by value) are carried by marine vessels, according to the statistics of U.S. Marine Administration [2]. Consequently, the safety, reliability and cost-effectiveness of marine surface vessels have attracted considerable attention and the industry is continuously seeking ways to improve all aspects of marine transportation. Among the research and development efforts, improving maneuverability has been an important subject of the industry and academic community. Maneuverability is defined as the capability to maintain or change the position, speed and orientation of vessels. Good maneuverability can be achieved through ship design in the design phase and ship motion control systems during operations. Maneuverability has always been a critical consideration in the ship design process for naval architects. A major invention of a local positioning system, namely the gyrocompass, was made in the 1910s that provided necessary signal for feedback control. Since then, many researchers have been turning to the employment of advanced ship motion control systems [24] for improving maneuverability.

The task of ship motion control is to make *"the ship to follow, as close as possible, a desired trajectory, which can be defined in terms of the ship's position, velocity and acceleration"* [53]. The control system generates appropriate commands for the

actuators (such as propeller and rudder) based on the states of the ship (obtained from sensors such as a gyrocompass and a GPS) so as to reduce the differences between the actual and desired trajectories. Depending on the types of ships and their operations performed, there are many different ship motion control problems in terms of their control goals, such as path following, course keeping, dynamic positioning, roll reduction, etc. Motivated by the importance of the ship motion control, this dissertation will focus on the design, analysis and evaluation of the ship motion control system, with the scope limited to *path following* under *roll constraints*.

The remainder of this chapter is divided into three sections. The first section presents background and literature review, followed by the summary of main contributions in the second section and the final section provides the dissertation overview.

1.1 Background and Literature Review

1.1.1 Modeling of Ship Dynamics

Mathematical models representing dynamic characteristics are a necessary prerequisite for model-based control design and analysis. There have been significant efforts for decades from both industrial and academic communities in developing accurate vessel models. Different reference frames and coordinates are adopted to describe the motion of vessels, such as north-east-down frame, geometric frame, body-fixed frame and hydrodynamic frame [53]. Each of these frames has its specific applications. Two frames have been adopted for modeling the six degrees of freedom (DoF) for the path following of marine surface vessels, which are described in Figure 1.1 [50, 52]. One is the inertial frame fixed on the earth (north-east-down frame); and the other is the body-fixed frame on the ship body.

The variables describing the position and orientation of the ship are usually expressed in the inertial frame, and the coordinates are noted: $[x, y, z]^T$ and $[\psi, \phi, \theta]^T$

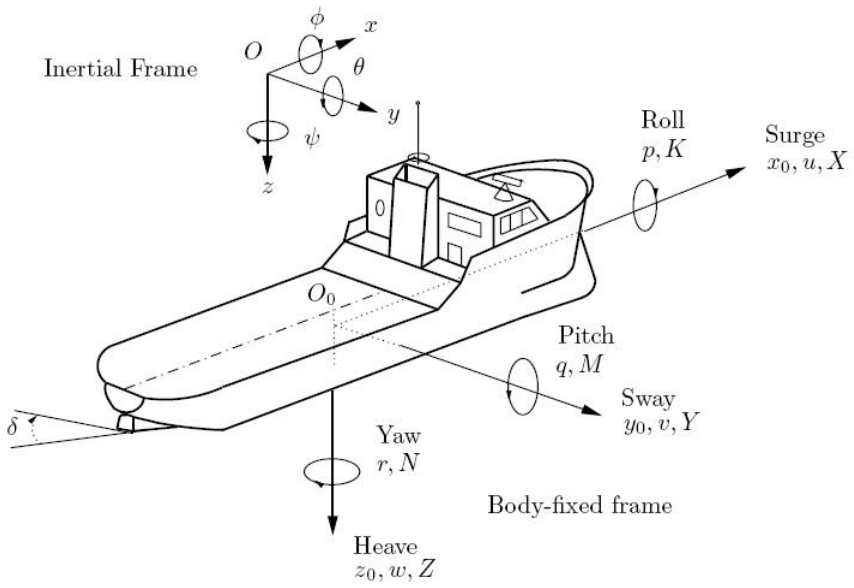

Figure 1.1: Reference frames and variables for ship motion description [50]. Figure adapted from [52].

respectively. The forces $[X, Y, Z]^T$, moments $[K, M, N]^T$, translational velocities $[u, v, w]^T$, and angular velocities $[p, q, r]^T$ are usually expressed in the body-fixed frame. δ is the rudder angle. See Figure 1.1 for the definitions of the symbols.

Numerous mathematical models have been built based on these frames for different applications [23, 24, 52]. For control purposes, two types of mathematical models are employed [52]: namely ***control-design models*** and ***high-fidelity simulation models***.

Control-design models are used for control system design and analysis (stability and robustness, etc.). They are normally linear models or simplified nonlinear models with benign nonlinearities to capture the essential behavior of the vessel. The first linear steering model was developed by Davidson and Schiff in 1946 [13]. The significant value of this model is still recognizable today. Based on the work of Davidson and Schiff, in 1957, Nomoto et al. [49] presented a first- and second-order transfer functions for yaw dynamics. This simple and effective Nomoto model is most popular for course-keeping control and autopilot design [24]. These linear models have

facilitated ship motion control design through well-developed linear control theory. Motivated by the breakthrough in nonlinear control theory in recent decades, many nonlinear vessel models for control design have emerged [23]. Among these simplified nonlinear models, the 3-DoF (surge, sway and yaw) vessel model developed by Fossen [23] in 1994 is the most widely adopted. It has been employed by numerous researchers ([7, 8, 14, 16, 25, 31, 37, 56]) to design a path following controller.

On the other hand, high-fidelity simulation models are developed to capture the behavior of the vessel as accurately as possible so that they can mimic the real hardware behavior and be used as the "virtual" ship for design and evaluation. Due to the highly nonlinear nature of the interaction between structure and fluid, the resulting models normally have intricate nonlinear terms and thus are not amenable to control design. However, these models are ideal candidates to serve as virtual vessels for performance evaluation and calibration of the control systems. Significant progress of developing these models was made by Abkowitz [1] in 1964 by applying Taylor-series expansions to the expression of the hydrodynamic forces. Using Abkowitz's idea, Son and Nomoto [67] presented a high fidelity 4-DoF high speed container model (S-175) in 1981, which has been widely adopted by subsequent research efforts. The high-fidelity modeling is greatly influenced by the work of Fossen, whose books [23, 24] presented the novel modeling approach inspired by robotics modeling and many other high accuracy vessel models. Very recently, Ross [59] improved the equations of motion by incorporating memory effect for vessels.

1.1.2 Modeling of Wave Disturbances

Environmental disturbances, such as waves, wind and current, will induce undesirable motion of a vessel in a seaway. For the vessel motion control problem considered in this dissertation, waves are the dominant environmental disturbances [53].

Normally, maneuvering studies have considered the vessel motion in the absence

of wave excitation, while seakeeping is associated with motion due to wave excitation [53]. With the assumption of calm water operation, typical path following designs for marine surface vessels do not consider wave excitation [24]. However, if we consider the performance of path following in wave fields, the seakeeping aspect should not be excluded. Over the past few decades, there are few overlaps between maneuvering and seakeeping studies, consequently accurate models incorporating ship dynamics and ship-wave interactions are not very mature yet. In the work of [7, 8], the wave effects, together with wind and current effects, are simply approximated by constant loads in the control design leading to wave load terms in the control laws. Aiming at bridging the gap between maneuvering and seakeeping to facilitate the judicious vessel motion control design in a seaway, Fossen [23, 24] and Perez [53] developed simplified wave load models based on linear seakeeping theory [38].

Given the stringent safety and performance requirements for both military and commercial ships and the cost associated with the testing and operation of vessels, detailed models that capture ship-wave interactions can be a great asset in the numerical evaluation of path following and trajectory tracking control system performance in a seaway. Recently, [54] presented a valuable 1st-order wave excitation force calculation program using force frequency response functions (FRF). While such a model provides credible wave excitation loads, the second-order drift loads are not included. However, the second-order wave loads are of importance in several contexts for marine systems such as added ship resistance and drift effects [21].

Motivated by these issues, this dissertation (Chapter 2) presents a test-bed, which combines the ship dynamics and the wave force calculations (both first-order excitation and second-order drift forces) based on Beck's progress on wave load calculation in the time domain [5]. The proposed test-bed is the proper tool to evaluate the performance of ship motion control systems such as path following, course keeping, roll stabilization, etc. The test-bed development has been summarized in [39] and

will be used to test the path following controllers in Chapter 3 and Chapter 6.

1.1.3 Path Following for Marine Surface Vessels

The objective of path following is to drive the vessel to converge to and follow the desired geometric path, without any temporal requirements [7]. In [7], the definition of path following is given as: *"Make the position of the vehicle converge to and follow a desired geometrical path."*

Several researchers [8, 9, 25] also incorporated speed regulation along the desired path, addressing the so-called dynamic path following and essentially a trajectory tracking problem. This dissertation studies the classical path following problem with the definition aforementioned.

In the open literature, the marine surface vessel path following has been addressed with two different approaches: one is to treat it as a tracking control problem [14, 15, 19, 31, 37, 57], the other is to simplify the tracking control into the regulation control problem by adopting proper path following error dynamics [7–9, 35, 56, 60, 65]. For the latter approach, the Serret-Frenet frame [46, 61], introduced from wheeled mobile robot control, is often adopted to derive the error dynamics.

Figure. 1.2 shows the Serret-Frenet frame used for path following control. The origin of the frame {SF} is located at the closest point on the curve C from the origin of the body-fixed frame {B}. The error dynamics based on the Serret-Frenet equations are introduced in [65], which are given by:

$$\dot{\bar{\psi}} = \dot{\psi} - \dot{\psi}_{SF} = \frac{\kappa}{1 - e\kappa}(u \sin \bar{\psi} - v \cos \bar{\psi}) + r, \tag{1.1}$$

$$\dot{e} = u \sin \bar{\psi} + v \cos \bar{\psi}, \tag{1.2}$$

where e, defined as the distance between the origins of {SF} and {B}, and $\bar{\psi} := \psi - \psi_{SF}$, are referred to as the cross-track error and heading error, respectively; u,

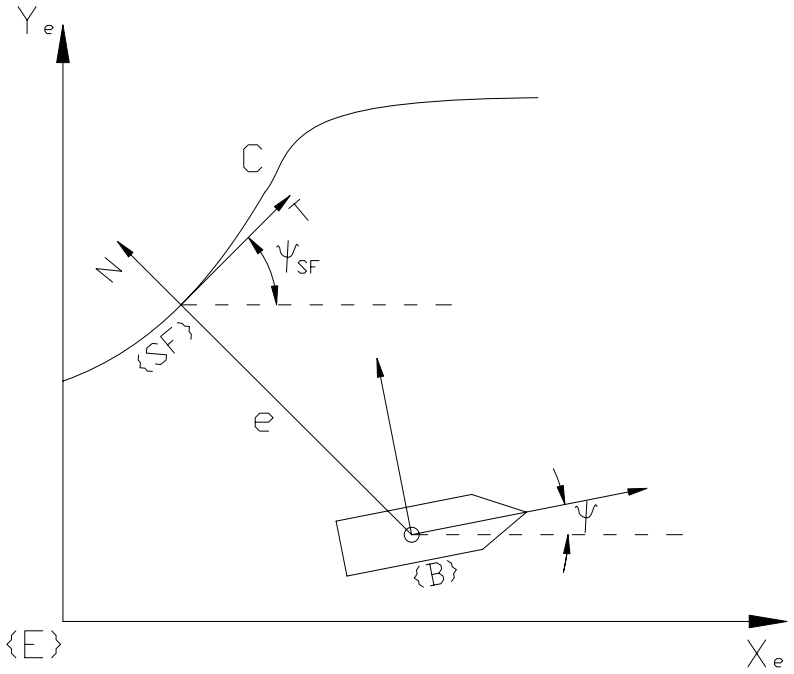

Figure 1.2: Illustration of the coordinates in the earth frame (inertial frame) {E}, the ship body-fixed frame {B} and the Serret-Frenet frame {SF}.

v, r are the surge, sway and yaw velocity, respectively. ψ is the heading angle of the vessel, ψ_{SF} is the path tangential direction as shown in Figure 1.2 [65] and κ is the curvature of the given path. In Figure 1.2, T and N are the tangent and normal directions of the curve C at the origin of {SF}. The control objective of the path following problem is to drive e and $\bar{\psi}$ to zero. When environmental disturbances (such as wind, wave and current) exist, the path following errors e and $\bar{\psi}$ often can not be eliminated simultaneously. In such circumstances, the primary objective is to maintain a small or near-zero cross-track error e, while keeping certain necessary heading error $\bar{\psi}$ to counteract disturbances.

For most path following problems for surface vessels in open sea, the path is often a straight line or a way-point path [15], which consists of piecewise straight lines with the curvature κ being zero. Even if the desired path has non-zero curvature, it is often possible to approximate the curve by many piecewise straight lines. Therefore

the heading error dynamics (1.1) can often be simplified as:

$$\dot{\tilde{\psi}} = r. \tag{1.3}$$

A challenge in the path following of marine surface vessels is the inherent nonlinearity, from either the ship dynamics or path following kinematics. Many different nonlinear design methodologies have been attempted. For example, Lyapunov's direct method is used in [8, 31] while the cascade control is employed in [37, 56]. Most papers published on this topic adopt the back-stepping as the design methodology [14–16, 19, 25, 35, 57, 65, 66]. Instead of using linear approximations, they often explore the inherit nonlinearities to achieve better performance. However, since the controller attempts to cancel or compensate for high-order nonlinearities, it yields a very complicated control law. Meanwhile, most of the control methodologies are explored with analytical and/or numerical investigation and no experimental efforts are reported, with the exception of [25,37] and [17], where the Cybership (I and II) with infrared camera system and a model ship with Differential Global Positioning System (DGPS) are used for experimental validation, respectively. Some path following algorithms for marine surface vessels, such as the LQR approach [29] and PID-type controllers [32], have already achieved industrial applications. All of these industrial path following systems pay great attention to the robustness and easy implementation.

Motivated by these recent developments in path following of marine surface vessels, this dissertation presents a novel back-stepping design for an integrated model of the surface vessel dynamics and 2-DoF path following kinematics. The focus is on developing the controller that lends itself for easy tuning and implementation, which is one of the key considerations of industrial path following systems. The details of this work, namely path following without roll constraints, will be presented in

Chapter 3 and also have been reported in [40, 41].

1.1.4 Path Following with Roll Constraints for Marine Surface Vessels

Roll motion, no matter whether it is induced by maneuvering or environmental disturbances, is normally considered to be detrimental to the operation and safety of marine surface vessels [24]. In particular, roll motion affects ship performance in the following ways [47, 53]:

- Acceleration induced by roll can contribute to the development of seasickness in the crew and passengers, resulting in reduced crew performance and passenger comfort.
- Roll acceleration may cause cargo damage, especially for high speed container ships.
- Large roll angles reduce the capability of equipment on board. For example, the performance of weapon launching systems, net fishing equipment and high precision electrical devices such as sonar will be strongly influenced.

Given that the roll motion produces high accelerations and is considered as the principal villain for seasickness and cargo/device damage, roll reduction in a seaway becomes an important consideration in hull design and vessel motion control. A noticeable amount of work has been reported in roll reduction and summarized in [64]. Although roll reduction in the course-keeping has been achieved by proper implementation of bilge keels [30], anti-rolling tanks [10, 26], active fin stabilizers [64,68] and rudder roll stabilizations (RSS) [4,6,33,55,68,71], roll reduction in course-changing, such as in path following and heading control, has not been thoroughly studied. Recently, a progress has been made in [22] to achieve roll reduction in the

track keeping using the rudder control. Given the stringent safety and performance requirements for both military and commercial vessels, achieving path following while enforcing roll constraints in a seaway deserves attention and will be one of the research foci of this dissertation.

Typical nonlinear control methodologies in path following such as those pursued in [8, 17, 19, 25, 31, 37, 40, 56, 66] do not take roll constraints explicitly into account in the design process. The constraint enforcement might be achieved through numerical simulations and trial-and-error tuning of the controller parameters. For the path following control with roll constraints considered in this dissertation, both the cross-tracking error and heading error are controlled by the rudder angle as an under-actuated problem and roll constraints need to be enforced simultaneously. The Model Predictive Control (MPC) [48, 58], which has the capability of handling input and state constraints explicitly, has been proposed to achieve satisfactory performance. The details of path following with roll constraints will be presented in Chapter 4 and Chapter 5 and also have been reported in [42, 43].

1.2 Contributions

The contributions of this dissertation on modeling and control of path following with roll constraints for marine surface vessels in wave fields are summarized as follows:

- A numerical test-bed combining the ship dynamics and wave effects (both first-order excitation and second-order drift loads) on vessels has been established to test the performance of the ship motion control systems in a wave field. This numerical test-bed is established in MATLAB, which is the most popular development environment for control community. Most importantly, this numerical test-bed is generic and can be widely used in many other ship motion

control applications, such as course keeping, roll stabilization and dynamical positioning.

- A novel robust feedback dominance back-stepping (FDBS) controller for path following of marine surface vessels has been developed. The novelty of the approach presented in this dissertation lies in the following aspects: (a) The back-stepping nonlinear controller design is based on feedback dominance, instead of feedback linearization and nonlinearity cancelation; (b) Additional design parameters are employed in the Lyapunov function that lead to simplification of the controller in the design procedure and normalization of different variables in the Lyapunov function to improve the controller performance; (c) Relying on feedback dominance and the introduction of the additional parameters in the Lyapunov function, the resulting controller is almost linear, with very benign nonlinearities allowing for analysis and evaluation; (d) The performance of the nonlinear controller, in terms of path following, is analyzed for robustness in the presence of model uncertainties. Simulation results are presented to verify and illustrate the analytic development and the effectiveness of the resulting control against rudder saturation and rate limits, delays in the control execution, as well as measurement noise. Furthermore, the control design is validated by experimental results conducted in a model basin using a model boat.

- The novel robust path following controller was evaluated by the proposed numerical test-bed for its performance in wave fields. Several issues, such as steady state errors and rudder oscillations, have been identified, thereby motivating controller modification and gain re-tuning. Mitigating strategies, such as gain re-tuning and gain scheduling, for improving the controller performance are proposed and numerically evaluated. The simulation results show that the performance of the modified controller can be substantially improved in wave

fields.

- A standard Model Predictive Control (MPC) approach for path following with roll constraints of marine surface vessels in calm water using the rudder as the control input has been proposed. The focus is on satisfying all the input (rudder) and state (roll) constraints while achieving satisfactory path following performance. The path following performance of the proposed MPC controller and its sensitivity to the major controller parameters, such as the sampling time, predictive horizon and weighting matrices in the cost-function, are analyzed by numerical simulations. This study is the first reported MPC application in path following for marine surface vessels, to the best knowledge of the author.

- To investigate the benefits as well as the associated cost, in terms of both path following and computational complexity, of using multiple actuator for path following control, the propeller is used as the second control actuator, in addition to the rudder angle, for solving the path following problem with roll constraints. MPC, where the design is based on multiple linear models, is used to handle the multi-variable control problem and roll constraints. The simulation results verify the effectiveness of the resulting two-actuator controller and show the advantage of the proposed controller over the one-input controller with a reduced roll responses.

- The effectiveness of the MPC path following controller in wave fields is also studied by simulation on the numerical test-bed. The feasibility issue due to roll constraint violations is identified and the mitigating strategies, such as gain re-tuning and constraint tightening and softening, are then proposed to guarantee the satisfaction of roll constraints. The satisfactory performance of the modified MPC controller is shown by the simulations on the numerical test-bed.

- Motivated by the constraint violation and feasibility issues of a MPC controller

for systems in the presence of disturbances, a novel disturbance compensating MPC (DC-MPC) algorithm has been proposed to guarantee the state constraint satisfaction in the presence of environmental disturbances. The effectiveness of the proposed algorithm has first been analyzed theoretically. The performance of DC-MPC algorithm in terms of constraint enforcement and error convergence is validated by numerical simulations, demonstrated on a ship heading control application. The DC-MPC algorithm has the potential to be applied to other motion control problems with environmental disturbances, such as flight, automobile and robotics control.

1.3 Dissertation Overview

The dissertation is organized as follows:

Chapter 2 first introduces the vessel dynamical models adopted in the path following controller design and evaluation, respectively. The numerical test-bed facilitating ship motion controller evaluation in wave fields is then presented, followed by the description of the experimental test-bed for the controller test.

Chapter 3 derives the path following control law based on back-stepping method using feedback dominance. Then the unmodeled dynamics are considered for the robustness analysis of the resulting control system. The simulation results are also presented and the experimental validation is summarized. Furthermore, the feedback dominance back-stepping (FDBS) controller is re-tuned to achieve satisfactory system performance in wave fields.

Chapter 4 applies the standard MPC algorithm to address the path following problem for marine surface vessels with input (rudder and propeller) and state (roll) constraints. The one-input (rudder) and two-input (rudder and propeller) MPC

controllers are both developed to achieve constrained path following and compared by simulations. The controller parameter tuning is also studied by simulations in this Chapter. Furthermore, the standard MPC controller is evaluated in wave fields and the state constraint violation is identified.

Chapter 5 aims at the state constraint satisfaction of the path following for marine surface vessels in wave fields. By the methods of gain re-tuning and constraint softening and tightening, the path following with roll constraints is achieved in wave fields. For both cases, the roll constraints is enforced successfully at the expense of slight slower path following convergence speed.

Chapter 6 presents a novel disturbance compensating MPC (DC-MPC) scheme. The capability of the DC-MPC algorithm is first analyzed theoretically. Then the proposed DC-MPC algorithm is applied to the ship heading control of marine surface vessels. The simulation results compared with standard MPC and time varying MPC schemes show the constraint satisfaction capability and good performance of the DC-MPC controller. The features and limitations of DC-MPC are also analyzed, which identify several suitable applications while at the same time rule out the path following control with roll constraints for marine surface vessels as a viable application.

Chapter 7 presents conclusions and future plans.

CHAPTER 2

Modeling and Controller Evaluation Test-bed Development

This dissertation focuses on the path following controller design and analysis for marine surface vessels in wave fields. For successful model based control design and analysis, the proper modeling of the dynamical system is critical and necessary. For our purposes, namely path following control with roll constraints, the appropriate modeling of ship dynamics and environmental loads are a pre-requisite.

In this chapter, ship dynamical models for control design and evaluation are first introduced, together with a wave model to calculate both the first- and second-order wave loads on ships. Based on that, the numerical test-bed, combining the ship dynamics and the ship-wave interactions, is developed to facilitate the ship motion controller evaluation in wave fields. Finally, the experimental test-bed for the controller performance validation and verification is presented.

2.1 Modeling of Marine Surface Vessels

The maneuvering and ship motion control community was largely influenced by Fossen's significant work on modeling of ship dynamics. He established the framework

of nonlinear dynamic equations of motion in six DoF in terms of Newtonian and Lagrangian formalism. Models developed in his books [23, 24] are widely adopted by subsequent researchers in this community. In this dissertation, his framework of ship dynamics modeling is also employed.

As mentioned in Chapter 1, two types of ship dynamical models are used for ship motion control [52]: high-fidelity models and control-design models. This section introduces the corresponding high-fidelity and control-design models adopted in this dissertation.

2.1.1 High-fidelity Model: A 4-DoF Nonlinear Container Ship

For maneuvering of surface vessels, normally 3-DoF are discussed, namely for surge, sway and yaw. When linearized, the surge is decoupled and 2-DoF are left. In this dissertation, in order to address the path following problem with roll constraints, a 4-DoF model is needed, including 3-DoF discussed in traditional maneuvering and the additional DoF focusing in seakeeping characteristics, namely the roll.

Fossen [23] summarized a nonlinear mathematical model for a single-screw high-speed container ship (so-called S175) in surge, sway, roll and yaw based on the results of [67]. The geometric parameters for the container ship modeled are given in Table 2.1.

The nonlinear equations of motion (surge u, sway v, roll p and yaw r) are given by:

$$(m' + m'_x)\dot{u}' - (m' + m'_y)v'r' = X', \tag{2.1}$$

$$(m' + m'_y)\dot{v}' + (m' + m'_x)u'r' + m'_y\alpha'_y\dot{r}' - m'_y l'_y\dot{p}' = Y', \tag{2.2}$$

$$(I'_x + J'_x)\dot{p}' - m'_y l'_y\dot{v}' - m'_x l'_x u'r' + W'GM'\phi' = K', \tag{2.3}$$

$$(I'_z + J'_z)\dot{r}' + m'_y\alpha'_y\dot{v}' = N' - Y'x'_G. \tag{2.4}$$

Table 2.1: Main parameters of the container ship

Length (L)	175.00(m)
Breadth (B)	25.40 (m)
Draft fore (d_F)	8.00 (m)
aft (d_A)	9.00 (m)
mean (d)	8.50 (m)
Displacement volume	21222 (m^3)
Height from keel to transverse metacenter (KM)	10.39 (m)
Height from keel to center of buoyancy	4.62 (m)
Block coefficient (C_b)	0.559
Rudder area (A_R)	33.04 (m^2)
Aspect ratio (Λ)	1.822
Propeller diameter (D)	6.53 (m)

Here, m' denotes the ship mass; m'_x and m'_y denote the added mass in the x and y directions respectively. I'_x and I'_z denote the moment of inertia and J'_x and J'_z denote the added moment of inertia about the x and z axes, respectively. Furthermore, α'_y denotes the x-coordinate of the center of m'_y; l'_x and l'_y the z-coordinates of the centers of m'_x and m'_y respectively. W' is the ship displacement, GM' is the metacentric height and x'_G is the location of the center of gravity in the x-axis. All the primes mean the corresponding dimensionless terms, please see Appendix E.1.3 in [23] for the details.

The hydrodynamic forces X', Y' and moments K', N' are given by [23]:

$$\begin{aligned} X' &= X'_{uu}u'^2 + (1-tt)T'(J) + X'_{vr}v'r' + X'_{vv}v'^2 \\ &\quad + X'_{rr}r'^2 + X'_{\phi\phi}\phi'^2 + c_{RX}F'_N sin\delta', \end{aligned} \tag{2.5}$$

$$\begin{aligned} Y' &= Y'_v v' + Y'_r r' + Y'_p p' + Y'_\phi \phi' + Y'_{vvv}v'^3 + Y'_{rrr}r'^3 + Y'_{vvr}v'^2 r' + Y'_{vrr}v'r'^2 \\ &\quad + Y'_{vv\phi}v'^2\phi' + Y'_{v\phi\phi}v'\phi'^2 + Y'_{rr\phi}r'^2\phi' + Y'_{r\phi\phi}r'\phi'^2 + (1+a_H)F'_N cos\delta', \end{aligned} \tag{2.6}$$

$$
\begin{aligned}
K' &= K'_v v' + K'_r r' + K'_p p' + K'_\phi \phi' + K'_{vvv} v'^3 + K'_{rrr} r'^3 + K'_{vvr} v'^2 r' \\
&\quad + K'_{vrr} v' r'^2 + K'_{vv\phi} v'^2 \phi' + K'_{v\phi\phi} v' \phi'^2 + K'_{rr\phi} r'^2 \phi' \\
&\quad + K'_{r\phi\phi} r' \phi'^2 - (1 + a_H) z'_R F'_N cos\delta', \qquad (2.7)
\end{aligned}
$$

$$
\begin{aligned}
N' &= N'_v v' + N'_r r' + N'_p p' + N'_\phi \phi' + N'_{vvv} v'^3 + N'_{rrr} r'^3 + N'_{vvr} v'^2 r' \\
&\quad + N'_{vrr} v' r'^2 + N'_{vv\phi} v'^2 \phi' + N'_{v\phi\phi} v' \phi'^2 + N'_{rr\phi} r'^2 \phi' \\
&\quad + N'_{r\phi\phi} r' \phi'^2 + (x'_R + a_H x'_H) F'_N cos\delta', \qquad (2.8)
\end{aligned}
$$

where, tt is the thrust deduction factor. c_{RX} , a_H and $a_H x'_H$ are interactive forces and moment coefficients between hull and rudder. x'_R and z'_R are the location of rudder center of effort in x and z direction, respectively. All the coefficients in X', Y', K' and N' are the corresponding hydrodynamic derivatives, and their values for S175 are given in the Appendix E.1.3 of [23].

The rudder force F'_N, according to [23] can be resolved as:

$$
F'_N = -\frac{6.13\Lambda}{\Lambda + 2.25} \frac{A_R}{L^2} ({u'_R}^2 + {v'_R}^2) sin\alpha_R, \qquad (2.9)
$$

$$
\alpha_R = \delta' + tan^{-1}({v'_R}^2 / {u'_R}^2), \qquad (2.10)
$$

$$
u'_R = u'_P \varepsilon \sqrt{1 + 8kK_T/(\pi J^2)}, \qquad (2.11)
$$

$$
v'_R = \gamma v' + c_{Rr} r' + c_{Rrrr} r'^3 + c_{Rrrv} r'^2 v, \qquad (2.12)
$$

where, Λ is the rudder aspect ratio and A_R is rudder area. L is the ship length. u'_R and v'_R are inflow velocities of the rudder in x and y directions, respectively. α_R is the relative angle between rudder and its inflow. δ' is the rudder angle. u'_P is the advance speed. ε and k are adjustment constants. K_T is the propeller thrust coefficient and J is the open water advanced coefficient. γ, c_{Rr}, c_{Rrrr} and c_{Rrrv} are the corresponding

hydrodynamic derivatives. Furthermore:

$$K_T = 0.527 - 0.455J, \tag{2.13}$$

$$J = u'_P U/(nD), \tag{2.14}$$

$$u'_P = cosv'[(1 - w_p) + \tau((v' + x'_p r')^2 + c_{pv}v' + c_{pr}r')], \tag{2.15}$$

where, $U = \sqrt{u^2 + v^2}$. n is the propeller shaft speed and D is the propeller diameter. w_p is the wake fraction number and τ is an adjustment constant. c_{pv} and c_{pr} are the corresponding hydrodynamic derivatives. The propeller force T' can be expressed as:

$$T' = 2\rho D^4 K_T n'|n'|, \tag{2.16}$$

where ρ is the water density. Also, the dynamics of the rudder and propeller are incorporated by:

$$\dot{\delta} = (\delta_c - \delta)/T_\delta, \tag{2.17}$$

$$\dot{n} = (n_c - n)/T_n. \tag{2.18}$$

T_δ and T_n are time constants. And the saturation of the rudder and propeller speed is given by $|\delta| \leqslant \delta_{max}$ and $0 \leqslant n \leqslant n_{max}$.

The motion equations can be transformed into the control-oriented dynamics equa-

tions as follows:

$$\begin{bmatrix} \dot{u} \\ \dot{v} \\ \dot{r} \\ \dot{x} \\ \dot{y} \\ \dot{\psi} \\ \dot{p} \\ \dot{\phi} \\ \dot{\delta} \\ \dot{n} \end{bmatrix} = \begin{bmatrix} \frac{X'}{m'_{11}} U^2/L \\ \frac{-(-m'_{33}m'_{44}Y'+m'_{32}m'_{44}K'+m'_{42}m'_{33}N')}{detM'} U^2/L \\ \frac{-m'_{42}m'_{33}Y'+m'_{32}m'_{42}K'+m'_{22}m'_{33}N'-{m'_{22}}^2N'}{detM'} U^2/L^2 \\ (u'cos\psi' - v'sin\psi'cos\phi')U \\ (u'sin\psi' - v'cos\psi'cos\phi')U \\ (r'cos\phi')U/L \\ \frac{-m'_{32}m'_{44}Y'+m'_{22}m'_{44}K'-{m'_{42}}^2K'+m'_{32}m'_{42}N'}{detM'} U^2/L^2 \\ p'U/L \\ \dot{\delta} \\ \dot{n} \end{bmatrix} \tag{2.19}$$

where, $m'_{11} = m' + m'_x$, $m'_{22} = m' + m'_y$, $m'_{32} = -m'_y l'_y$, $m'_{42} = -m'_y \alpha'_y$, $m'_{33} = I'_x + J'_x$, $m'_{44} = I'_z + J'_z$ and $detM' = m'_{22}m'_{33}m'_{44} - {m'_{32}}^2 m'_{44} - {m'_{42}}^2 m'_{33}$.

When environmental forces are neglected, the model (2.19) can be simulated for different rudder angles and the same forward speed. The results are given in Figure 2.1.

It is worth noting that while larger rudder angles normally lead to smaller turning diameter (as shown in Figure 2.1(a)), larger surge velocity reduction (Figure 2.1(b)), larger sway, yaw and roll motion (Figure 2.1(c)(d)(e)), some of these trends are reversed for very large rudder angles (say 35 deg), which are shown in Figure 2.1(c)(e). This is due to the decrease in centrifugal force with a large rudder angle input, which causes great forward velocity deduction.

This 4-DoF nonlinear container ship model is one of the most comprehensive ship models available in open literature. It captures the fundamental characteristics of the ship dynamics and covers a wide range of operating conditions. However, due to the complexity of this original nonlinear model and the non-affine input terms,

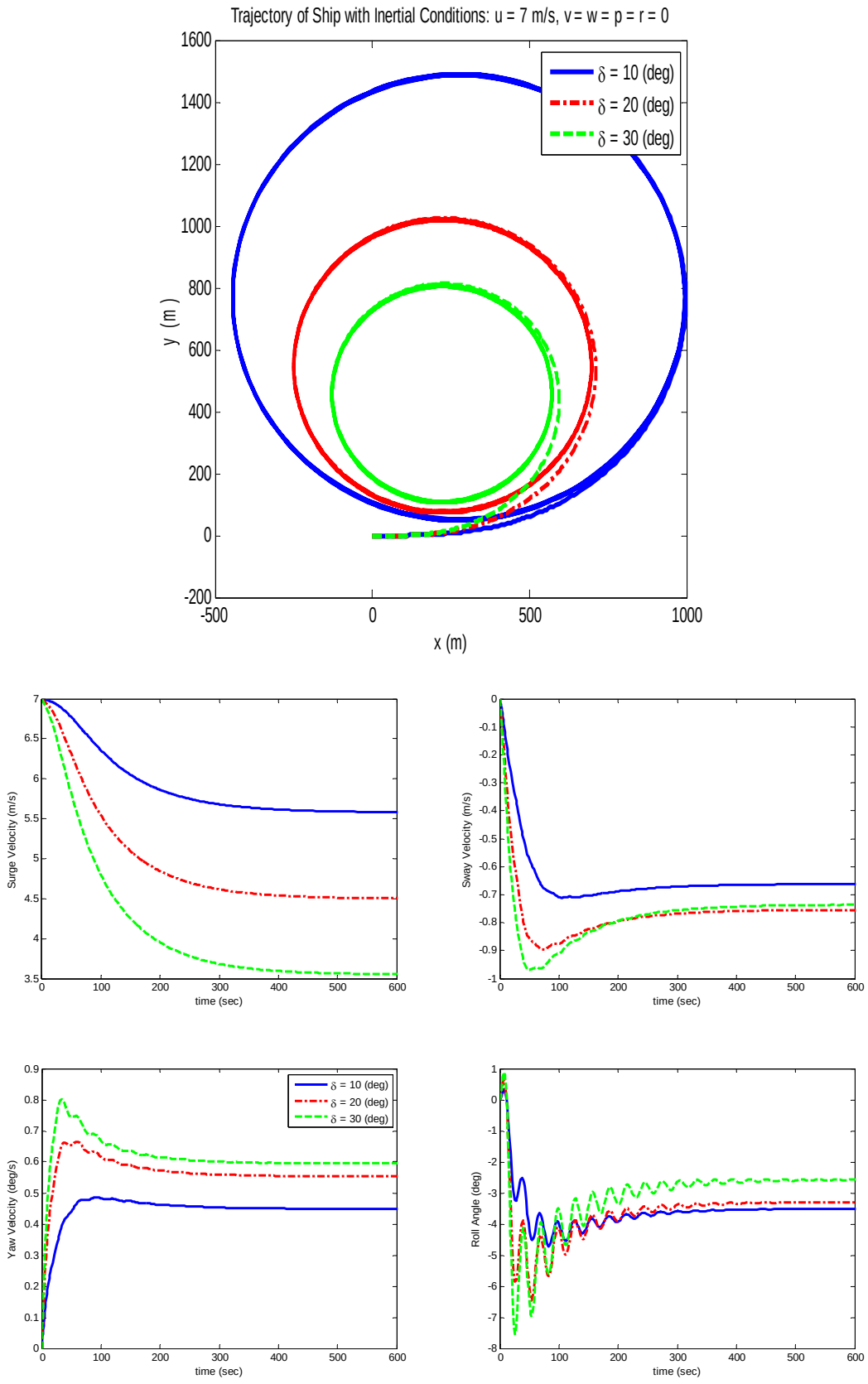

Figure 2.1: Open-loop simulation results of the original nonlinear container model.

the model is not amenable to model-based control design methodology and tools. In our work, this 10th-order nonlinear model is used for simulation and performance evaluation. For control design, however, a reduced-order model is used to make the problem tractable.

2.1.2 Control-design Model Development

For typical path following, which seeks to control the ship in the horizontal plane, only three degrees, namely the surge u, sway v and yaw r, are critical and the heave w, roll p and pitch q are normally neglected. The most widely used ship model in the path following research was developed in [23], which is in the following form:

$$\dot{u} = \frac{m_{22}}{m_{11}} vr - \frac{d_{11}}{m_{11}} u + \frac{1}{m_{11}} u_1, \tag{2.20}$$

$$\dot{v} = -\frac{m_{11}}{m_{22}} ur - \frac{d_{22}}{m_{22}} v, \tag{2.21}$$

$$\dot{r} = \frac{m_{11} - m_{22}}{m_{33}} uv - \frac{d_{33}}{m_{33}} r + \frac{1}{m_{33}} u_2, \tag{2.22}$$

where the parameters $m_{ii} > 0$ are given by the ship inertia and added mass effects. The parameters $d_{ii} > 0$ are given by the hydrodynamic damping. The available controls are the surge force u_1 and the yaw moment u_2.

Many different nonlinear design methodologies have been applied to the above model (2.20)-(2.22) [7, 8, 14, 16, 25, 31, 37, 56]. However, due to the nonlinearities involved, the resulting control laws often have complex expressions, making the controller difficult for gain tuning and its performance sensitive to model parameters. In our work, the following reduced-order linear model is developed based on (2.20)-(2.22) to facilitate the model-based approach:

$$\dot{v} = a_{11} v + a_{12} r, \tag{2.23}$$

$$\dot{r} = a_{21}v + a_{22}r + b_2\delta, \tag{2.24}$$

where a_{11}, a_{12}, a_{21}, a_{22} and b_2 are constant parameters. The validity of the model (2.23-2.24) is demonstrated through performance evaluation of the resulting control system on the high-fidelity simulation.

Remark 2.1 *The 2-DoF linear model (2.23)-(2.24) is developed from the nonlinear 3-DoF model (2.20)-(2.22) based on the assumption that surge velocity u is constant and the yaw moment u_2 is proportional to the rudder angle δ. An independent control system can be used to maintain the ship surge speed. Even without such a control system, the surge velocity deduction is not significant if the engine is operating at its rated power. The constant surge velocity assumption is adopted by many researchers [56, 65]. Notice that the rudder angle is the control input in the linear model (2.23)-(2.24), while the yaw moment is used as the input in (2.20)-(2.22). However, the former is the real actuator variable, but the latter is not.*

For the path following problem without roll constraints, the control design, summarized in Chapter 3, is based on the linear system (2.23)-(2.24). However, if we consider path following with roll constraints, the additional DoF, namely roll, should be also included. Based on the high-fidelity nonlinear container ship model, which is described in Section 2.1.1, a 3-DoF (sway, yaw and roll) linear system is developed and adopted in the control design in Chapter 4. The model has the following form:

$$\dot{v} = a_{11}v + a_{12}r + a_{13}p + a_{14}\phi + b_1\delta, \tag{2.25}$$

$$\dot{r} = a_{21}v + a_{22}r + a_{23}p + a_{24}\phi + b_2\delta, \tag{2.26}$$

$$\dot{\psi} = r, \tag{2.27}$$

$$\dot{p} = a_{31}v + a_{32}r + a_{33}p + a_{34}\phi + b_3\delta, \tag{2.28}$$

$$\dot{\phi} = p, \tag{2.29}$$

where a_{11}, a_{12}, a_{21}, a_{22}, a_{31}, a_{32}, a_{33}, a_{34}, b_1, b_2 and b_3 are constant parameters. Note agian that the surge speed is also assumed to be constant and the surge dynamics are neglected.

2.2 Modeling of Wave Disturbances

Marine surface vessels maneuvered in a seaway will be bearing loads from environmental disturbances, such as waves, wind and current. In this dissertation, we only consider the wave disturbances, which are the dominant environmental disturbances in the course-keeping or path following problem [53].

The wave-induced loads can be represented by the sum of the first-order and second-order effects, where the first-order terms correspond to the wave excitation load while the second-order terms represent the wave drift load [21]. The summation of these two terms serves as the total wave loads acting on the vessels.

The coordinate system used in the wave force calculation is shown in Figure 2.2. β, the ship heading angle with respect to the wave heading angle, is defined as:

$$\beta = \theta_{wave} - \theta_{ship}. \tag{2.30}$$

where θ_{wave} and θ_{ship} are the wave heading angle and ship heading angle in the inertial frame, respectively.

2.2.1 First-Order Wave Excitation Force and Moment

The calculation of the first-order wave excitation forces is very involved. An irregular sea [38] surface can be expressed as a sum of single frequency waves with different frequencies (ω_i), wavenumbers ($\underline{\mathrm{k}}_i$), and uniformly distributed random phase

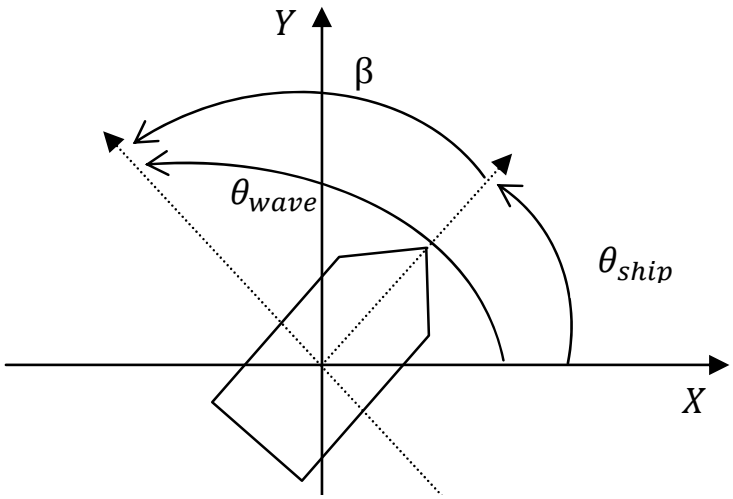

Figure 2.2: Wave angle definition.

angles (α_i):

$$\eta(\underline{\mathrm{x}}, t) = \sum_{i=1}^{N} A_i \cos(\omega_i t - \underline{\mathrm{k}}_i \underline{\mathrm{x}} + \alpha_i), \tag{2.31}$$

where A_i is the corresponding wave amplitude and $\underline{\mathrm{x}}$ is the position vector.

By linear seakeeping theory [5], the wave excitation forces and moments can be expressed by the following equations:

$$f_j(\underline{\mathrm{x}}, t) = \sum_{i=1}^{N} A_i |H_j(\omega_i, \beta, u)| \cos(\omega_i t - \underline{\mathrm{k}}_i \underline{\mathrm{x}} + \alpha_i + \delta_j(\omega_i, \beta, u)), \tag{2.32}$$

for directional index $j = 1, 2, 3, 4, 5, 6$, which stand for surge, sway, heave, roll, pitch and yaw, respectively. $H_j(\omega_i, \beta, u)$ is the response amplitude operator (RAO) in the j direction, with a magnitude $|H_j(\omega_i, \beta, u)|$ and a phase angle $\delta_j(\omega_i, \beta, u)$. By definition, the RAO (such as $H_j(\omega_i, \beta, u)$) is the response of the ship system, such as the ship motion variable, to wave forces, per wave height due to a wave of frequency ω, a wave heading β and ship speed u [38]. For our purpose, only the index 1, 2, 4 and 6 are used for surge, sway forces and roll, yaw moments, respectively. For further details, please see [5].

In the calculation of first-order wave loads, a quasi-steady approach is adopted

where the transient effects are neglected in order to greatly simplify the computation, because the calculation of transients involves computational convolution integrals. The similar approach is employed in [54].

2.2.2 Second-Order Wave Drift Force and Moment

For the wave-induced drift force in the surge direction ($\bar{f}_1$), we approximate the second-order drift forces by an empirical equation [18] which is a sixth-order polynomial function of forward speed u (m/s) and relative ship heading angle β (rad):

$$\begin{aligned}\bar{f}_1 &= C_0 + C_{10}u + C_{01}\beta + C_{20}u^2 + C_{11}u\beta + C_{02}\beta^2 + C_{21}u^2\beta + C_{12}u\beta^2 + C_{03}\beta^3 \\ &\quad + C_{22}u^2\beta^2 + C_{13}u\beta^3 + C_{04}\beta^4 + C_{23}u^2\beta^3 + C_{14}u\beta^4 + C_{24}u^2\beta^4, \end{aligned} \tag{2.33}$$

where C_0, C_{10}, C_{01}, C_{20}, C_{11}, C_{02}, C_{21}, C_{12}, C_{03}, C_{22}, C_{13}, C_{04}, C_{23}, C_{14} and C_{24} are the empirical coefficients fitted using data generated from a detailed ship numerical simulation program (see [18] for the details). For the container ship S175 in sea state 5 (corresponding to 3.25 m of significant wave height), the coefficients in (2.33) are summarized in Table 2.2.

Table 2.2: Empirical coefficients for calculation of second order drift wave force in surge.

C_0	C_{10}	C_{01}	C_{20}	C_{11}
84.988	32.040	-487.122	-2.436	40.734
C_{02}	C_{21}	C_{12}	C_{03}	C_{22}
1076.446	-0.348	-135.610	-577.089	5.582
C_{13}	C_{04}	C_{23}	C_{14}	C_{24}
77.390	91.061	-3.558	-12.646	0.606

For the drift sway force and the drift yaw moment, the following empirical equations were developed in [12]:

$$\bar{f}_2{}^* = \frac{1}{2}\rho g L \zeta^2 \sin\beta C_Y, \tag{2.34}$$

$$\bar{f_6}^* = \frac{1}{2}\rho g L^2 \zeta^2 \sin\beta C_N, \tag{2.35}$$

where ρ is the water density, g is the acceleration due to gravity, L is the ship length, ζ is the mean wave amplitude, C_Y and C_N are the corresponding empirical coefficients, whose expressions are given as follows:

$$C_Y = 0.46 + 6.83\frac{\lambda}{L} - 11.65(\frac{\lambda}{L})^2 + 8.44(\frac{\lambda}{L})^3, \tag{2.36}$$

$$C_N = 0.11 + 0.68\frac{\lambda}{L} - 0.79(\frac{\lambda}{L})^2 + 0.21(\frac{\lambda}{L})^3, \tag{2.37}$$

where λ is the mean wave length. However, (2.36) and (2.37) are regressed from the data of the specific ship with zero speed in [20]. For different ships with nonzero speed, these two coefficients need to be corrected. We introduce speed dependent correction coefficients $C_{f2}(u)$ and $C_{f6}(u)$ to adjust the second order drift loads by the following equations:

$$\bar{f_2} = C_{f2}(u)\bar{f_2^*}, \tag{2.38}$$

$$\bar{f_6} = C_{f6}(u)\bar{f_6^*}. \tag{2.39}$$

It was pointed out in [21] that the ratio between the magnitudes of the mean wave drift forces and linear first-order wave forces is about $\zeta/100$. For different speeds, the coefficients $C_{f2}(u)$ and $C_{f6}(u)$ adopted in this dissertation are calculated using the magnitude of the first-order excitation loads, which is calculated based on the detailed information of the ship hull form using the linear seakeeping theory. Specifically, given the vessel speed and mean wave amplitude ζ, we first calculate the mean amplitudes of the first-order wave loads in sway and yaw, namely F_{f2} and F_{f6}, for β equal to 45, 90 and 135 deg. Then the correction coefficients $C_{f2}(u)$ and $C_{f6}(u)$ are obtained by averaging the corresponding three values of $F_{f2}\zeta/(100|\bar{f_2^*}|)$ and $F_{f6}\zeta/(100|\bar{f_6^*}|)$. For the container ship S175 with a speed of 10 m/s in sea state 5, the values of $C_{f2}(u)$

and $C_{f6}(u)$ are 0.2535 and 0.5211, respectively.

2.3 Numerical Test-bed for Controller Evaluation in wave fields

A numerical test-bed for controller evaluation in wave fields, based on the high-fidelity ship model S175 presented in Section 2.1.1 and the wave load calculation described in Section 2.2, is developed in this section.

As mentioned before, the forces/moments X', Y', K' and N' that appear in the system (2.1)-(2.4) are the calm water hydrodynamic forces and moments. In an incident wave field, the following modifications should be adopted:

$$X'_w = X + f'_1 + \bar{f}'_1, \tag{2.40}$$

$$Y'_w = Y + f'_2 + \bar{f}'_2, \tag{2.41}$$

$$K'_w = K + f'_4, \tag{2.42}$$

$$N'_w = N + f'_6 + \bar{f}'_6, \tag{2.43}$$

where X'_w, Y'_w, K'_w and N'_w are the corresponding hydrodynamic forces and moments in the incident wave field and will replace X', Y', K' and N' in the equations (2.1)-(2.4) when waves exist. As mentioned in Section 2.2, f'_1, f'_2, f'_4 and f'_6 are the corresponding dimensionless first-order wave loads and $\bar{f}'_1$, $\bar{f}'_2$, $\bar{f}'_4$ and $\bar{f}'_6$ are the corresponding dimensionless second-order wave loads. Note that the second-order moment in roll is neglected. Using (2.40)-(2.43) in (2.1)-(2.4), the wave induced loads are incorporated into the ship dynamics, with the assumption that the damping and added mass of the ship are unchanged in wave fields. The similar approach is employed to incorporate the wave loads into calm water maneuvering model in the work

of [23, 24, 53].

Figure 2.3 shows the block diagram of the overall model. The wave load program calculates the wave induced forces and moments based on the wave field information (sea state, dominant wave direction) and the ship states (position, heading and speed). The ship maneuvering model is driven by the wave forces and moments, together with the control input (rudder angle calculated based on a control law using the current ship state measurement or estimation).

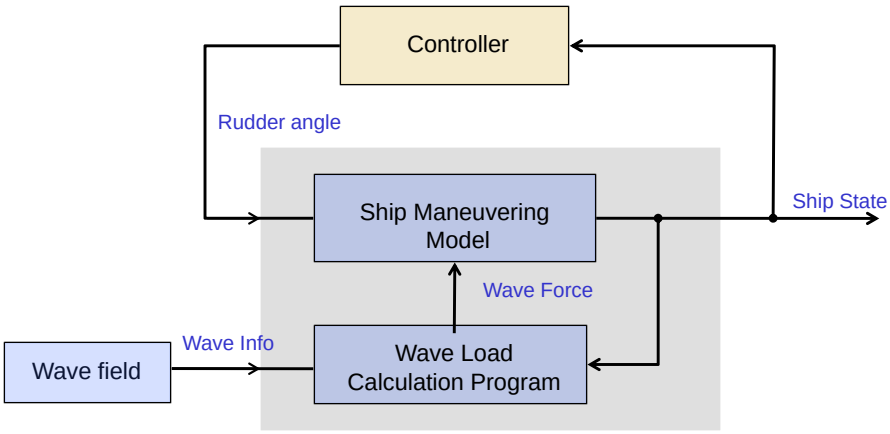

Figure 2.3: Block diagram of the simulation model.

As an example, Figure 2.4 shows the wave-induced first-order excitation forces and moment for four different heading angles, namely following sea ($\beta = 0$ deg), stern quartering sea ($\beta = 45$ deg), beam sea ($\beta = 90$ deg) and head sea ($\beta = 180$ deg). In simulations, the JONSWAP spectrum [21] was adopted with 3.25 m significant wave height (sea state 5), 9.53 sec peak period and default Gamma peak factor 3.3. The ship used in the simulation is the container ship S175, which is widely used in research and is described in Section 2.1.1. The ship velocity is maintained at 10 m/sec. From Figure 2.4, we can see that the wave load calculation program captures the key characteristics of the wave excitation loads on vessels in a short crested wave field. For example, the head sea has the highest encounter frequency while the following has the lowest frequency; the beam sea has the largest sway force and roll moment

among these four cases while these loads are relatively small in the following sea and head sea cases; the head sea has the largest surge force and the following sea and head sea have very small sway force.

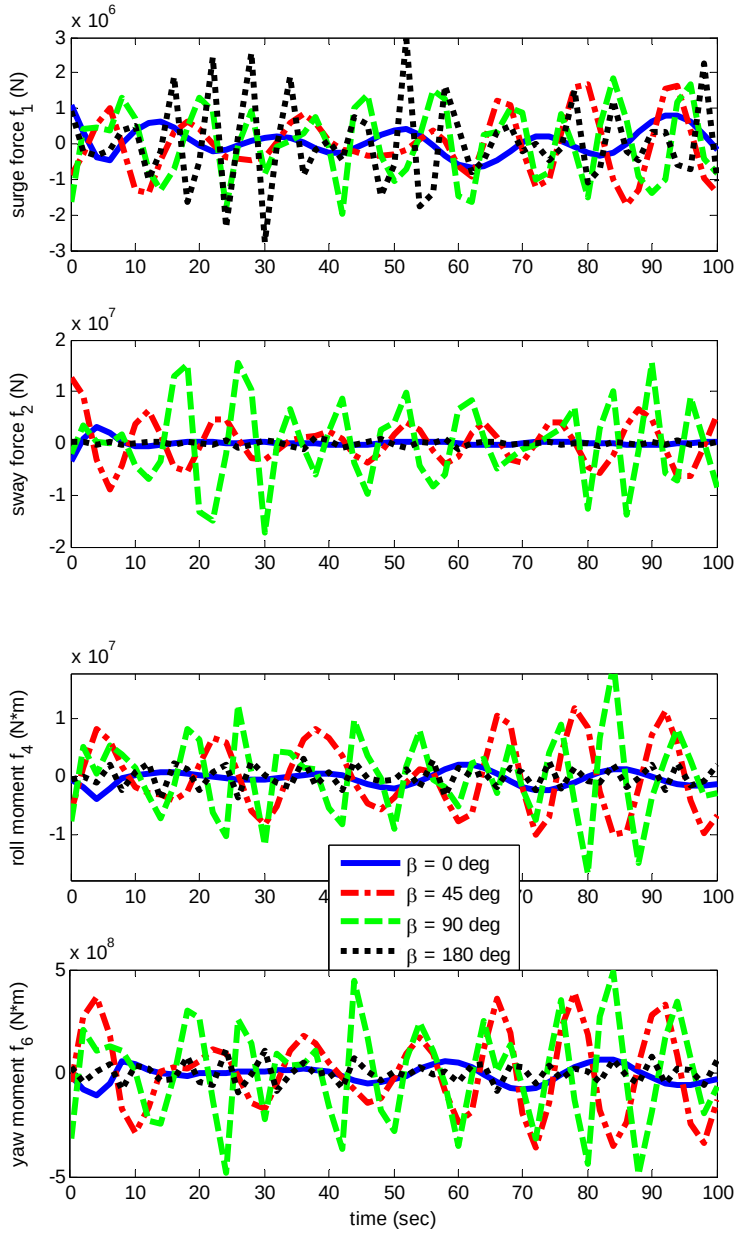

Figure 2.4: First-order wave excitation forces and moments with different wave heading angles.

The proposed numerical test-bed is used to evaluate the path following controller in this dissertation. This numerical test-bed is established in MATLAB, which is the

most popular software in the control community. The program calculating the first-order wave induced loads is coded in FORTRAN and called from the main program in MATLAB for computational efficiency. It should be pointed out that this model is generic and can be used in many other applications, such as course keeping, roll stabilization and dynamical positioning, and its utility is independent of the control design methodology used.

2.4 Experimental Test-bed Introduction

To support the control development, a fully instrumented model ship was designed so that the control algorithm developed in Section 3 could be experimentally evaluated. The model ship is actuated with two opposite rotating main propellers with two rudders aft. Propellers and rudders are actuated by two DC servo motors fitted with encoders and tachometers, respectively. The main parameters of the model ship are given in Table 2.3.

Table 2.3: Principal particulars of the model ship.

Item	Symbol	Value
Length	L	1.60 m
Beam	B	0.38 m
Draft	H	0.17 m
Mass	m	38 kg
Inertia	I_z	2.7 kgm^2

When the model ship is tested in the towing tank ($320ft. \times 22ft. \times 10.5ft.$) located in the Marine Hydrodynamics Laboratories (MHL) of the University of Michigan, GPS signals are not available (even if available, the accuracy of GPS signals is not high enough for the model test). Thus, four infra-red cameras are used, in lieu of the GPS system, to provide the feedback signal to the control system. A picture of the instrumented model is shown in Figure 2.5.

The real-time feedback control is accomplished using a PC-based PC104 hardware

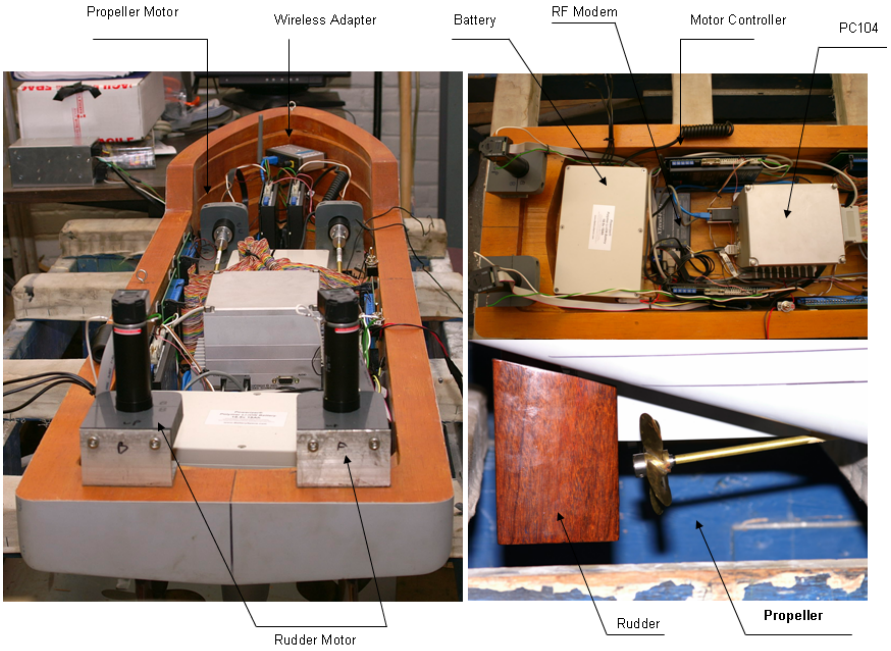

Figure 2.5: A system overview of the fully instrumented model ship.

which runs the QNX real-time operating system. PC104 communicates, through a wireless LAN, to a host PC, on which the control algorithm is programmed and tuned, data acquisition function is performed, and ship position signals are collected from the camera system and transmitted to PC104. The key control and communication devices are shown in Figure 2.6, together with the connections among the devices.

For the experimental validation conducted later in Chapter 3, the onboard computer controls and coordinates the motion of two propeller motors and two rudder motors according to the control algorithm. At the higher level, the desired path to be tracked is specified and communicated wirelessly to the on-board controller. In the MHL towing tank where the experiments were conducted, the speed of the towing carriage (on which the camera position tracking system is mounted) and the ship position data captured by the camera motion tracking system are transmitted in real time to PC104 through two pairs of wireless RF modems. The actuators have their low level inner loop control for the propeller speed and the rudder angle. PI controllers with the gains $K_{prop} = (0.05, 1.0)$ and $K_{rudder} = (3, 5)$ are used. The control

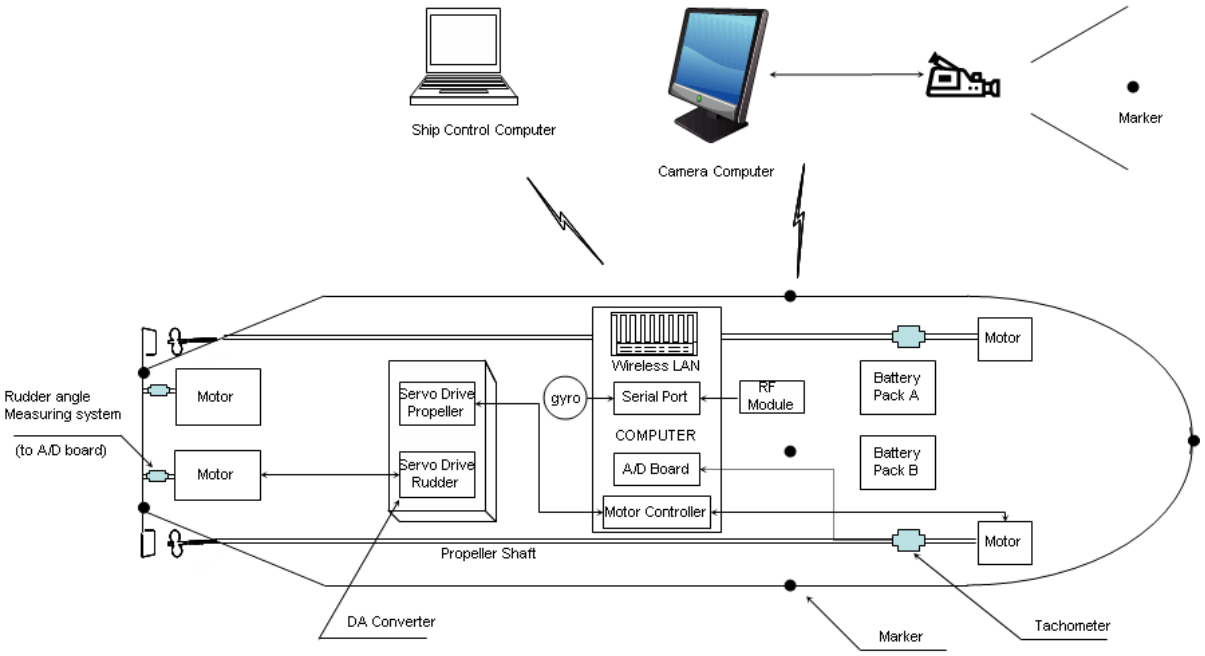

Figure 2.6: Wireless link between devices.

system runs at a sample rate of 1 mSec. In the experiments, the same controller parameters used in the simulation are downloaded to the onboard processor.

The initial conditions of the model ship are not specified. Instead, the boat is first running in the manual mode where the operator is trying to position the ship to the launching area. Then the system is switched to the autonomous mode where the rudders are controlled according to the specific algorithm tested. In the test, the control algorithm was tested with a constant propeller speed, and the rudder was constrained to turn only ± 30 deg to prevent the potential mechanical damage to the model ship.

Using this experimental test-bed, a successful evaluation of a back-stepping path following controller (please see details in Chapter 3) and a path following controller using dynamic surface control technique [51] have been conducted. Other path following controllers, such as MPC and disturbance compensating MPC, will be tested in the future.

CHAPTER 3

Path Following without Roll Constraints for Marine Surface Vessels

In this chapter, the simplified 2-DoF linear model is first presented along with the Serret-Frenet formulation to facilitate the path following control design without roll constraints. Then the path following control law based on the back-stepping method using feedback dominance is derived, and the control law is shown to have a simple expression. The robustness of the resulting control system is also analyzed, where unmodeled dynamics are considered, followed by the simulation results and experimental validation. The controller evaluation and modification in wave fields are finally summarized in Section 3.6.

3.1 Control-design Model for Path Following without Roll Constraints

As mentioned in Section 1.1.3, two different approaches have been adopted to address the path following problem for marine surface vessels: one treats it as a tracking control problem [14, 15, 19, 31, 37, 57], and another simplifies the tracking control problem into the regulation control problem by adopting proper path following

error dynamics [7–9,35,56,60,65]. In this chapter, the latter approach with the Serret-Frenet error dynamics [46, 61] is employed to design the path following controller.

The error dynamics [65] based on the Serret-Frenet equations are given by equations (1.1) and (1.2) (please see details in Section 1.1.3). For the most common straight line or way-point path for marine surface vessels in open sea, the heading error dynamics (1.1) can often be simplified as equation (1.3) since the path curvature κ in these cases is zero.

In this study, the path following error dynamics adopted for control design are (1.2) and (1.3). Notice the control objective for path following of marine surface vessels is to drive e and $\bar{\psi}$ to zero.

As discussed in Section 2.1.2, many path following controllers in the literature [7, 8, 14, 16, 25, 31, 37, 56] based on the most popular design model (2.20)-(2.22) have complex expressions, making the controller difficult for gain tuning to achieve good performance and its performance sensitive to model parameters. To address these issues, in our work, the reduced-order 2 DoF linear model (2.23) and (2.24) are used to facilitate the control design.

Before proceeding to the controller design, an additional assumption can be made to further simplify the model and to avoid the under-actuation problem. In ship maneuvering, the sway velocity is relatively small compared with other motion variables [65]. Therefore we assume that the sway velocity was small enough to be neglected, which means $v = 0$. With this assumption, the final model for control design, that captures the dominant ship maneuvering dynamics and path following error dynamics, with one control variable δ, has been simplified into:

$$\dot{e} = u \sin \bar{\psi}, \tag{3.1}$$

$$\dot{\bar{\psi}} = r, \tag{3.2}$$

$$\dot{r} = a_{22}r + b_2\delta. \tag{3.3}$$

This overall model (3.1)-(3.3) will be used in this chapter to design the path following controller without roll constraints for marine surface vessels.

3.2 Feedback Dominance Back-Stepping Controller Design

With u being treated as a constant, which is a common assumption for many design [56,65], the dynamic system (3.1)-(3.3) assumes a triangular structure where the control action δ influences only r while r affects $\bar{\psi}$ and in turn $\bar{\psi}$ influences e. This triangular structure naturally renders the back-stepping control design [34]. However, given the nonlinearity of the dynamics and the "explosive nature" of the back-stepping design approach, the controller resulting from the standard back-stepping design approach involves many nonlinear terms [65]. As such, the controller may be susceptible to unmodeled dynamics and implementation errors.

In this work, in an attempt to enhance system robustness and implementation ease, we propose a design approach that will result in a relatively simple control law. Instead of feedback linearization and nonlinearity cancelation, our back-stepping design is based on feedback dominance. The design procedure is delineated as follows:

Step 1:

Define the first Lyapunov function as:

$$V_1 := \frac{1}{2}e^2 > 0. \tag{3.4}$$

Differentiating V_1 with respect to time yields:

$$\dot{V}_1 = e\dot{e} = ue\sin\bar{\psi}. \tag{3.5}$$

Normally, according to the back-stepping design procedure, a virtual control of $\bar{\psi} = -\arcsin(c_1 e)$ would be chosen to stabilize (3.1). However, this approach will result in a very complex controller when $\bar{\psi}$ is differentiated in the subsequent design steps. In our work, the stabilizing virtual control $\alpha_1 := -c_1 e$, $c_1 > 0$ is selected, then for $\bar{\psi} \in (-\pi, \pi)$, $\dot{V}_1$ becomes:

$$\dot{V}_1 = -c_1 u e^2 \frac{\sin\bar{\psi}}{\bar{\psi}} + ue\frac{\sin\bar{\psi}}{\bar{\psi}}(\bar{\psi} - \alpha_1). \tag{3.6}$$

For $\bar{\psi} = \alpha_1$, this becomes:

$$\dot{V}_1 = -c_1 u e^2 \frac{\sin\bar{\psi}}{\bar{\psi}} \leq 0. \tag{3.7}$$

In deriving the inequality for V_1 in (3.7), the property $\sin(x)/x > 0, \forall x \in (-\pi, \pi)$ has been used.

Step 2:

Let $z_2 = \bar{\psi} - \alpha_1$ and differentiating with respect to time, giving:

$$\dot{z_2} = \dot{\bar{\psi}} - \dot{\alpha_1} = r + c_1 u \frac{\sin\bar{\psi}}{\bar{\psi}}(z_2 + \alpha_1). \tag{3.8}$$

Augment the first Lyapunov function into the second Lyapunov function as $V_2 := V_1 + \frac{p_1}{2} z_2^2 > 0$ where p_1 is a positive constant, whose role will become apparent in the subsequent analysis. Differentiating V_2 with respect to time yields:

$$\begin{aligned} \dot{V}_2 &= e\dot{e} + p_1 z_2 \dot{z_2} \\ &= -c_1 u e^2 \frac{\sin\bar{\psi}}{\bar{\psi}} + p_1 z_2 [r + c_1 u z_2 \frac{\sin\bar{\psi}}{\bar{\psi}} + (\frac{1}{p_1} - c_1^2) eu \frac{\sin\bar{\psi}}{\bar{\psi}}]. \end{aligned} \tag{3.9}$$

If $p_1 = 1/c_1^2$, equation (3.9) becomes:

$$\dot{V}_2 = -c_1 u e^2 \frac{\sin\bar{\psi}}{\bar{\psi}} + \frac{1}{c_1^2} z_2 [r + c_1 u z_2 \frac{\sin\bar{\psi}}{\bar{\psi}}]. \tag{3.10}$$

Remark 3.1. *Note that the introduction of p_1 in V_2 allows us to eliminate the cross-product term in $\dot{V}_2$ that involves nonlinearity. Without this flexibility in V_2, one has to rely on the virtual control to cancel the nonlinear term to achieve $\dot{V}_2 \leq 0$. It should be noted that since both c_1 and p_1 are design parameters and no model parameters are involved in meeting the condition $p_1 = 1/c_1^2$, therefore the equation (3.10) is not subject to modeling errors.*

To design the next virtual control for the (e, z_2) dynamics, feedback dominance is used instead of feedback linearization (which will involve the exact cancelation of nonlinearities) to form the stabilizing virtual control. By selecting $\alpha_2 := -c_2 z_2$ and making c_2 satisfy $c_2 > c_1 u$, $\dot{V}_2$ becomes:

$$\dot{V}_2 = -c_1 u e^2 \frac{\sin\bar{\psi}}{\bar{\psi}} - \frac{c_2}{c_1^2} z_2^2 [1 - \frac{c_1 u}{c_2} \frac{\sin\bar{\psi}}{\bar{\psi}}] + \frac{1}{c_1^2} z_2 (r - \alpha_2). \tag{3.11}$$

If $r = \alpha_2$, this becomes:

$$\dot{V}_2 = -c_1 u e^2 \frac{\sin\bar{\psi}}{\bar{\psi}} - \frac{c_2}{c_1^2} z_2^2 [1 - \frac{c_1 u}{c_2} \frac{\sin\bar{\psi}}{\bar{\psi}}] \leq 0, \tag{3.12}$$

where the inequality in (3.12) is a direct result of $c_2 > c_1 u$ and $0 < \sin(\bar{\psi})/\bar{\psi} < 1$. Note that in (3.12), the linear virtual control $-c_2 z_2$ is used to dominate, instead of canceling, the nonlinear term, thus the name "feedback dominance".

Step 3:

Define $z_3 = r - \alpha_2$ and differentiating with respect to time, giving:

$$\dot{z_3} = \dot{r} - \dot{\alpha_2} = a_{22} r + b_2 \delta - \dot{\alpha_2}. \tag{3.13}$$

Further augmenting the second Lyapunov function as $V_3 := V_2 + \frac{p_2}{2} z_3^2 > 0$, where p_2 is a positive constant, $\dot{V}_3$ becomes:

$$\dot{V}_3 = -c_1 u e^2 \frac{\sin\bar{\psi}}{\bar{\psi}} - \frac{c_2}{c_1^2} z_2^2 [1 - \frac{c_1 u}{c_2} \frac{\sin\bar{\psi}}{\bar{\psi}}] + p_2 z_3 [\frac{1}{c_1^2 p_2} z_2 + a_{22} r + b_2 \delta - \dot{\alpha_2}]. \quad (3.14)$$

If δ is selected to be

$$\delta = \frac{1}{b_2}(-c_3 z_3 - \frac{1}{c_1^2 p_2} z_2 - a_{22} r + \dot{\alpha_2}), \quad (3.15)$$

then (3.14) turns into:

$$\dot{V}_3 = -c_1 u e^2 \frac{\sin\bar{\psi}}{\bar{\psi}} - \frac{c_2}{c_1^2} z_2^2 [1 - \frac{c_1 u}{c_2} \frac{\sin\bar{\psi}}{\bar{\psi}}] - p_2 c_3 z_3^2 \leq 0, \quad (3.16)$$

and the second inequality holds if $\bar{\psi} \in (-\pi, \pi)$ and $c_2 > c_1 u$. Furthermore, $\dot{V}_3 = 0$ only if $(e, z_2, z_3) = (0, 0, 0)$, which means the control law (3.15) renders the system (3.1), (3.2), (3.3) asymptotically stable.

Substituting the expressions for z_2, z_3 and $\dot{\alpha_2}$ in terms of the original states, (3.15) becomes:

$$\delta = -\bar{c}_1 e - \bar{c}_2 \bar{\psi} - \bar{c}_3 r - \bar{c}_4 u \sin\bar{\psi}, \quad (3.17)$$

where

$$\bar{c}_1 = \frac{1}{b_2}(c_1 c_2 c_3 + \frac{1}{c_1 p_2}), \quad (3.18)$$

$$\bar{c}_2 = \frac{1}{b_2}(c_2 c_3 + \frac{1}{c_1^2 p_2}), \quad (3.19)$$

$$\bar{c}_3 = \frac{a_{22} + c_2 + c_3}{b_2}, \quad (3.20)$$

$$\bar{c}_4 = \frac{c_1 c_2}{b_2}. \quad (3.21)$$

As shown in the equation (3.17), the final control law has a very simple structure. The first three terms in the control law are linear and the only nonlinearity comes

from the last term.

Remark 3.2. *Besides their functions as mentioned in Remark 2, namely, to eliminate the nonlinear term in the design procedure and therefore simplify the resulting control, the parameters p_1 and p_2 also serve to normalize the effects of different variables in the Lyapunov function. For example, three variables in V_3 are e, $z_2 = \psi - \alpha_1$ and $z_3 = r - \alpha_2$, which have the order of magnitude of 1000, π and 0.01, respectively in the case of the four DoF container ship. Thus, p_1 and p_2 have the order of 10^5 and 10^{11} to make all the three variables have the comparable influences on the V_3.*

In contrary, the nonlinear control designed using the standard back-stepping and feedback linearization, instead of "feedback dominance", would have the form (3.22):

$$\delta = -\frac{1}{b_2}(k_3\bar{z}_3 + \cos(\arcsin(\bar{z}_2 + \beta_1))\bar{z}_2 + a_{22}r - \dot{\beta}_2). \tag{3.22}$$

where

$$\beta_1 = -k_1 e, \tag{3.23}$$

$$\bar{z}_2 = \sin\bar{\psi} - \beta_1, \tag{3.24}$$

$$\beta_2 = \frac{-ue - k_2\bar{z}_2 + \dot{\beta}_1}{cos(\arcsin(\bar{z}_2 + \beta_1))}, \tag{3.25}$$

$$\bar{z}_3 = r - \beta_2, \tag{3.26}$$

and k_1, k_2 and k_3 are positive control parameters. When $\bar{z}_2$, $\bar{z}_3$, β_1 and $\dot{\beta}_2$ are replaced by their corresponding expressions in terms of the original states, the control law

(3.22) becomes:

$$\begin{aligned}\delta &= -\frac{1}{b_2}[(a_{22}+k_1u+k_2+k_3)r+(k_1u+k_2)r\tan^2\bar{\psi} \\ &\quad +(k_3u+k_1k_2k_3)e\sec\bar{\psi}+(u+k_1k_2)er\sin\bar{\psi}\sec\bar{\psi} \\ &\quad +(u^2+k_1k_2u+k_2k_3-k_1k_3u)\tan\bar{\psi} \\ &\quad +\sin\bar{\psi}\cos\bar{\psi}+k_1e\cos\bar{\psi}]. \end{aligned} \tag{3.27}$$

The resulting control law (3.27) has a lengthy expression comprising of many nonlinear terms, most of which are due to the non-affine function of the input that the feedback design is trying to cancel. The complexity will not only make the controller difficult to tune, but also make it susceptible to implementation errors and model uncertainties.

Remark 3.3. *Note that the controller (3.17) has the proportional, integral and derivative terms when e and r are expressed in terms of $\bar{\psi}$, the tuning of the controller gains are relatively easy in the sense that the effects of each parameter on the system dynamics and control saturation can be interpreted in physical variables and many of the PID tuning algorithms can be used.*

3.3 Robustness Analysis of the Resulting FDBS Controller

In deriving the path following controller, the linear vessel model was used and the sway velocity was neglected. To incorporate the nonlinearities and non-zero sway velocities, the following model is used in robustness analysis:

$$\dot{e} = u\sin\bar{\psi}+v\cos\bar{\psi}, \tag{3.28}$$

$$\dot{\psi} = r, \tag{3.29}$$

$$\dot{r} = a_{21}v + a_{22}r + b_2\delta + \Delta, \tag{3.30}$$

where Δ captures the unmodeled dynamics.

For the uncertainties Δ, it is assumed that:

Assumption 3.1. There exist positive constants γ_0, γ_v and γ_r such that:

$$|\Delta| \leq \gamma_0 + \gamma_v|v| + \gamma_r|r|. \tag{3.31}$$

For the sway dynamics, which is not considered in the controller design, the following assumption is made:

Assumption 3.2. There exist positive constants $\bar{\gamma}_0$ and $\bar{\gamma}_r$ such that:

$$|v| \leq \bar{\gamma}_0 + \bar{\gamma}_r|r|. \tag{3.32}$$

Remark 3.4. *Comparing (2.24) with the nonlinear yaw dynamical equation (2.22) and assuming* $a_{22} = -\frac{d_{33}}{m_{33}}$*, yields:*

$$\Delta = (\frac{m_{11} - m_{22}}{m_{33}}u - a_{21})v + \frac{1}{m_{33}}u_2 - b_2\delta. \tag{3.33}$$

Given the constant surge speed assumption, the term $\frac{m_{11}-m_{22}}{m_{33}}u - a_{21}$ *is zero since* $a_{21} = \frac{m_{11}-m_{22}}{m_{33}}u$*. However, in the actual maneuvering, the varying surge speed will lead to nonzero values for* $\frac{m_{11}-m_{22}}{m_{33}}u - a_{21}$*. Therefore,* γ_v *in equation (3.31) is introduced to capture this surge speed effect and other parameter uncertainties. On the other hand, the assumption that the yaw moment induced by the rudder action is proportional to the rudder angle is an approximation for the ship physical responses observed in simulations of the high fidelity model and*

experiments. Recognizing that the rudder induced yaw moment also depends on the ship state such as u, v and r, we introduce the γ_0 term to capture the higher-order but bounded nonlinear terms in control input (the difference between $b_2\delta$ and $\frac{1}{m_{33}}u_2$) and other model dynamics. Furthermore, the effects of parameter uncertainties in the r term are captured by γ_r.

Remark 3.5. *For surface vessel maneuvering in calm water, the nonzero rudder angle, which is the only control input considered here, will result in corresponding nonzero sway velocity v and yaw rate r. Normally, the magnitudes of v and r are both related to the magnitude of rudder angle. Extensive simulation using a high-order nonlinear model shows that there exists a phase lag between the response v and r. Therefore, we use $\bar{\gamma}_0$ in Assumption 3.2 to capture this lag and $\bar{\gamma}_r$ for the proportional relation between v and r.*

To study the stability of the closed loop system with the proposed controller implemented to the system (3.28)-(3.30), the Lyapunov function V_3 used in the controller derivation in the previous section is adopted. Differentiating V_3 with respect to time, yields,

$$\begin{aligned}\dot{V}_3 &= -c_1 u e^2 \frac{\sin\bar{\psi}}{\bar{\psi}} - \frac{c_2}{c_1^2} z_2^2 [1 - \frac{c_1 u}{c_2}\frac{\sin\bar{\psi}}{\bar{\psi}}] - p_2 c_3 z_3^2 \\ &\quad + ve\cos\bar{\psi} + \frac{1}{c_1} v z_2 \cos\bar{\psi} + p_2 c_1 c_2 v z_3 \cos\bar{\psi} + p_2 a_{21} v z_3 + p_2 z_3 \Delta. \quad (3.34)\end{aligned}$$

Defining $d_1 := c_1 u\frac{\sin\bar{\psi}}{\bar{\psi}}$, $d_2 := \frac{c_2}{c_1^2}(1 - \frac{c_1 u}{c_2}\frac{\sin\bar{\psi}}{\bar{\psi}})$ and $d_3 := p_2 c_3$, it follows from (3.34) that:

$$\begin{aligned}\dot{V}_3 &\leq -d_1 e^2 - d_2 z_2^2 - d_3 z_3^2 \\ &\quad + |v|(|\cos\bar{\psi}||e| + \frac{|\cos\bar{\psi}|}{c_1}|z_2| + p_2 c_1 c_2 |\cos\bar{\psi}||z_3| \\ &\quad + p_2|a_{21}||z_3|) + p_2|z_3||\Delta|. \quad (3.35)\end{aligned}$$

If Assumption 3.1 and 3.2 are satisfied and notice that $|r| \leq |z_3| + c_2|z_2|$, (3.35) leads to:

$$\begin{aligned} \dot{V}_3 \;\; \leq \;\; & -d_1 e^2 - d_2 z_2^2 - d_3 z_3^2 + l_1|e| + l_2|z_2| + l_3|z_3| \\ & + n_1 z_2^2 + n_2 z_3^2 + q_1|e||z_2| + q_2|e||z_3| + q_3|z_2||z_3|, \end{aligned} \tag{3.36}$$

where

$$l_1 = \bar{\gamma}_0 |\cos\bar{\psi}|, \tag{3.37}$$

$$l_2 = \frac{\bar{\gamma}_0 |\cos\bar{\psi}|}{c_1}, \tag{3.38}$$

$$l_3 = p_2(c_1 c_2 \bar{\gamma}_0 |\cos\bar{\psi}| + \bar{\gamma}_0 |a_{21}| + \gamma_0 + \bar{\gamma}_0 \gamma_v), \tag{3.39}$$

$$n_1 = \frac{c_2 \bar{\gamma}_r |\cos\bar{\psi}|}{c_1}, \tag{3.40}$$

$$n_2 = p_2(c_1 c_2 \bar{\gamma}_r |\cos\bar{\psi}| + \bar{\gamma}_r |a_{21}| + \gamma_r + \bar{\gamma}_r \gamma_v), \tag{3.41}$$

$$q_1 = c_2 \bar{\gamma}_r |\cos\bar{\psi}|, \tag{3.42}$$

$$q_2 = \bar{\gamma}_r |\cos\bar{\psi}|, \tag{3.43}$$

$$q_3 = p_2 c_2 (c_1 c_2 \bar{\gamma}_r |\cos\bar{\psi}| + |a_{21}| \bar{\gamma}_r + \bar{\gamma}_r \gamma_v + c_1 \gamma_r) + \frac{c_3 \bar{\gamma}_r}{c_1}. \tag{3.44}$$

Using the arithmetic mean geometric mean inequality in (3.36), we have:

$$\dot{V}_3 \leq -\bar{d}_1 e^2 - \bar{d}_2 z_2^2 - \bar{d}_3 z_3^2 + l_1|e| + l_2|z_2| + l_3|z_3|. \tag{3.45}$$

where

$$\bar{d}_1 = d_1 - \frac{q_1}{2} - \frac{q_2}{2}, \tag{3.46}$$

$$\bar{d}_2 = d_2 - n_1 - \frac{q_1}{2} - \frac{q_3}{2}, \tag{3.47}$$

$$\bar{d}_3 = d_3 - n_2 - \frac{q_2}{2} - \frac{q_3}{2}. \tag{3.48}$$

From (3.45), it follows that the system will converge to a region around the origin that is characterized by $\{\,(e, z_2, z_3) \mid |e| \leq \frac{l_1}{\bar{d}_1}, |z_2| \leq \frac{l_2}{\bar{d}_2}, |z_3| \leq \frac{l_3}{\bar{d}_3}\,\}$. By a proper selection of the controller gains c_1, c_2, c_3 and p_2, we can make the region very small if there are no significant unmodeled dynamics, which means γ_0, γ_v and γ_r are small, and the sway velocity is relatively small, which means $\bar{\gamma}_0$ and $\bar{\gamma}_r$ are small.

Remark 3.6. *In order to eliminate the steady state error in cross-track error e when environmental disturbances exist (such as the lateral current), we could design a controller with an integral term e by augmenting the system dynamics (3.1)-(3.3) with $\dot{e}_I = e$, where e_I is the integral of cross-track error e. However, the feedback dominance technique for simplifying the backstepping controller is not applicable in this case. Thus, the resulting controller derived by following the standard backstepping technique is very complex, which defeats our purpose to develop a simple controller for easy gain-tuning and analysis. In fact, an integral term $-\bar{c}_4 e_I$ ($\bar{c}_4$ is positive gain) could be directly added into the control law (3.17) to achieve good performance with environmental disturbances. However, rigorous analysis would be difficult to establish stability and converging performance in this case.*

3.4 Simulation Results in Calm Water

To verify and illustrate the theoretical results, the proposed control law is implemented and simulated with the 4-DoF nonlinear container model (S175 described in Section 2.1.1) along with the corresponding reduced-order model. The actuator saturation and its rate limits ($|\delta| \leq 20$ degree and $|\dot{\delta}| \leq 5$ degree/second) are incorporated in the performance evaluations. In the simulation, $u = 7$ m/s, $a_{22} = -0.10676$ and $b_2 = 0.0028385$. Different controller gains are used to achieve different transient performance; the numerical values of the gains used for simulations are listed in Table

3.1. Notice that the large value assumed by p_2 is used to normalize the variables in the Lyapunov function.

Table 3.1: Controller gains for simulations of FDBS path following controller.

	c_1	c_2	c_3	p_2
gain1	0.0005	0.2	0.005	10^{11}
gain2	0.001	0.2	0.006	10^{11}
gain3	0.006	0.2	0.008	10^{11}

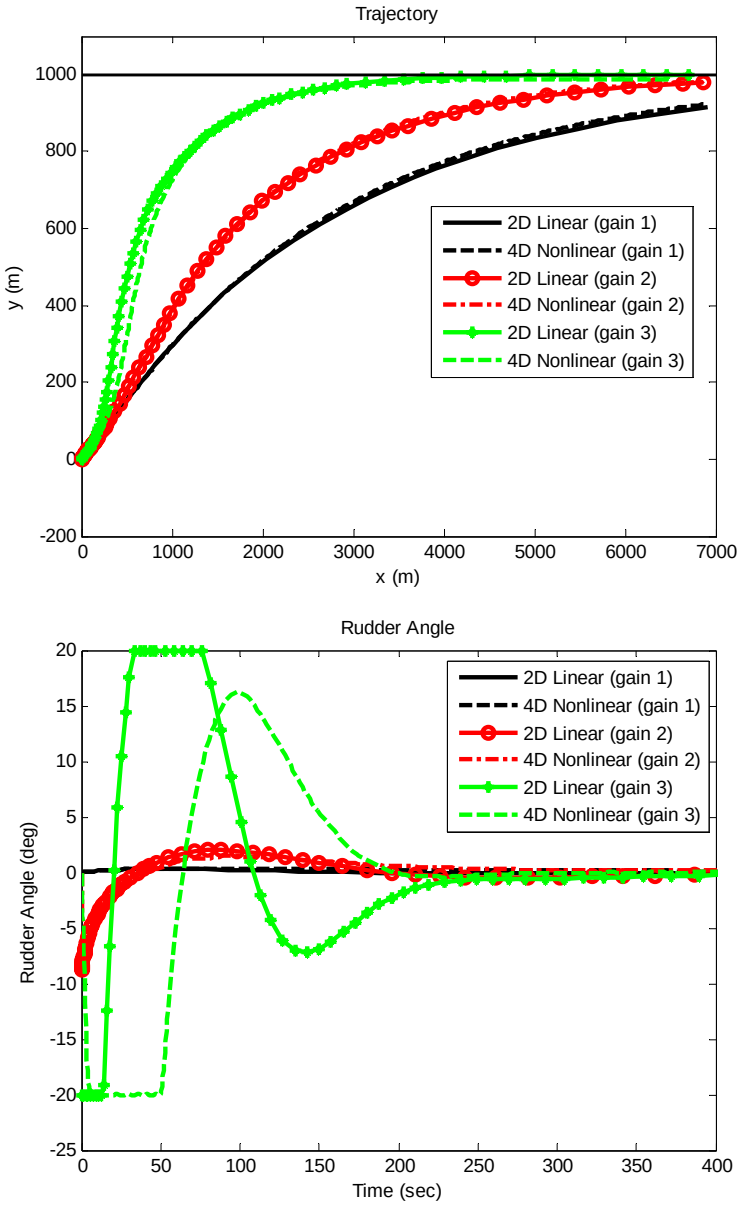

Figure 3.1: Simulation results of the ship response with different control gains.

The effects of the controller gains on the dynamic response are first illustrated in Figure 3.1. The controller with gain3 (corresponding to the largest c_1) has the fastest convergence speed. This response speed, however, is achieved at the expense of the large rudder angle and actuator saturation. From Figure 3.1 (where the legends linear and nonlinear indicate the response of linear and nonlinear model, respectively), one can also see that the response of the linear model is in excellent agreement with that of the nonlinear model. This demonstrates the robustness of the control law against the potential modeling errors.

The control algorithm is also tested with different initial conditions, see Figure 3.2. The ship is placed with the initial heading angles, -5, -45, and 15 [deg] and the cross-track errors, 100, 500 and 1000 [m], respectively. The initial v and r are set to zero. Figure 3.2 shows that the controller (with gain2) is capable of achieving path following for all the initial conditions tested. It is also shown that the rudder angle and the convergence rate depend in general on the magnitude of the initial errors, which verifies the nonlinear nature of the underlying dynamics.

To evaluate the robustness of the control system, additional uncertainties, such as time-delays and measurement noise, are considered. A time delay (1 sec and 5 sec) is introduced in the control execution, while the measurement noise (white noise with standard deviation of $p|S|$ with p being the noise factor and S being the order of the magnitude of the measured signal) is introduced for all the signals (e, $\bar{\psi}$ and r) used in the control implementation. Figure 3.3 and Figure 3.4 show the simulation results of the vessel response in the presence of time delay and measurement noise, respectively (both with gain2). One can see that while the path following performance is almost un-affected by these adverse factors in both cases, these uncertainties introduce oscillations in the rudder responses.

Furthermore, we compared the LQR, feedback dominance backstepping controller (FDBS) and linearized FDBS controllers by simulations. The LQR controller is de-

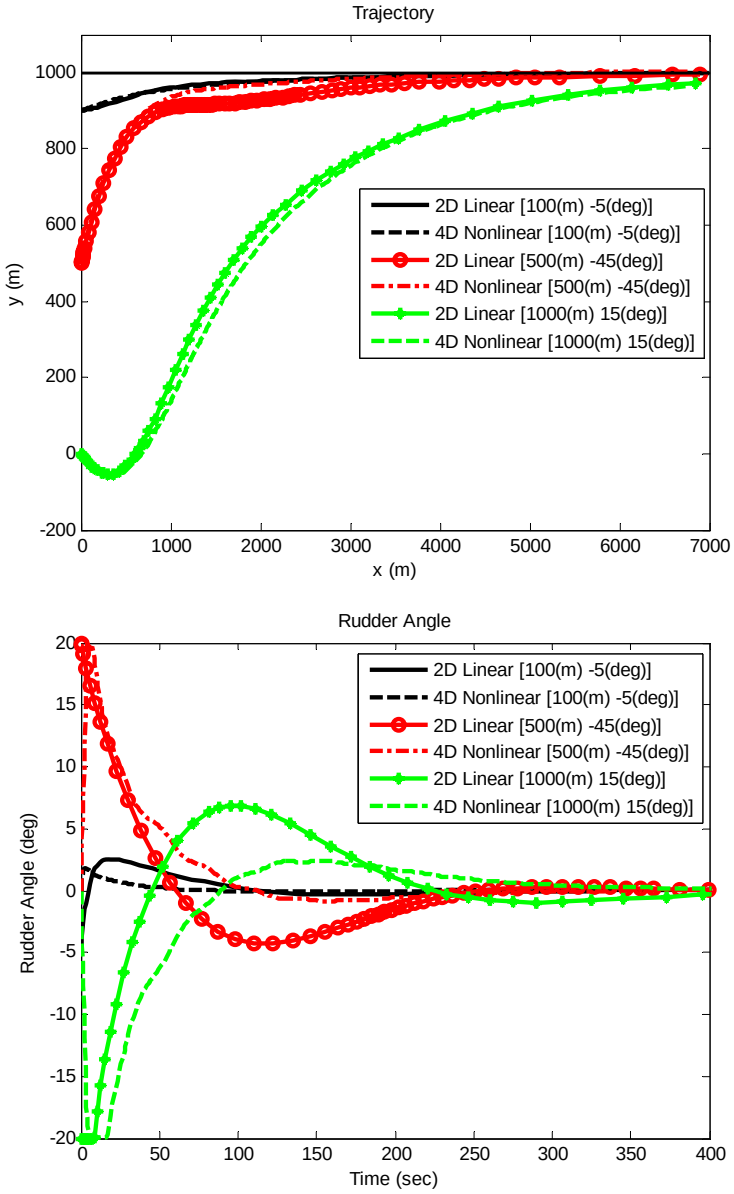

Figure 3.2: Simulation results of the control system for different initial conditions (number in the brackets are the initial cross-track error and heading error).

signed based on the linearized version of system (3.1)-(3.3) (which is also referred to as the Nomoto model in [24]) and the linearized FDBS is developed by replacing $\sin\bar{\psi}$ with $\bar{\psi}$ in (3.17). To get the best path following performance in terms of the fast convergence speed and overshoot avoidance, we tuned the controller gains for both the LQR and the FDBS controller carefully. The Q and R matrix employed in LQR

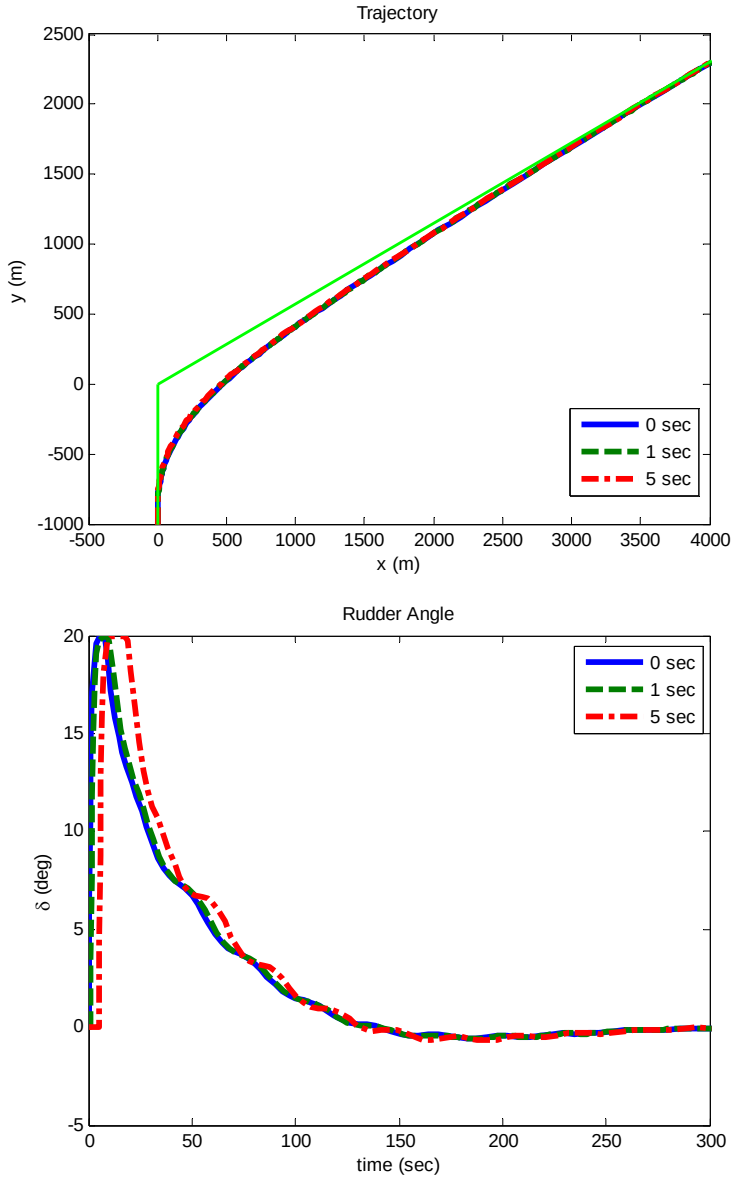

Figure 3.3: Simulation results with time delay.

controller are $[0.018^2, 0, 0; 0, 3.5^2, 0; 0, 0, 0]$ and 1, respectively. The gains adopted in FDBS and linearized FDBS are $c_1 = 0.0028$, $c_2 = 0.1$, $c_3 = 0.1$ and $p_2 = 10^{11}$. The simulation results for three different controllers are shown in Figure 3.5. It can be seen from Figure 3.5 that the FDBS controller achieves the fastest path following convergence speed with the least rudder action, while the LQR controller has slower path following and more rudder action than the FDBS controller. We also notice that

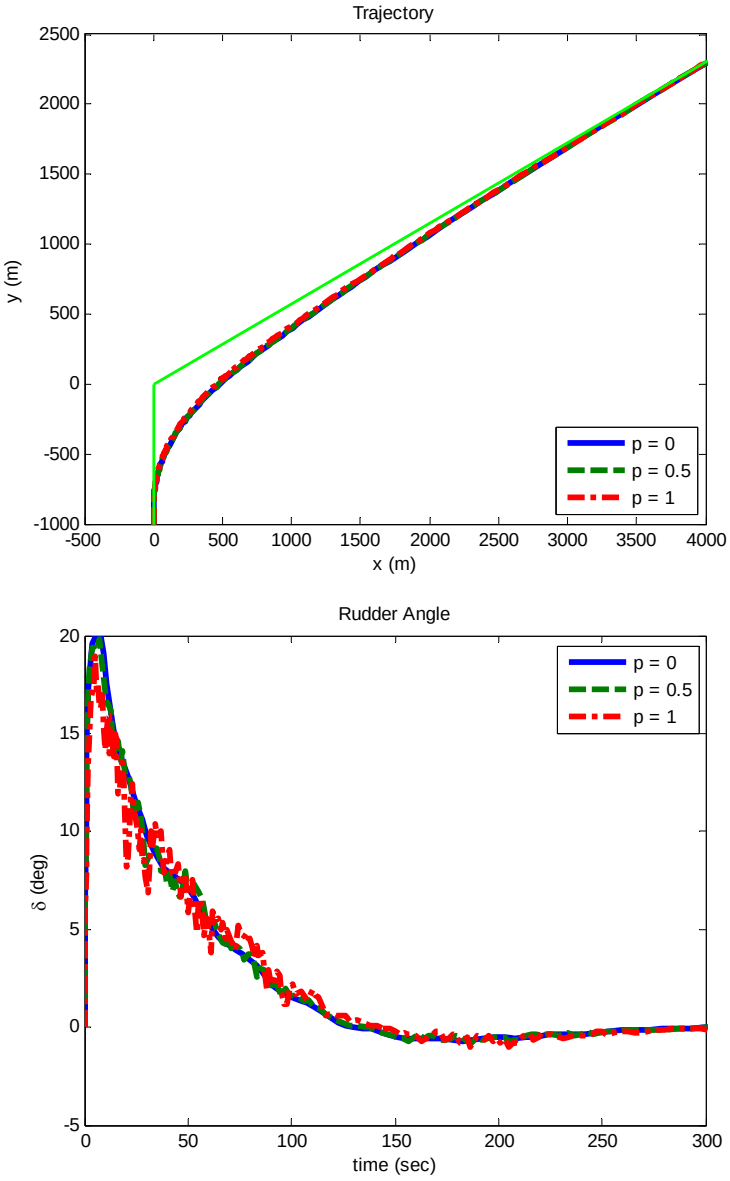

Figure 3.4: Simulation results with measurement noises.

the linearized FDBS controller has a slight overshoot in both cross-track and heading errors.

To further verify the controller performance and prepare for the experimental validation, the numerical simulations of a model boat (the details of this boat has been given in Section 2.4) with the controller proposed in this paper were conducted. The numerical model of the model boat has 2 DoF of sway and yaw by assuming the

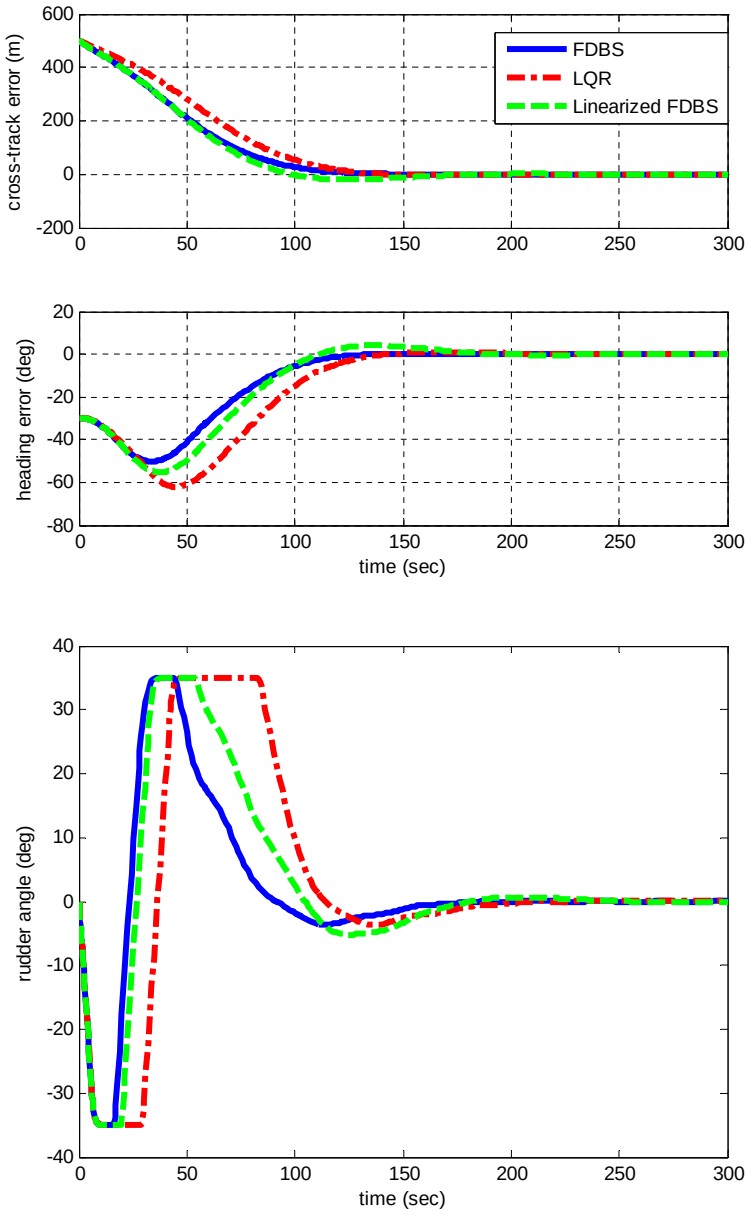

Figure 3.5: Comparison of simulation results of FDBS, LQR and Linearized FDBS controllers.

surge velocity is constant. In these simulations, the gains of the controller are set to $c_1 = 0.35$, $c_2 = 0.5$, $c_3 = 10$ and $p_2 = 10000$. The c_1, c_2 and c_3 used here are much bigger and p_2 is much smaller than the ones in Table 3.1 . The difference is due to the different scales used in two applications. Figure 3.6 shows that path following is achieved as all the path following errors are going to zero for all the initial conditions tested.

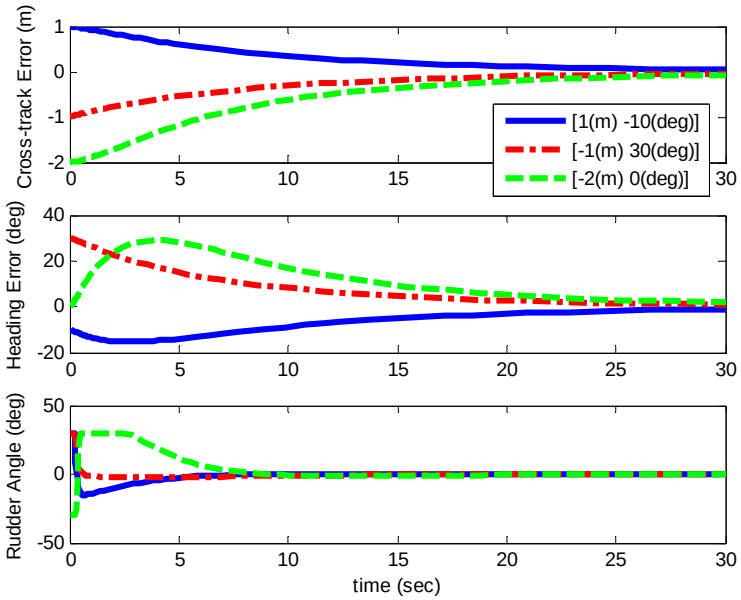

Figure 3.6: Simulation results of the model boat for different initial conditions (number in the brackets are the initial cross-track error and heading error).

3.5 Experimental Results in Calm Water

The experimental validation was conducted in the Marine Hydrodynamics Laboratories (MHL) towing tank with a model boat, which has been introduced in Section 2.4.

In all experiments, the model ship could converge to the desired path, regardless of where it actually started in the towing tank. Figure 3.7 shows one example of the experiment results, giving the time evolution of the states y, $\bar{\psi}$ and the rudder angle δ. The first and second plots given in Figure 3.7 show that the ship tracks the path well given that the cross-track and heading errors are intended to approach zero. The control algorithm was also validated to be effective under other different propeller speeds.

Figure 3.7 also shows the comparison between the simulation and experimental validation results of the model boat. Figure 3.7 shows the good match between the simulation and experimental results. In Figure 3.7, the simulation result is shown to have less rudder effort than the experimental results and this error could be attributed

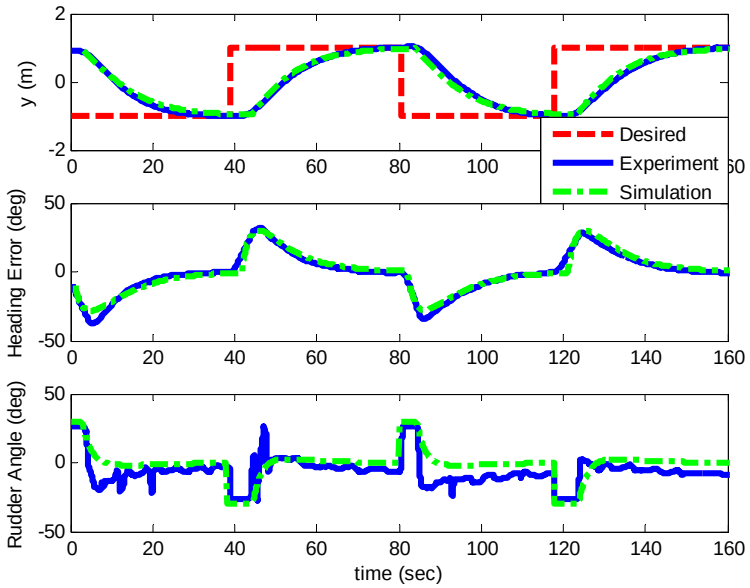

Figure 3.7: Comparison of simulation (with a reduced surge speed) and experiment results.

to the measurement bias in rudder angle detection sensor. This error tends to be small for the initial phase of the experiments. It expands over time as the error accumulates, and disappears after the sensor reset. Furthermore, model uncertainties, environmental disturbances and implementation delay and error might all contribute to the discrepancies between simulation and experiment results.

3.6 Controller Evaluation and Modification in wave fields

The proposed robust path following controller, developed based on the reduced-order linear ship model in calm water, was tested with the numerical test-bed introduced in Section 2.3 to evaluate the performance in a seaway. The actuator saturation and its rate limits ($|\delta| \leq 35$ degree and $|\dot{\delta}| \leq 5$ degree/second) are also incorporated in the evaluations. In the simulation, $u = 10$ m/s, $a_{22} = -0.10676$ and $b_2 = 0.0028385$ and the propeller speed is maintained as constant (99.50 RPM).

The controller gains were chosen to be: $c_1 = 0.0033$, $c_2 = 0.1$, $c_3 = 0.1$, $p_2 = 10^{11}$ (this gain set is named gain set 1 in the subsequent discussions), which corresponds to good closed-loop path following performance in calm water. The effects of the waves on the dynamic response of the controller are first illustrated in Figure 3.8, compared with the calm water case. The beam sea is used in the simulation since it often introduces the largest motions in sway and roll. The significant wave height in the simulations is 3.25 m (sea state 5) and it will be kept the same in all other simulations.

From Figure 3.8, it can be seen that the waves do have an impact on the container ship's response. The proposed path following controller achieves the path following with a steady state error. The wave force pushes the vessel off the desired trajectory. Furthermore, undesired oscillations in rudder response can be observed from Figure 3.8.

The steady state error in the path following and rudder oscillations are also reported in the simulation results of a fuzzy controller in [73], where there exist external disturbances from a passing ship or sea current. They solved this problem by introducing an adaptive fuzzy controller [72]. However, neither of the algorithms provided in these papers could eliminate the rudder oscillations. The rudder oscillations in the course-keeping stage cause wear and tear of the steering gear, and efforts have been reported in the literature to reduce or eliminate their impacts. Typical mitigating solutions include using low gains or dead zone, limiting rudder actions and filtering of the signals [69, 70]. It should be pointed out that each solution has its associated limitations. For example, using low gain has to compromise fast course changing for good course keeping, while the dead zone might lead to sluggish course steering. On the other hand, the effectiveness of the filtering depends on a good knowledge of the cut-off frequency, whose estimation will further complicate the overall control system.

To search for an alternative solution to mitigate the problems for the path fol-

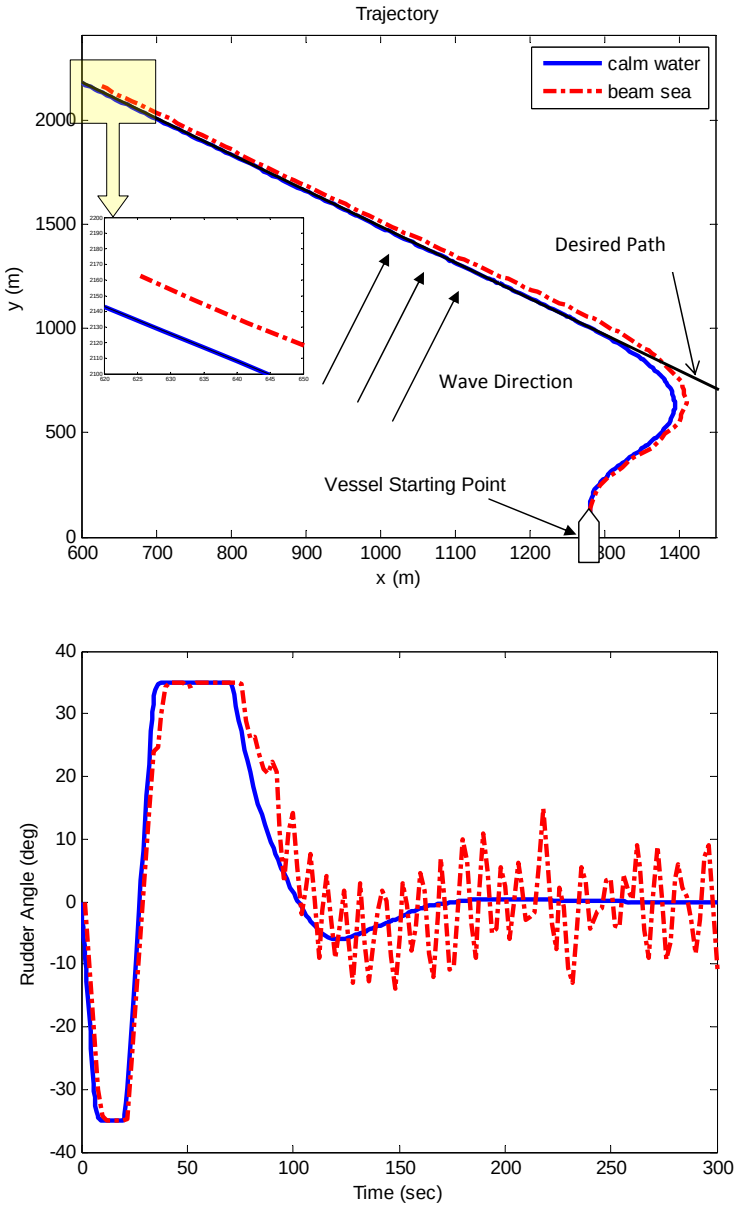

Figure 3.8: Simulation results of the ship response in beam sea and calm water with gain set 1.

lowing control in the seaway, the wave impacts on the controller performance will be analyzed to identify the reasons for the steady state error and rudder oscillations.

Steady state error is largely due to the second-order drift force, which results in a non-zero equilibrium point if the controller gains are not properly selected. The simplified vessel model will be used to analyze the reason of the steady state error.

When the waves exist, the overall system dynamics can be described as follows:

$$\dot{e} = usin(\bar{\psi}) + vcos(\bar{\psi}), \tag{3.49}$$

$$\dot{\bar{\psi}} = r, \tag{3.50}$$

$$\dot{v} = a_{11}v + a_{12}r + b_1\delta + \frac{m_{66}(\bar{f}_2 + f_2) - m_{62}(\bar{f}_6 + f_6)}{m_{22}m_{66} - m_{62}^2}, \tag{3.51}$$

$$\dot{r} = a_{21}v + a_{22}r + b_2\delta + \frac{m_{22}(\bar{f}_6 + f_6) - m_{62}(\bar{f}_2 + f_2)}{m_{22}m_{66} - m_{62}^2}, \tag{3.52}$$

where (3.49) and (3.50) are the original path following error dynamics. Moreover, $m_{22} = m + m_y$, $m_{66} = I_z + J_z$ and $m_{62} = m_y\alpha_y$.

The equilibrium point of the overall system (3.49)-(3.52) in the average sense is the solution of the equations:

$$usin(\bar{\psi}) + vcos(\bar{\psi}) = 0, \tag{3.53}$$

$$a_{11}v + b_1\delta + \frac{m_{66}\bar{f}_2 - m_{62}\bar{f}_6}{m_{22}m_{66} - m_{62}^2} = 0, \tag{3.54}$$

$$a_{21}v + b_2\delta + \frac{m_{22}\bar{f}_6 - m_{62}\bar{f}_2}{m_{22}m_{66} - m_{62}^2} = 0. \tag{3.55}$$

Notice that $r = 0$ and the zero-mean oscillating 1st-order wave loads are neglected. According to the control law (3.17), δ is a function of e and $\bar{\psi}$. Therefore, the above three equations (3.53)-(3.55) have three unknowns, namely v, e and $\bar{\psi}$. And the solution of these three equations depends on the controller gains c_1, c_2, c_3 and p_2. If gain set 1 is selected, the steady state error given by the (3.53)-(3.55) is:

$$e_0 = -16.67 \text{ (m)}, \tag{3.56}$$

$$\bar{\psi}_0 = 4.6 \text{ (deg)}, \tag{3.57}$$

$$v_0 = -0.64 \text{ (m/s)}, \tag{3.58}$$

which match the simulation result given in Figure 3.8. To reduce or eliminate the steady state error, the gains c_1,c_2,c_3 and p_2 should be properly selected. The proper gains that eliminate the steady state cross-track error should satisfy the following two equations:

$$a_{11}v_0 - \frac{b_1}{b_2}[(c_2c_3 + \frac{1}{c_1^2p_2})\bar{\psi_0} + c_1c_2usin\bar{\psi_0}] + \frac{m_{66}\bar{f}_2 - m_{62}\bar{f}_6}{m_{22}m_{66} - m_{62}^2} = 0, \tag{3.59}$$

$$a_{21}v_0 - (c_2c_3 + \frac{1}{c_1^2p_2})\bar{\psi_0} - c_1c_2usin\bar{\psi_0} + \frac{m_{22}\bar{f}_6 - m_{62}\bar{f}_2}{m_{22}m_{66} - m_{62}^2} = 0. \tag{3.60}$$

Notice that e_0 is set to zero to derive (3.59)-(3.60) from (3.53)-(3.55). To find the proper parameters so that (3.59)-(3.60) are satisfied, let $\bar{\psi_0} = 4.6$ (deg) and $v_0 = -0.64$ (m/s), which is the same as the solution of gain set 1. For a given wave field with a specific sea state, the steady state errors in the heading error and sway velocity should be the same to counteract the same wave drift loads, regardless of the controller gains. For this particular case, the control gain c_1, c_2, c_3 and p_2 should satisfy the following condition:

$$(c_2c_3 + \frac{1}{c_1^2p_2}) + 9.9893c_1c_2 - 0.0039 = 0. \tag{3.61}$$

The reason for the rudder oscillations is the state oscillations induced by the first-order wave excitation load, especially the yaw rate r. The correlation between the rudder angle and yaw rate can be clearly seen in Figure 3.9. One intuitive solution to reduce the rudder oscillations is to use the low gain corresponding to the yaw rate term to make the controller insensitive to the oscillating state. More specifically, proper c_2 and c_3 should be selected to make the coefficient of the r term $(a_{22}+c_2+c_3)$ in control law to be zero or small. For this particular case, the following condition

should be satisfied:

$$c_2 + c_3 - 0.1068 \approx 0. \tag{3.62}$$

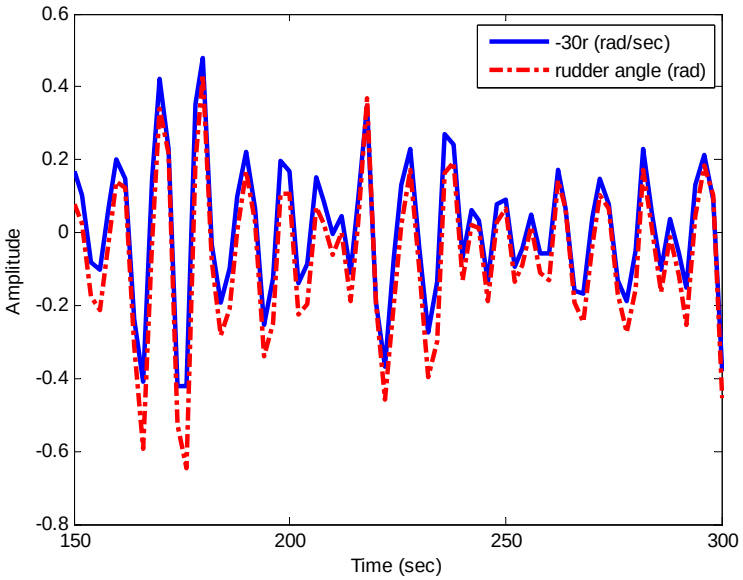

Figure 3.9: The state histories in wave fields (gain set 1)

From the above analysis, the gain set 2, which corresponds to $c_1 = 0.0023$, $c_2 = 0.05$, $c_3 = 0.05676$ and $p_2 = 10^{11}$ satisfies these two conditions (3.61)-(3.62) for small or no steady state error in cross-track error and rudder oscillations. However, the path following performance of gain set 2 is not satisfactory in the sense that sluggish path following convergence speed is observed in simulation, as shown in Figure 3.10. To achieve good path following performance and small steady state error and rudder oscillations, a gain scheduling approach is proposed: 1), if the cross-track error is larger than 20m, gain set 1 is adopted for good path following performance and 2), otherwise gain set 2 is employed to have small steady state error in cross-tracking error and rudder oscillations. The simulation results of modified controller with gain scheduling compared with the original controller are summarized in Figure 3.10. From Figure 3.10, the steady state error in path following and the rudder oscillations are reduced to an acceptable extent without compromising the path following convergent

speed.

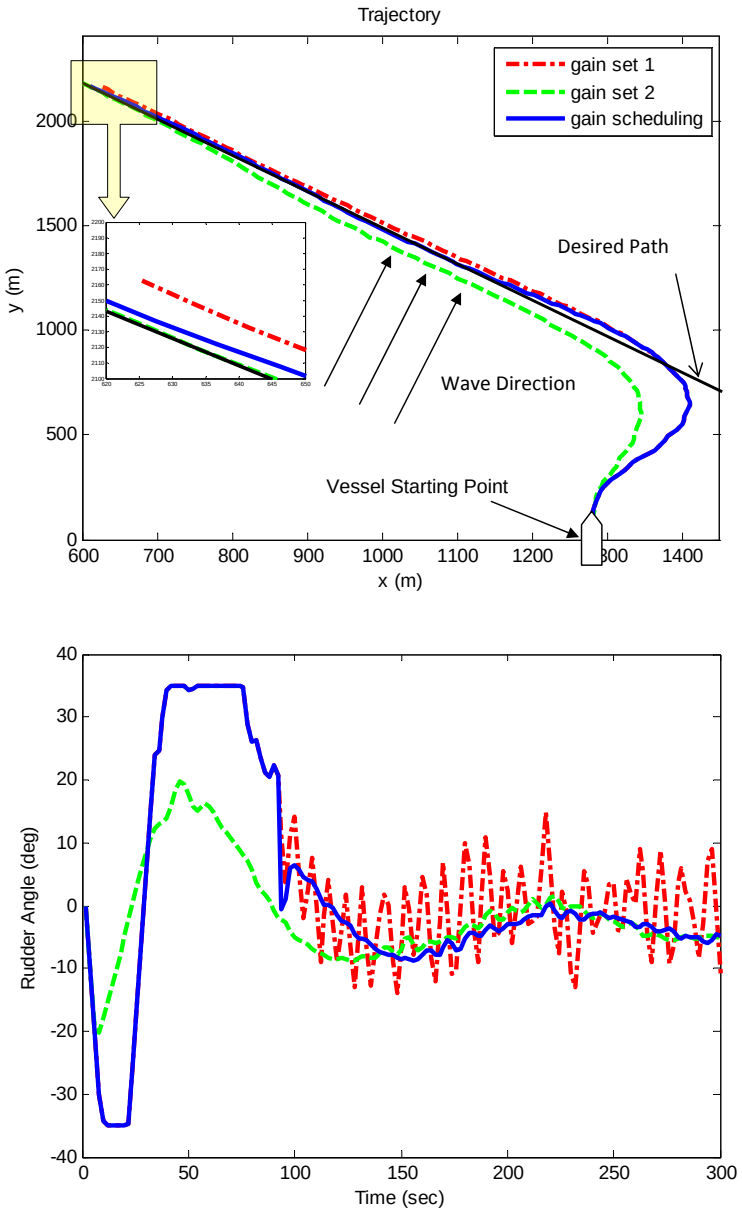

Figure 3.10: Simulation results of gain scheduling controller to reduce the steady state error and rudder oscillations.

The proposed path following gain scheduling controller has the great advantage of easy re-tuning to address the environmental disturbance because of its simple form. Furthermore, since no adaptation mechanism and signal filters are adopted in the gain scheduling controller, the complexity of the control system can be largely reduced.

3.7 Summary

In this chapter, a control system for marine surface vessel path following was proposed. The back-stepping design, based upon feedback dominance, leads to a simple control law that achieves asymptotic path following. Robustness analysis against unmodeled dynamics was also performed. Simulation results revealed that the controller enhanced the path following capability while demonstrating robust performance against model uncertainties, communication delays and measurement noise. The effectiveness of the designed controller was also validated by the successful experimental results. Because of the simple form of the controller, it is expected that very limited on-board computational power will be required to implement the control. The FDBS controller for marine surface vessels was also evaluated in wave fields. Since a steady state cross-track error and the rudder oscillations were observed in the evaluation, controller tuning was performed to modify the system response to reduce the steady state cross-track error and rudder oscillations. Simulation validated that the re-calibrated controller with gain scheduling achieved satisfactory performance in terms of both path following convergence speed and steady state behavior.

CHAPTER 4

Path Following with Roll Constraints for Marine Surface Vessels

This chapter presents a Model Predictive Control (MPC) design of the path following for an integrated model of the surface vessel dynamics and path following kinematics. The focus is on satisfying all the inputs and state constraints while achieving satisfactory path following performance. The one-input (rudder) and two-input (rudder and propeller) MPC controllers are both developed to achieve constrained path following and their performance are compared by simulations. The path following performance of the proposed MPC controller and its sensitivity to the major controller parameters, such as the sampling time, predictive horizon and weighting matrices in the cost-function, are analyzed by numerical simulations.

4.1 Introduction

One challenge for path following of marine surface vessels stems from the fact that the system is often underactuated. Conventional ships are usually equipped with one or two main propellers for forward speed control, and rudders for course keeping of the ship. For ship maneuvering, such as path following and trajectory tracking,

where we seek control for all three degrees of freedom (surge, sway and yaw), the two controls can not influence all three variables independently, thereby leading to under-actuated control. Another challenge in the path following of marine surface vessels is the inherent physical limitations in the control inputs, namely the rudder saturation and rudder rate limit. More recently, given that the roll motion produces the highest acceleration and is considered as the principal villain for the seasickness and cargo damage [24], enforcing roll constraints while maneuvering in a seaway becomes an important design consideration in surface vessel control. While typical nonlinear control methodologies do not take these input and output constraints explicitly into account in the design process, the constraint enforcement is often achieved through numerical simulations and trial-and-error tuning of the controller parameters. Few other control methodologies, such as the MPC [48, 58] and reference governor [28], have a clear advantage in addressing input and state constraints explicitly. [74] considers rudder saturation in its MPC controller for tracking control of marine surface vessels and [55] achieves the roll reduction for the heading control problem using an MPC approach. For the path following control problem considered in this dissertation where both the cross-track error and heading error are controlled by the rudder angle as an under-actuated problem and rudder limitation and roll constraints need to be enforced simultaneously, MPC applications have not been found in the open literature, to the best knowledge of the author.

MPC, also known as the receding horizon control (RHC), is a control technique which embeds optimization within feedback to deal with systems subject to constraints on inputs and states [48, 58]. Over the last few decades, MPC has proven to be successful for a wide range of applications including chemical, food processing, automotive and aerospace systems [58]. Using an explicit model and the current state as the initial state to predict the future response of a plant, it determines the control action by solving a finite horizon open-loop optimal control problem on-line

at each sampling interval. Furthermore, because of its natural ability to treat multi-variable systems, MPC can handle underacuated problem gracefully by combining all the objectives into a single objective function.

4.2 MPC for Path Following of Marine Surface Vessels using Rudder

4.2.1 Control-design Model for MPC using Rudder

The Serret-Frenet error dynamics (1.2) and (1.3) described in Section 1.1.3 are employed to design the MPC path following controller. The control objective is to drive e and $\bar{\psi}$ to zero.

For the path following problem without roll constraints, the control design, summarized in Chapter 3, is based on the linear system (2.23)-(2.24). However, the additional DoF roll should be also included for path following with roll constraints. Therefore, the corresponding 3-DoF (sway, yaw and roll) linear system (2.25)-(2.29), described in Section 2.1.2, will be adopted in the one-input MPC control design. Notice that the surge speed is assumed to be constant and the surge dynamics are neglected.

The performance of the control system designed using the reduced-order model ((1.2)-(1.3) and (2.25)-(2.29)) will be presented to justify the utility of the reduced-order model when the same controller is applied to the full-order model S175 (see Section 2.1.1).

4.2.2 MPC Formulation for Path Following using Rudder

This section presents the formulation of the MPC for the path following problem of marine surface vessels using rudder. For notational convenience, the ship dynamics

(2.25)-(2.29) together with linearized path following error dynamics (1.1)-(1.2) are written into the matrix form:

$$\dot{\bar{x}} = \bar{A}\bar{x} + \bar{B}\delta, \tag{4.1}$$

where

$$\bar{x} = \begin{bmatrix} e \\ \bar{\psi} \\ v \\ r \\ p \\ \phi \end{bmatrix}, \tag{4.2}$$

$$\bar{A} = \begin{bmatrix} 0 & u & 0 & 0 & 0 & 0 \\ 0 & 0 & 0 & 1 & 0 & 0 \\ 0 & 0 & a_{11} & a_{12} & a_{13} & a_{14} \\ 0 & 0 & a_{21} & a_{22} & a_{23} & a_{24} \\ 0 & 0 & a_{31} & a_{32} & a_{33} & a_{34} \\ 0 & 0 & 0 & 0 & 1 & 0 \end{bmatrix}, \qquad \bar{B} = \begin{bmatrix} 0 \\ 0 \\ b_1 \\ b_2 \\ b_3 \\ 0 \end{bmatrix}. \tag{4.3}$$

Given a specific sampling time T_s, the plant (4.1) is easily transformed into its discrete-time version:

$$\bar{x}_{k+1} = A\bar{x}_k + B\delta_k. \tag{4.4}$$

Using the discrete-time plant (4.4), the future state of the plant can be predicted by:

$$\bar{X}_k = F\bar{x}_k + HU_k, \tag{4.5}$$

where

$$\bar{X}_k = \begin{bmatrix} \bar{x}_{k+1} \\ \bar{x}_{k+2} \\ \vdots \\ \bar{x}_{k+N_p} \end{bmatrix}, \qquad U_k = \begin{bmatrix} \delta_k \\ \delta_{k+1} \\ \vdots \\ \delta_{k+N_p-1} \end{bmatrix}, \tag{4.6}$$

$$F = \begin{bmatrix} A \\ A^2 \\ \vdots \\ A^{N_p} \end{bmatrix}, \qquad H = \begin{bmatrix} B & 0 & 0 & \cdots & 0 \\ AB & B & 0 & \cdots & 0 \\ \vdots & \vdots & \vdots & \ddots & \vdots \\ A^{N_p-1}B & A^{N_p-2}B & A^{N_p-3}B & \cdots & B \end{bmatrix}, \tag{4.7}$$

and N_p is the predictive horizon.

Then the MPC online optimization problem can be formulated as follows: at each time k, find the optimal control sequence $\{\delta_k^*, \delta_{k+1}^*, \cdots, \delta_{k+N_p-1}^*\}$ to minimize the following cost function (4.8):

$$J(U_k, \bar{x}_k) = \sum_{j=1}^{N_p} (\bar{x}_{k+j}^T Q \bar{x}_{k+j} + \delta_{k+j-1}^T R \delta_{k+j-1}), \tag{4.8}$$

subject to

$$-\delta_{max} \leq \delta_{k+j} \leq \delta_{max}, \ j = 0, 1, \cdots, N_p - 1, \tag{4.9}$$

$$-\Delta\delta_{max} \leq \delta_{k+j} - \delta_{k+j-1} \leq \Delta\delta_{max}, \ j = 0, 1, \cdots, N_p - 1, \tag{4.10}$$

$$-\bar{x}_{max} \leq \bar{x}_{k+j} \leq \bar{x}_{max}, \ j = 1, 2, \cdots, N_p, \tag{4.11}$$

where (4.9), (4.10) and (4.11) stand for rudder saturation, rudder rate limit and state limit respectively. Q and R are the corresponding weighting matrices and N_p is the predictive horizon. The control law is given by $\delta_k = \delta_k^*$.

Since the cost function (4.8) is quadratic in $\bar{x}$ and δ and all the constraints are linear, we can use quadratic programming (QP) to solve the optimization problem. In this study, the optimization and simulation are performed in MATLAB.

4.2.3 Simulation Results and Controller Parameter Tuning

The proposed control law is implemented and simulated on the full-order nonlinear model. The actuator saturation and its rate limits ($|\delta| \leq 35$ deg and $|\dot{\delta}| \leq 5$ deg/sec) are incorporated in simulations, while different roll constraints are imposed to evaluate the effectiveness of the MPC and the trade-offs between tightening the roll constraint and achieving path following. For all simulations of the MPC controller using the rudder, the propeller speed is maintained as constant (99.50 RPM). Since only the relative penalty on $\bar{x}$ and δ will influence the performance, Q and R are chosen to have the form of $Q = \{0.0001, c_1, 0, 0, 0, 0\}$, $R = c_2$, namely, the cost function is $J = \sum_{j=1}^{N_p}(0.0001{e_{k+j}}^2 + c_1\bar{\psi}_{k+j}^2 + c_2\delta_{k+j-1}^2)$, with c_1, c_2 being positive constants. The numerical values of these different gains used for simulations are listed in Table 4.1.

Table 4.1: Controller gains for simulations of MPC path following controller.

	G1	G2	G3	G4	G5
c_1	8	1.6	40	8	8
c_2	1	1	1	0.1	10

Selection of the Sampling Time

The general guideline for selecting the sampling rates for discrete-time dynamical system is about 4-10 samples per rise time [3], which is about 18 second for the roll dynamics (which is the fastest among yaw, sway and roll) of the container ship. Therefore, a rational choice of the sampling is between 1 to 4 seconds. For the MPC application, small sampling times provide more timely feedback but require more frequent optimization, and a good trade-off between the path following performance and real-time implementation consideration can be achieved through the sensitivity analysis. The roll, sway and yaw responses of the closed-loop system with the MPC corresponding to different sampling times are summarized in Figure 4.1. For each simulation, the predictive time window is set to 120 seconds (considering that the

time constant for the maneuvering dynamics is around 20 seconds), which leads to different predictive steps N_p for different sampling intervals. The gain set G1 is employed in this simulation. From Figure 4.1, the responses with 1 second and 2 second sampling period can be seen to be almost indifferentiable, while the responses with 3 or 4 second sampling interval start to deviate. Figure 4.1 shows that $T_s = 2$ sec is a good choice for the implementation of MPC controller for the container ship under consideration. Simulations performed for many other gain sets yield the same conclusion.

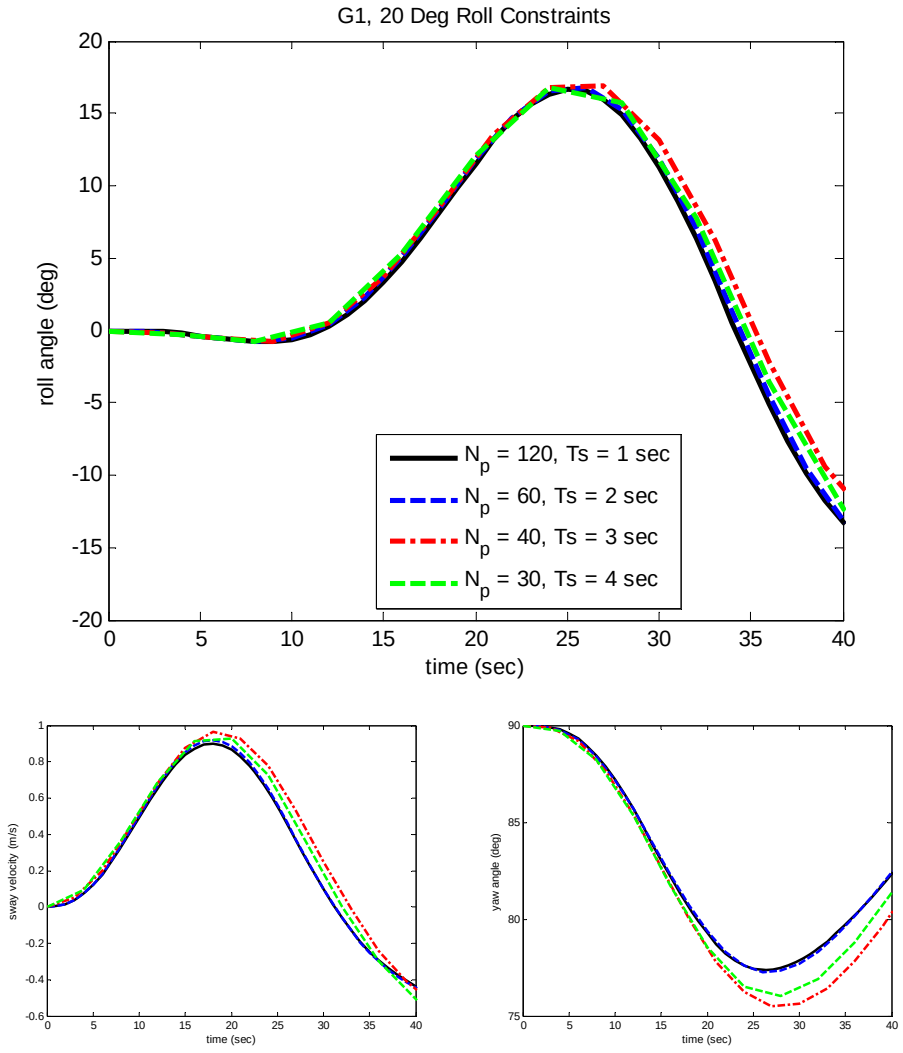

Figure 4.1: Simulation results of the ship response with different sampling time.

Prediction Horizon

The length of the predictive horizon N_p is a basic tuning parameter for MPC controllers. Generally speaking, controller performance improves as N_p increases, at the expense of additional computation effort [58]. The effects of predictive horizon N_p on the path following performance are studied by simulations with results given in Figure 4.2. The gain set G1 is employed in this simulation. It is clear from Figure 4.2 that longer predictive horizon leads to faster path following and avoids over-steering, but the benefits of extending the prediction horizon diminishes beyond $N_p = 40$. Given the heavy computational cost associated with long prediction horizon (in our simulations, the computational time for each optimization with $N_p = 160$ and $N_p = 80$ are about 16 and 4 times of the one for $N_p = 40$, respectively), it can be concluded that a value of 40-60 achieves a good trade-off for the predict horizon N_p, given 2 seconds as the sampling period. The same conclusion can be drawn from simulations performed for many other gain sets.

Putting it all in the context of computational effort required for MPC implementation for a marine surface vessel path following control, the optimization problem with 2 second sampling interval and 60 step predictive horizon can be solved in about 0.6 second in simulations on a desktop computer with P4 2.4 CPU and 2G RAM. Experience with the real-time optimization implementation shows that this number can be substantially reduced, using real-time computing technology, to a small fraction of sampling time. This moderate computational demand makes the MPC path following control promising for real-time implementation.

Effects of Weighting Matrices Q and R

The weighting matrices Q and R are used as the main tuning parameters to shape the closed-loop response for desired performance [48]. Investigating the performance sensitivity to the weighting matrix leads to useful insights that will be discussed in

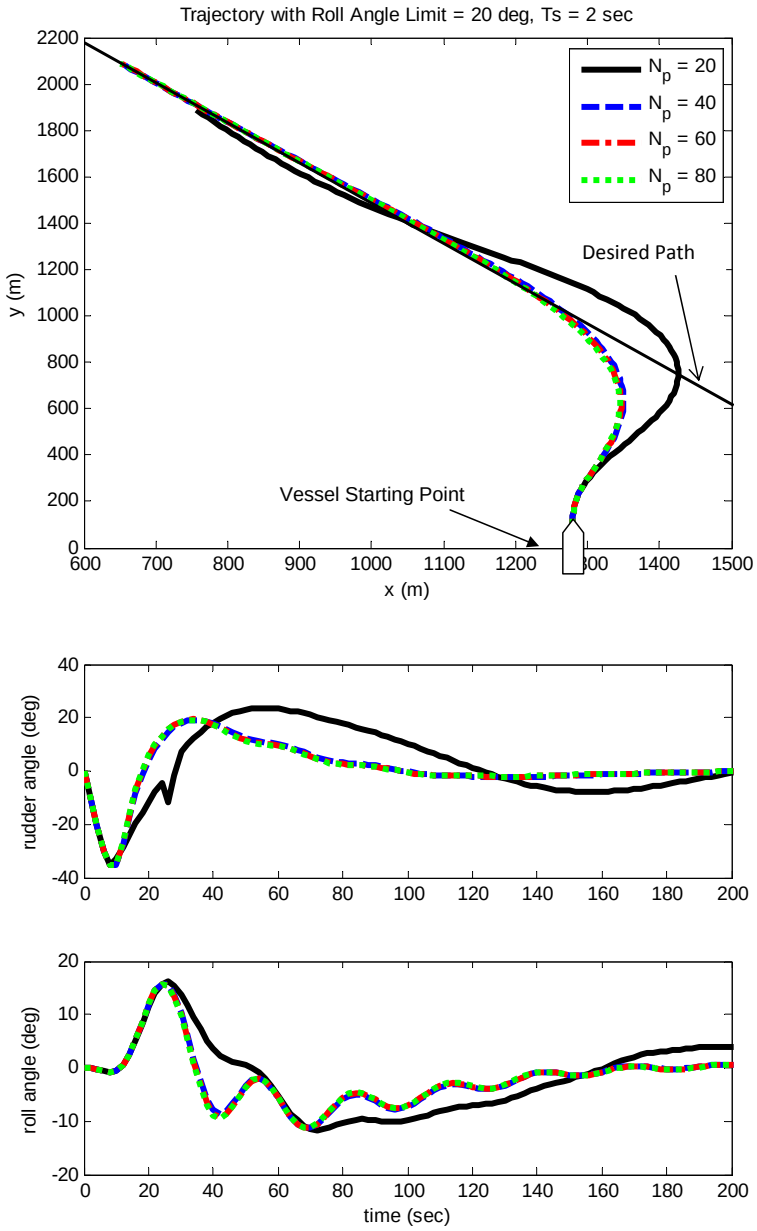

Figure 4.2: Simulation results of the ship response with different predictive horizons.

the sequel.

First, it is observed that the path following performance is primarily determined by the value of c_1 and is almost independent of the penalty of rudder c_2. This characteristic is revealed by inspecting the responses of Figure 4.3 with weighting matrix selection G1, G4 and G5 on Figure 4.3. Simulations are performed for many other combinations of c_1 and c_2, the same results are obtained. To further confirm

this, linear analysis of the closed-loop system with LQR controller was performed, and it can be shown that the slowest eigenvalue, which dominates the cross-track error dynamics, is essentially un-affected by the R matrix. The sensitivity of the path following performance to the parameter c_1 is shown in Figure 4.3 that compares the responses with weighting matrix selection G1, G2 and G3. In these simulations, the value of c_1 in the range of $[1.6, 40]$ yields reasonable path following performance, measured in the cross-tracking convergence speed.

Furthermore, once c_1 is determined to achieve the desired path following performance, the parameter c_2 can be used to tune for different rudder response and roll response. Again considering responses corresponding to weighting matrix selection G1, G4 and G5, the difference in the rudder behavior reflects the impact of c_2.

This analysis leads to the following guidelines for parameter tuning of the proposed MPC path following controller: 1) Set $c_2 = 1$, and vary c_1 to achieve desired path following performance; 2) Fix c_1 as selected in 1), vary c_2 to tune for different rudder and roll responses.

Enforcing Roll Constraints

Generally speaking, a trade-off exists between the path following convergence speed and the roll minimization, namely, imposing roll constraints will deteriorate the path following performance of vessels. To understand this trade-off, simulations are performed with different roll constraints being imposed, and the results are summarized in Figure 4.4. From Figure 4.4, it can be seen that initially the roll constraints slow down the heading changing speed because the large rudder action is not permissible due to the roll constraints. However, the final convergence time of all scenarios are very close because the MPC scheme can compensate the initial slow maneuvering later by increasing the rudder angle. However, if the constraints on the roll is tightened further beyond 2 deg, the vessel will take very long time to converge to the path

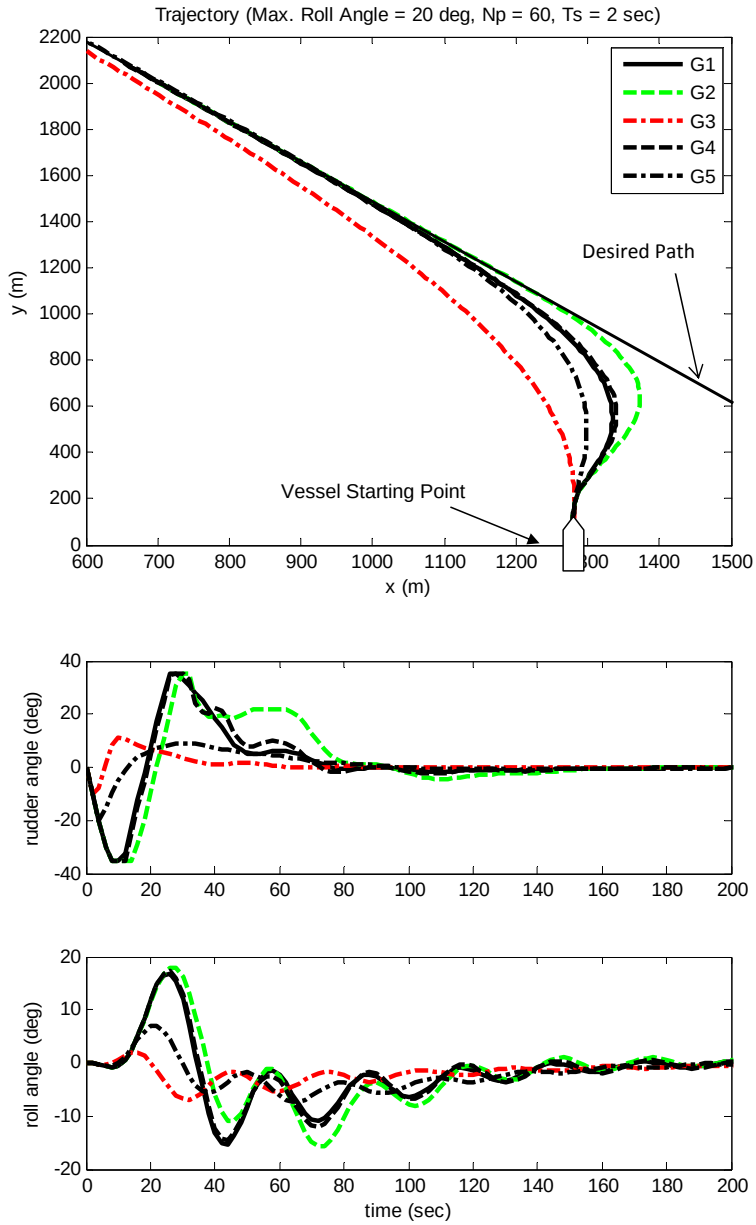

Figure 4.3: Simulation results of the ship response with different weighting matrix.

or even go into the infeasible region. When simulations are performed for many other gain sets, the similar tendency is obtained.

4.2.4 Summary

The MPC approach using rudder as the sole control was presented to address the path following of marine surface vessels with input and state constraints. The

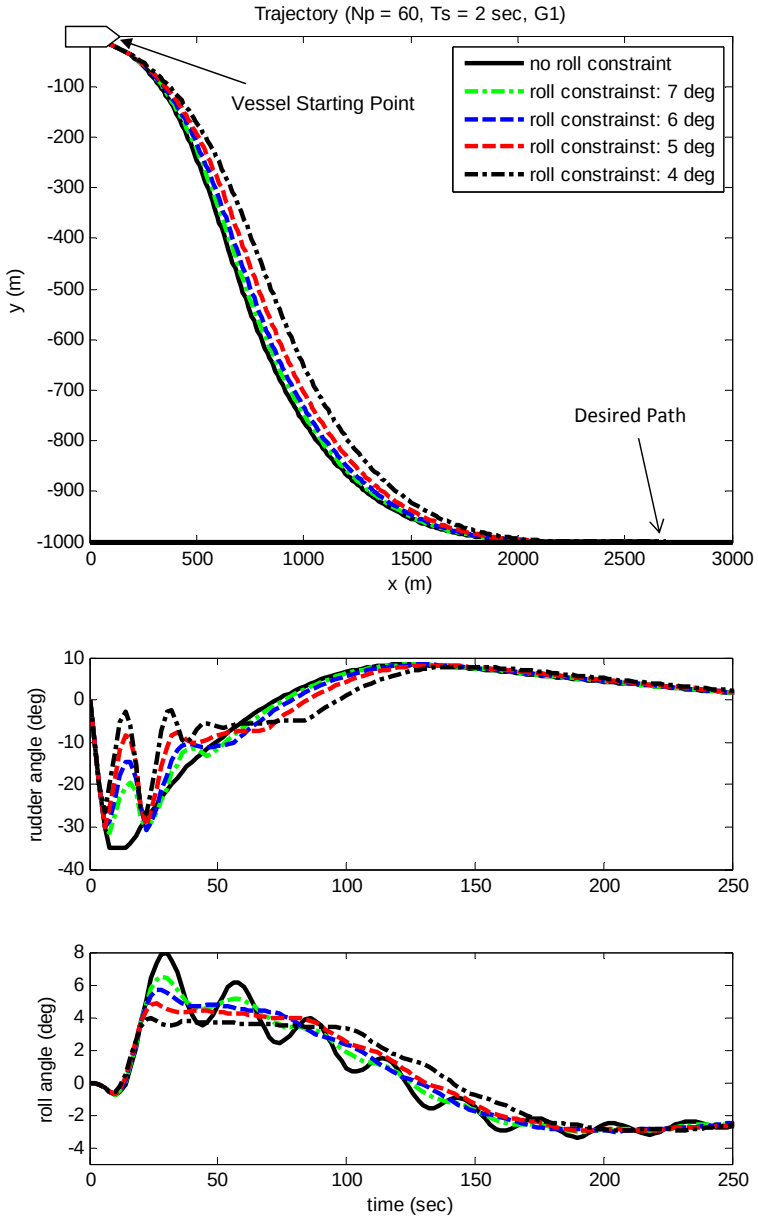

Figure 4.4: Simulation results of the ship response with different roll constraints.

detailed MPC formulation was described and the simulation results showed that the MPC design can achieve the path following of marine surface vessels while satisfying the pre-scribed input and state constraints. Furthermore, the sensitivity analysis of the performance to the sampling time, predictive horizon and weighting matrices were also performed, which leads to the guidelines in the MPC parameter tuning. The sampling rate (2 seconds) and the prediction horizon ($N_p \simeq 50$) determined from

simulations provided evidence that the real-time implementation of the MPC scheme in path following of marine surface vessels is feasible with moderate computational resources.

4.3 MPC for Path Following of Marine Surface Vessels with Coordinated Rudder and Propeller Actuation

In this study, the propeller control, in addition to the rudder control, is proposed to improve the roll reduction performance of the MPC path following controller, motivated by the fact that the dynamic coupling between the vessel forward speed and roll response can be leveraged to mitigate excessive roll with properly designed propeller actions. The significant influence of the forward speed on the roll angle can be clearly seen from Figure 4.5, which shows the simulation results of S175 for different forward speeds and the same rudder angle. Therefore, it is expected that the roll response can be reduced by properly controlling the propeller speed, which largely determines the forward speed.

4.3.1 Control-design Model for MPC Controller with Rudder and Propeller as Inputs

The matrix form of the two-input linearized model of the ship dynamics together with path following error dynamics is as follows:

$$\dot{\bar{x}} = \bar{A}\bar{x} + \bar{B}'\bar{u}, \tag{4.12}$$

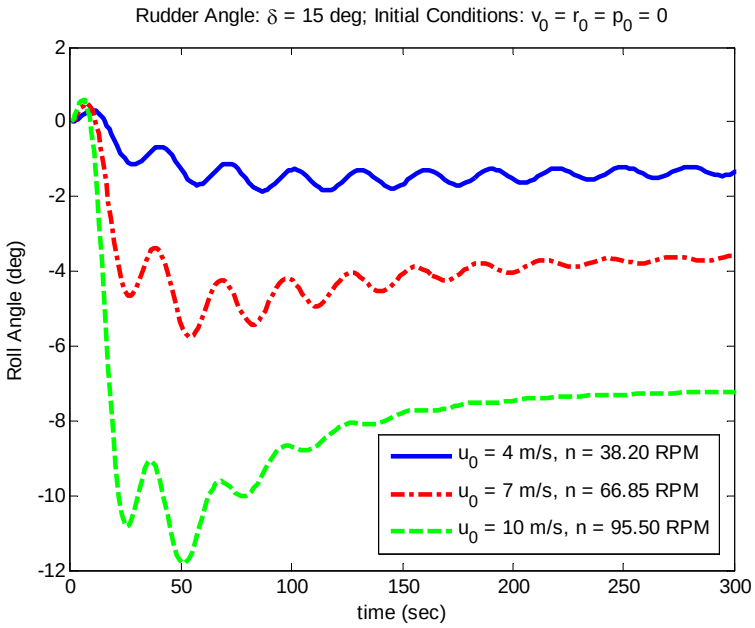

Figure 4.5: Roll response with different surge speeds.

where $\bar{x}$ and $\bar{A}$ are in the forms of (4.6) and (4.7), respectively. Furthermore,

$$\bar{B}' = \begin{bmatrix} 0 & 0 \\ 0 & 0 \\ b_{11} & b_{12} \\ b_{21} & b_{22} \\ b_{31} & b_{32} \\ 0 & 0 \end{bmatrix}, \qquad \bar{u} = \begin{bmatrix} \delta \\ n \end{bmatrix}. \tag{4.13}$$

For control design, three linear models, obtained by linearizing the original nonlinear model S175 (see Section 2.1.1 (2.19)) at different equilibrium points, are used to facilitate the model-based design. To incorporate the propeller effects on the system dynamics, the nonlinear model is linearized around the equilibrium points corresponding to $\delta_0 = 0$ (for the operating range corresponding to the rudder angle from -10 to 10 deg), $\delta_0 = 15$ (for the operating range corresponding to the rudder angle large than 10 deg) and $\delta_0 = -15$ deg (for the operating range corresponding to the rudder

angle less than -10 deg). Those three models will be denoted as M_1, M_2 and M_3, respectively, in the sequel. The different values of matrix $\bar{A}$ and $\bar{B}'$ of three linearized models are given in Table 4.2.

Table 4.2: System parameters for different linear models.

	M_1	M_2	M_3
a_{11}	-0.02276	-0.04062	-0.04062
a_{12}	-2.7910	-0.1899	-0.1899
a_{13}	-0.09211	-0.06664	-0.06664
a_{14}	-0.1169	-0.09348	-0.09348
a_{21}	-0.0009168	0.0001167	0.0001167
a_{22}	-0.1068	-0.1468	-0.1468
a_{23}	0.009949	0.007198	0.007198
a_{24}	0	-0.0008284	-0.0008284
a_{31}	0.002032	0.002594	0.002594
a_{32}	-0.3058	-0.3051	-0.3051
a_{33}	-0.01982	-0.01434	-0.01434
a_{34}	-0.04486	-0.04471	-0.04471
b_{11}	-0.05699	-0.04575	-0.04575
b_{12}	0	-0.0002503	0.0002503
b_{21}	0.002838	0.002279	0.002279
b_{22}	0	0.00001247	-0.00001247
b_{31}	0.004081	0.003277	0.003277
b_{32}	0	0.00001793	-0.00001793

The reason of adopting multiple linear models instead of using a single linear model employed in Section 4.2 is that the single linear model linearized around the equilibrium point $\delta_0 = 0$, designated as M_1, can not capture the dynamic relation between the system response and propeller speed. If a single linear model M_1 is adopted, the values of b_{12}, b_{22} and b_{32}, shown in Table 4.2 are all zeros. For the linear model M_1, the propeller speed has no effective influence on state variables. However, for M_2 and M_3 (linearized at $\delta \neq 0$), the nonlinearities of the dynamics render some control authority to the propeller speed on vessel responses for all the considered degrees of freedom sway v, yaw r and roll p. In order to incorporate this nonlinearity without incurring substantial computational penalty, the multiple linear models are

adopted for the MPC design.

4.3.2 MPC Formulation for Path Following Control using Rudder and Propeller

This section presents the formulation of the MPC for the path following problem of marine surface vessels. For notational convenience, we rewrite the multiple linear models into the matrix form:

$$\dot{\bar{x}} = \bar{A}(M)\bar{x} + \bar{B}(M)\bar{u}. \tag{4.14}$$

Notice that the matrix $\bar{A}$ and $\bar{B}$ are now dependent on which linear model is employed. Specifically, one of the three linear models will be selected in the MPC optimization, based on the yaw rate r, as follows:

$$M = \begin{cases} M_1, \text{ if } -r_c < r < r_c; \\ M_2, \text{ if } r \leq -r_c; \\ M_3, \text{ otherwise,} \end{cases} \tag{4.15}$$

where r_c is the steady state value of the yaw velocity when the rudder angle is -10 deg. The reason of adopting yaw velocity as the criteria of model-switching is that the vessel forward speed effects on the roll response are largely influenced by the yaw rate, which can be clearly seen from Figure 4.6 that shows the simulation results of S175 for different yaw rates and the same propeller speed. Yaw rates 0.0058, 0.0078 and 0.0089 rad/sec are the steady state values when the rudder angle is set to 5, 10 and 15 deg, respectively.

Given a sampling time T_s and yaw rate (which determine M), the plant (4.14) can be discretized as:

$$\bar{x}_{k+1} = A(M)\bar{x}_k + B(M)\bar{u}_k. \tag{4.16}$$

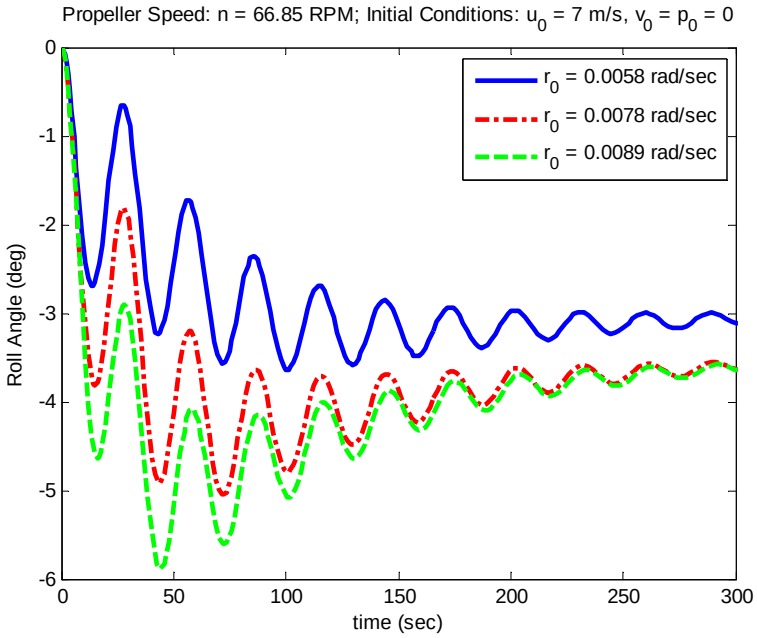

Figure 4.6: Roll response with different yaw rates.

Then the MPC online optimization problem can be formulated as follows: at each time k, find control sequence $\{\bar{u}_k, \bar{u}_{k+1}, \cdots, \bar{u}_{k+N_p-1}\}$ to minimize the following cost function (4.17):

$$J(\bar{x}_k) = \sum_{j=1}^{N_p} (\bar{x}_{k+j}^T Q \bar{x}_{k+j} + \bar{u}_{k+j-1}^T R' \bar{u}_{k+j-1}), \tag{4.17}$$

subject to state equation (4.16) and

$$\bar{u}_{min} \leq \bar{u}_{k+j-1} \leq \bar{u}_{max}, \ j = 1, 2, \cdots, N_p, \tag{4.18}$$

$$-\Delta\bar{u}_{max} \leq \Delta\bar{u}_{k+j-1} \leq \Delta\bar{u}_{max}, \ j = 1, 2, \cdots, N_p, \tag{4.19}$$

$$-\bar{x}_{max} \leq \bar{x}_{k+j} \leq \bar{x}_{max}, \ j = 1, 2, \cdots, N_p, \tag{4.20}$$

where (4.18), (4.19) and (4.20) stand for the control input saturation, input rate limit and state limit, respectively (the inequalities (4.18), (4.19) and (4.20) have to be satisfied element-by-element). Q and R' are the corresponding weighting matrices and N_p is the predictive horizon. Notice that R' here has one more dimension than

R used in the one-input case.

Since the cost function (4.17) is quadratic in $\bar{x}$ and $\bar{u}$ and all the constraints are linear, QP can be used to solve the optimization problem. In this study, the optimization and simulation are performed in MATLAB.

4.3.3 Simulation Results

The MPC using rudder and propeller is implemented and simulated on the 4 DoF nonlinear S175 container model. The propeller speed limit ($0 \leq n \leq 160$ RPM), together with the rudder saturation and its rate limits ($|\delta| \leq 35$ deg and $|\dot{\delta}| \leq 5$ deg/sec), are incorporated in the simulations. No rate limit is imposed on the change of the propeller speed.

Sampling Time and Prediction Horizon Choices

The philosophy of selecting the sampling time and prediction horizon for the MPC using rudder and propeller is basically the same as the case using rudder only. Considering the rise time of the fastest dynamics, the sampling time $T_s = 2$ sec is still a rational choice. For the selection of the prediction horizon, simulations were performed using different prediction horizons, which are shown in Figure 4.7. The gain set G1 and $c_3 = 0$ are employed in these simulations with the sampling time of 2 seconds. Figure 4.7 shows that longer predictive horizon leads to faster path following but the benefits of extending the prediction horizon diminishes beyond $N_p = 60$. Considering the associated computational cost, $N_p = 60$ was selected for this particular case, given 2 seconds as the sampling period. The same conclusion can be drawn from simulations performed for many other gain sets.

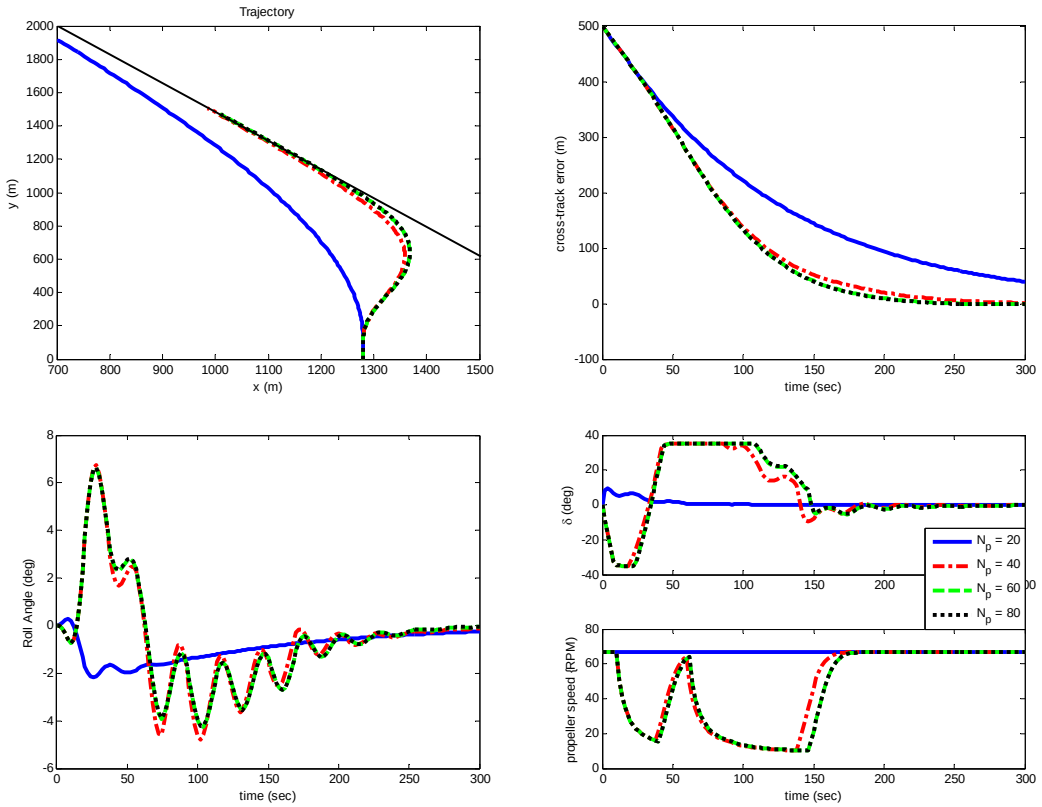

Figure 4.7: Simulation results of the ship response with different prediction horizon.

Effects of Weighting Matrix R'

The guidelines given in Section 4.2 for tuning matrix Q of the MPC path following controller using just the rudder are also useful for the tuning of controller using rudder and propeller. Additional simulations are conducted to study the effect of matrix $R' = \{c_2, c_3\}$ on the system response. The impact of c_2 has been analyzed in Section 4.2, which is similar in two-input case as shown in simulations. In this section, focus is on investigating the performance sensitivity to the gain c_3. With gain set G1, three values of c_3 , namely 0, 0.00002 and 0.2, are adopted in simulations, which are summarized in Figure 4.8. Please notice the different magnitudes for values of rudder angle ($\sim \pi/5$) and propeller speed (~ 70). Thus, with $c_3 = 0.2$, the penalty on propeller speed is significantly large compared with the rudder angle penalty with $c_2 = 1$.

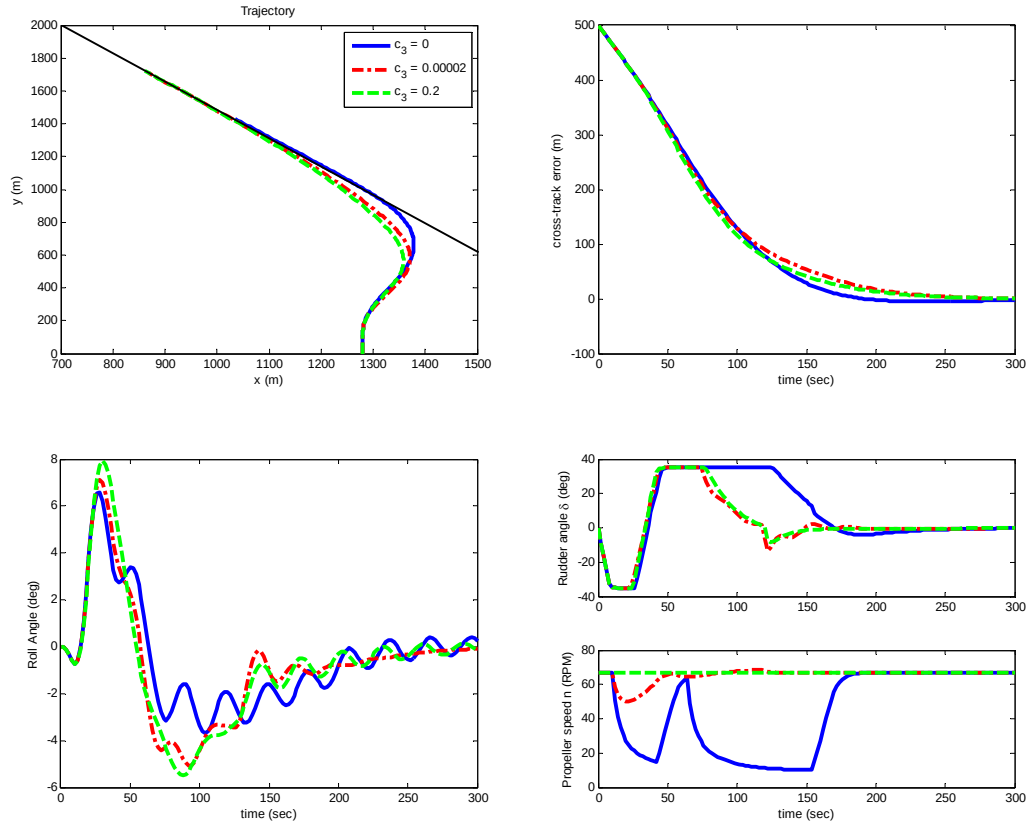

Figure 4.8: Simulation results of the ship response with different penalties on the propeller speed.

The simulation results employing different values of c_3 are illustrated in Figure 4.8. Figure 4.8 shows that the value of c_3 has significant effect on the propeller response. A large value of c_3 will prevent the change of propeller speed. Specially, if the c_3 is extremely large ($c_3 = 0.2$), the propeller speed almost can not be changed and it results in the MPC controller using rudder, which is discussed in Section 4.2. It is also shown in Figure 4.8 that smaller c_3 results in faster path following convergence speed and smaller maximum roll angle. Because the propeller has more freedom to slow down the ship speed, which helps to make a faster turn and reduce roll action, when c_3 is small.

Comparisons of One-input (Rudder) and Two-input (Rudder and Propeller) MPC

The MPC designed using multiple reduced-order linear models with rudder and propeller as inputs is implemented and simulated with the full-order original nonlinear model S175 and compared with simulations of the one-input case.

First the performance of these two controllers are compared when no roll constraint is imposed. In this simulation, the gain set G1 is employed and c_3 is set to be zero to maximize the capability of the propeller speed in changing the vessel's forward speed to affect the roll response. The simulation results are summarized in Figure 4.9. Figure 4.9 shows that the introduction of additional propeller control helps to enhance the roll reduction capability when making abrupt turns. Moreover, this improvement is achieved without compromising the path following convergence speed. When the vessel makes large turns, the two-input controller predicts that the large roll motion will happen and thus the propeller speed is slowed down in order to reduce the vessel forward speed, not significantly. As the result of forward speed reduction, the vessel has the capability to make the easier turn while keeping the roll motion small. In this case, the propeller speed never exceed the initial value because the linear model M_1 is used when the vessel approaches the path, which can not reflect the propeller effect in system responses. If a better prediction model is adopted, which can involve the dynamic relation between propeller speed and ship states, the propeller speed might exceed the initial value to make the path convergence speed even faster.

To quantitatively evaluate the controller performance, four performance indices are introduced, namely maximum roll angle ϕ_{max}, Root Mean Squares (RMS) roll angle ϕ_{RMS} and path convergence time t_{con}, with the definitions given by:

$$\phi_{RMS} = \sqrt{\frac{1}{T_{final}} \int_0^{T_{final}} \phi^2 \, dt}, \tag{4.21}$$

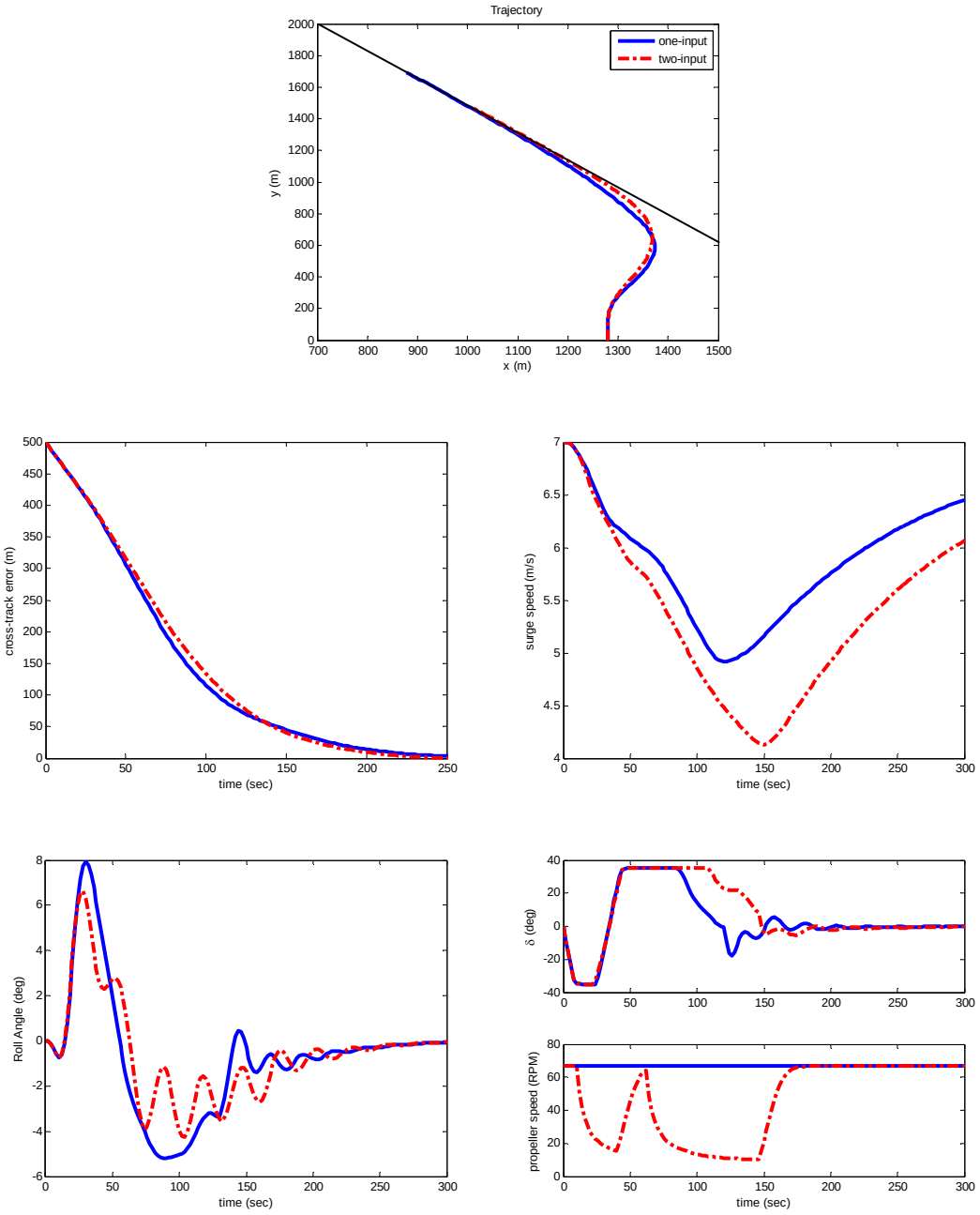

Figure 4.9: Comparisons of one-input and two-input MPC performance without roll constraints.

and path convergence time t_{con} is the time the vessel finally approaches the path (cross-track error less than 10 m). T_{final} is the total simulation time, which is 300 sec in this case.

The summary of these three performance indices without roll constraints is given

in Table 4.3, which shows that the roll action of two-input case is largely reduced, both in maximum and RMS roll angle. The path following performance depends on which performance index is considered. The two-input case has smaller convergence time compared with one-input case.

Table 4.3: Comparisons of performance indices for one-input and two-input MPC without roll constraints.

	ϕ_{max} [deg]	ϕ_{RMS} [deg]	t_{con} [sec]
One-input	7.78	1.44	188
Two-input	6.60	1.30	172
Change Percent	-15.17	-9.72	-8.51

Furthermore, these two controllers implemented in the original nonlinear system were compared with roll constraints. In simulations, the maximum allowed roll angle is set to 5 deg. The corresponding results are summarized in Figure 4.10. As shown in Figure 4.10, these two controllers both achieve path following while satisfying the roll constraints. The path following convergence speeds for the two cases are very close. Although they have the same maximum roll angle, which is due to the constraint enforcement capability of MPC, the two-input MPC controller has less overall roll motion because it slows down the vessel forward speed when making the turns.

The performance index comparisons for these two controllers with 5 deg roll constraints are summarized in Table 4.4. Table 4.4 shows that the introduction of additional propeller control helps to reduce the roll response. However, the two-input case approaches the path with a slightly slower speed.

Finally, the simulations are performed with tighter rudder saturation to further compare the performance of one-input and two-input MPC controllers. These results are shown in Figure 4.11. In the simulations, the maximum rudder angle allowed is 20 deg. Figure 4.11 shows that the two-input MPC controller can effectively reduce the roll actions compared with the one-input case. Meanwhile, the path following

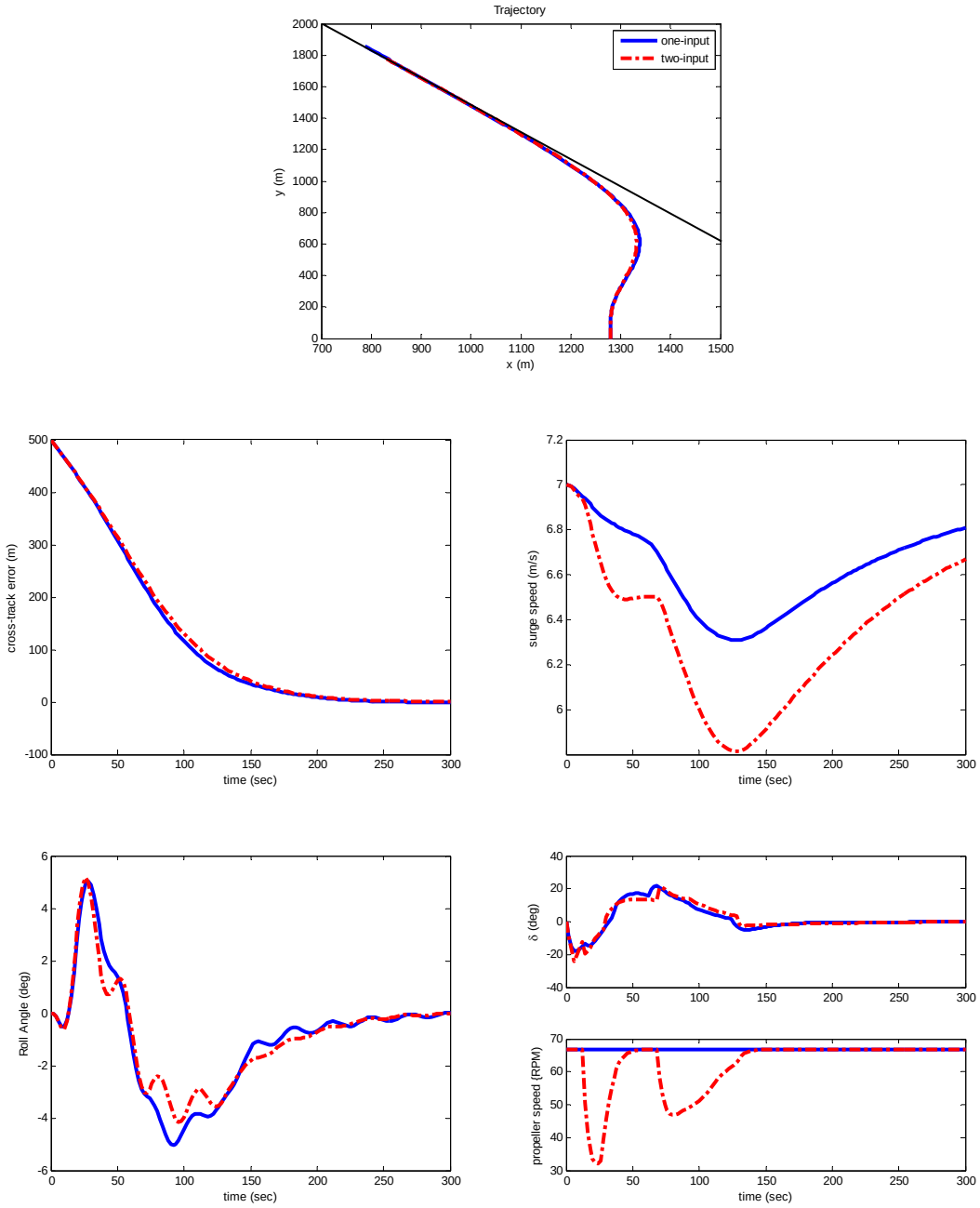

Figure 4.10: Comparisons of one-input and two-input MPC performance with roll constraints.

convergence speed is very close. Furthermore, due to the tightened rudder constraints, the overshoot is observed in both cases.

Table 4.5 presents the performance index comparisons for these two controller with 20 deg rudder saturation. Table 4.5 shows that the advantage of the introduction

Table 4.4: Comparisons of performance indices for one-input and two-input MPC with 5 deg roll constraints.

	ϕ_{max} [deg]	ϕ_{RMS} [deg]	t_{con} [sec]
One-input	4.99	1.29	198
Two-input	4.99	1.23	202
Change Percent	0	-4.65	2.02

of the propeller control is more pronounced when there is a tighter rudder limit. Particularly, the RMS of the roll angle is reduced by 21.60 percent, which is achieved with almost the same path following performance.

Table 4.5: Comparisons of performance indices for one-input and two-input MPC with tighter rudder saturations (20 deg).

	ϕ_{max} [deg]	ϕ_{RMS} [deg]	t_{con} [sec]
One-input	6.35	1.62	266
Two-input	5.34	1.27	260
Change Percent	-15.59	-21.60	-2.26

To sum up all the comparisons, the additional propeller control helps to reduce the roll response, and this improvement is achieved without compromising the path following convergence speed. Using a desktop computer with P4 2.4 CPU and 2G RAM, the optimization problem of two-input MPC with 2 second sampling interval and 60 step predictive horizon can be solved in about 0.9 second in simulations, compared to around 0.6 second for one-input case. Real-time implementation should not be a problem given this moderate computational demand.

4.3.4 Summary

The two-input (rudder and propeller) MPC design of the path following controller with roll constraints for an integrated model of the surface vessel dynamics and 2-DoF path following kinematics was presented. Two inputs, namely the rudder angle

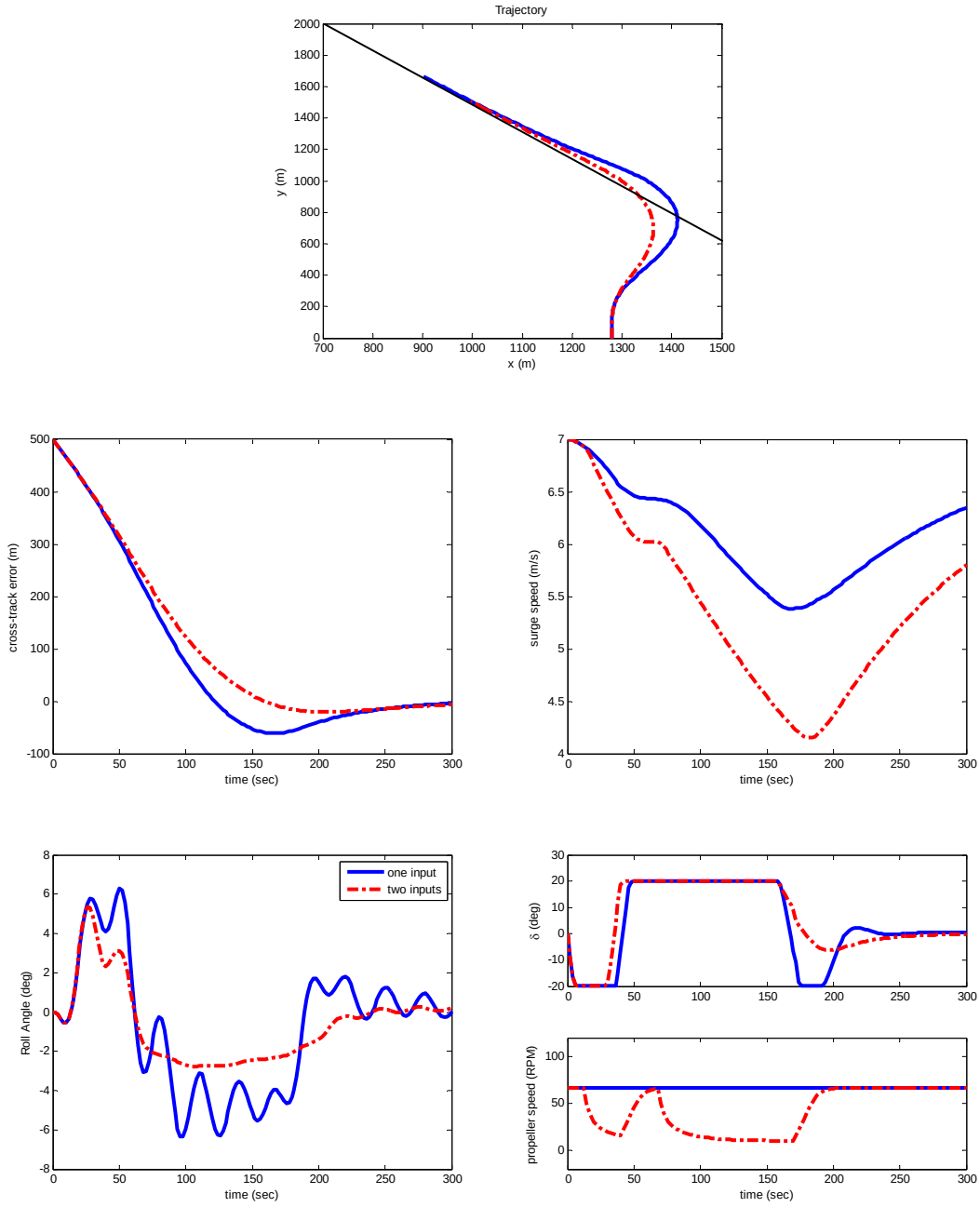

Figure 4.11: Comparisons of one-input and two-input MPC performance with tighter rudder saturation.

and propeller speed, were employed and coordinated to control the vessel. Multiple 3-DoF simplified linear vessel models were adopted in the controller design and a corresponding 4-DoF nonlinear container model was used in simulations in order to investigate the interactions between the path following maneuvering control and

roll dynamics. The path following performance and roll response were analyzed by numerical simulations and compared with the one-input (rudder) MPC performance. The simulations show that the two-input controller has the advantage over the single-input controller with improved roll response. Moreover, the improvement in the roll response was achieved without compromising the path following performance in terms of convergence speed.

CHAPTER 5

Path Following with Roll Constraints for Marine Surface Vessels in Wave Fields

This chapter first evaluates the standard MPC path following controller using rudder as the input, developed in Chapter 4, in wave fields by the numerical test-bed introduced in Chapter 2. Since roll constraint violation and feasibility issues were found in the evaluation, the mitigating strategies such as gain re-tuning and constraint tightening and softening are then proposed to guarantee the feasibility of MPC scheme and satisfaction of roll constraints. The satisfactory performance of the modified MPC controller is shown by the simulations on the numerical test-bed.

5.1 MPC Controller Evaluation in wave fields

The MPC path following controller using rudder, developed based on the reduced-order linear ship model in calm water, is implemented and simulated in the numerical test-bed (original nonlinear model of S175) incorporating the wave effects (described in Section 2.3) to evaluate the performance. The ship maneuvering model is driven by the wave forces and moments, together with the control input. In the evaluation, the propeller speed is maintained as constant (99.50 RPM). The significant wave height

in the simulations is 3.25 m, which corresponds to sea state 5, and kept the same in all simulations of this chapter.

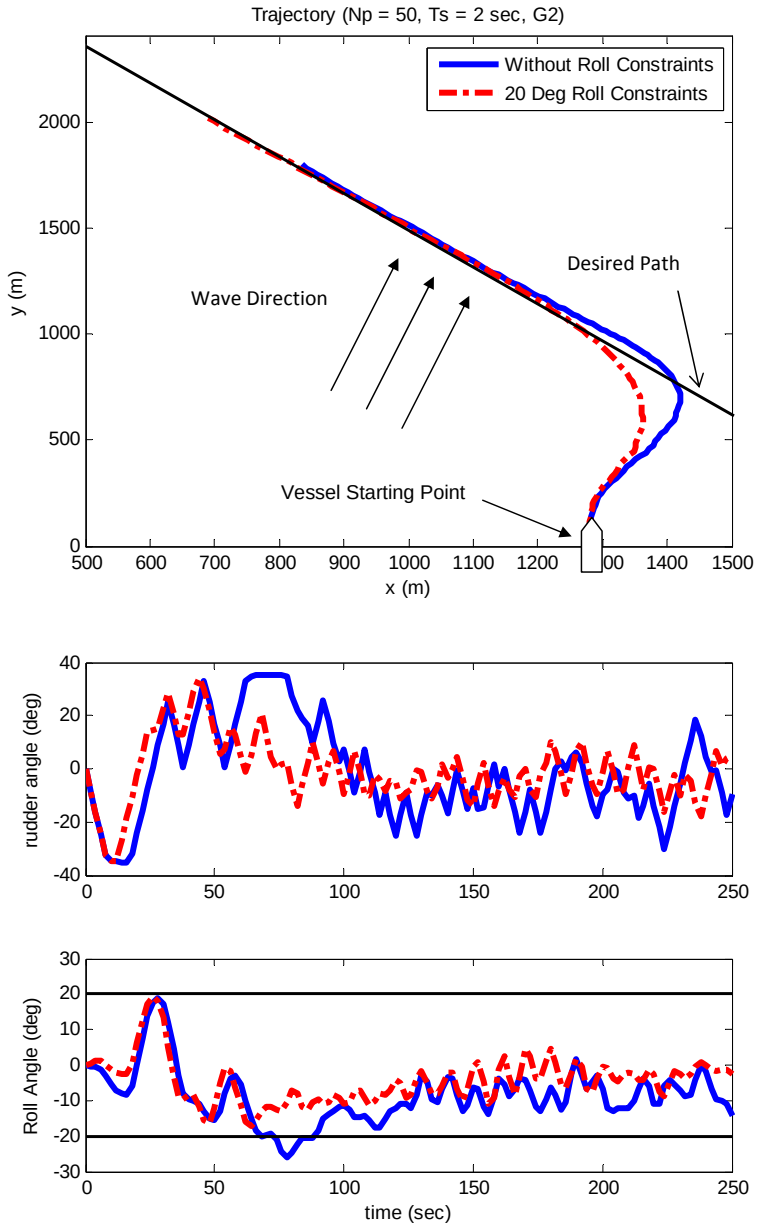

Figure 5.1: Simulation results of the ship response with one-input MPC path following controller in wave fields.

The evaluation results of the one-input MPC path following controller in wave fields without roll constraints and with 20 degree roll constraints are summarized in Figure 5.1. In this simulation, the controller gain G2 is employed (see Chapter 4

Table 4.1 for the information on G2). Figure 5.1 shows that the proposed MPC controller achieves path following while satisfying the roll constraints. Without roll constraints, the extreme roll angle reaches 26 degrees, while the maximum roll angle with the constraints is 19 degrees.

It is worthy to point out that the proposed MPC controller is addressing the roll motion induced by maneuvering, not that due to wave impacts, since the model embedded here can not predict the future wave loads on the vessel. As a result, the robustness of the standard MPC controller without incorporating the wave effects in the design is vulnerable. If we further tighten the roll constraints, the constraints might be violated and thus the feasibility issue emerges. The simulation result with 15 deg roll constraints is shown by Figure 5.2, where the roll constraint violations can be clearly seen. Furthermore, this feasibility issue can not be solved by simply introducing additional propeller control in the design. Therefore, research to address the feasibility of the path following MPC controller in wave fields has been motivated and the progress is summarized in the remainder of this chapter.

> **Remark 5.1.** *In the simulation of MPC with 15 deg roll constraints, which shown in Figure 5.2, the optimization problem of MPC has no solution to satisfy all the constraints in many time steps. In such circumstances, we temporarily remove the roll constraints to avoid the breakdown of the MPC controller so that the simulation can continue.*

5.2 Roll Constraint Satisfaction in wave fields

One of the primary merits of MPC is the input and state constraint enforcement. The input constraints often come from physical limitations of the actuators and it is always beneficial to enforce them in the control design. Even if these constraints are not enforced by the control design, they will be satisfied in the physical imple-

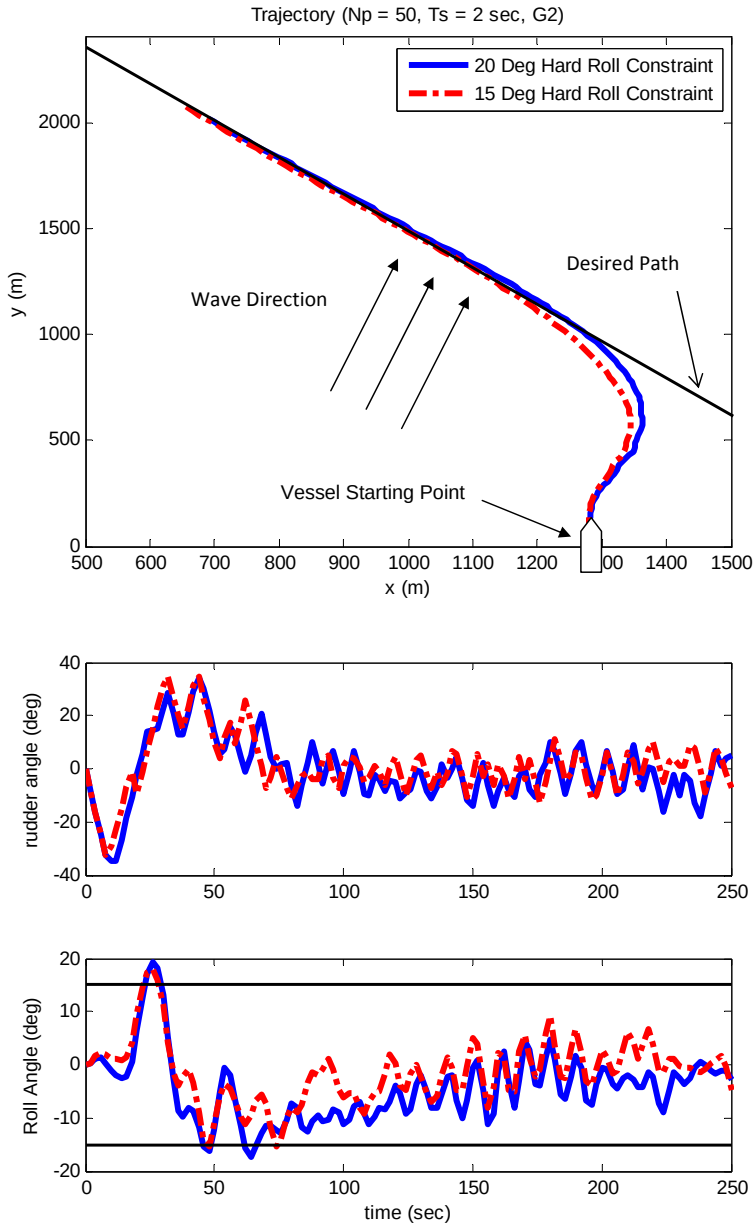

Figure 5.2: Simulation results of the ship response with one-input MPC path following controller with 15 deg hard roll constraints in wave fields.

mentation because of the physical constraints of the actuator. However, the state constraints are normally associated with the safety and device protection, and they can not be enforced directly in physical implementation (unless additional hardware is included). If these state constraints are enforced as hard constraints in the optimization, the feasibility problem may arise, especially if the system is subject to

large disturbances. As an example, the hard roll constraint enforcement results in infeasibility of the MPC scheme in wave fields, as shown in Figure 5.2.

Although many robust MPC algorithms have been proposed in the open literature ([44, 48, 58] and references therein), the industrial applications of such schemes are still very limited due to their conservatism and computational complexity [58]. The feasibility guarantee in industrial applications is often achieved by re-tuning parameters [75] and using soft constraint approaches [63, 77]. The latter approach is by far the most popular one to avoid feasibility issues in real applications. In all commercial algorithms, the hard state constraints are softened by introducing slack variables and augmenting the cost function [58]. In this study, these two approaches have been explored, namely gain re-tuning and constraint softening, to deal with the roll constraints in wave fields.

5.2.1 Gain Re-tuning for Roll Constraint Satisfaction

In Chapter 4, the guideline for tuning the controller gains, namely c_1 and c_2, has been presented to achieve good path following performance in calm water. In that case, the guidelines were: 1) Set $c_2 = 1$, and vary c_1 to achieve desired path following performance; 2) Fix c_1 as selected in 1), vary c_2 to tune for different rudder and roll responses.

Similar guidelines can be used here for gain re-tuning to reduce roll motion in wave fields, where the feasibility can not always be guaranteed. The selection of c_2, the penalty on rudder angle, to achieve the desired roll response is the focus here. On one hand, the roll constraints are removed from the optimization problem, thus the feasibility of resulting MPC scheme can be always guaranteed. On the other hand, the roll constraints are satisfied by the proper selecting of c_2. The input constraints are still enforced to improve the controller performance because they do not induce the feasibility issue. For this strategy, the roll constraint satisfaction is achieved

by trial-and-error. However, such an MPC scheme is still expected to have better performance than traditional control methodologies such as PID and LQR, because it considers the input limitations, which are normally neglected in the design process and imposed afterwards in the traditional control design.

For gain re-tuning strategy, $c_1 = 1.6$ is adopted, since it achieves good performance in calm water. By proper selection of the rudder gain c_2, the roll response of the vessel is shaped and kept within the desired limits.

The simulation of the re-tuned one-input MPC path following controller is summarized in Figure 5.3. The goal here is to achieve 15 and 10 deg roll constraint satisfaction, respectively. Figure 5.3 shows that although no roll constraints are enforced in the MPC scheme, the roll is reduced by the proper choice of gain c_2 as the penalty for rudder action. With the value of 5 and 20, respectively, the roll constraints of 10 and 15 deg can be satisfied, respectively. Figure 5.3 also shows that the roll reduction and roll constraint satisfaction are achieved at the expense of slightly lower path following convergence speed.

5.2.2 Constraint Softening and Tightening for Roll Constraint Satisfaction

Soft-constraint MPC has wide and successful applications because it is easy to implement and there is no feasibility issue. In soft-constraint MPC, violations of the state constraints are allowed, while an additional term is introduced in the cost function, which penalizes the constraint violations.

In reality, many constraints can be violated for a short period of time. It is the long period of sustained violation that causes detrimental problems to the system. The roll constraint in the marine surface vessel path following problem is of this type. Slight violation of roll constraints for short periods, caused by big waves, normally will not deteriorate ship performance greatly, nor endanger the ship safety. But large

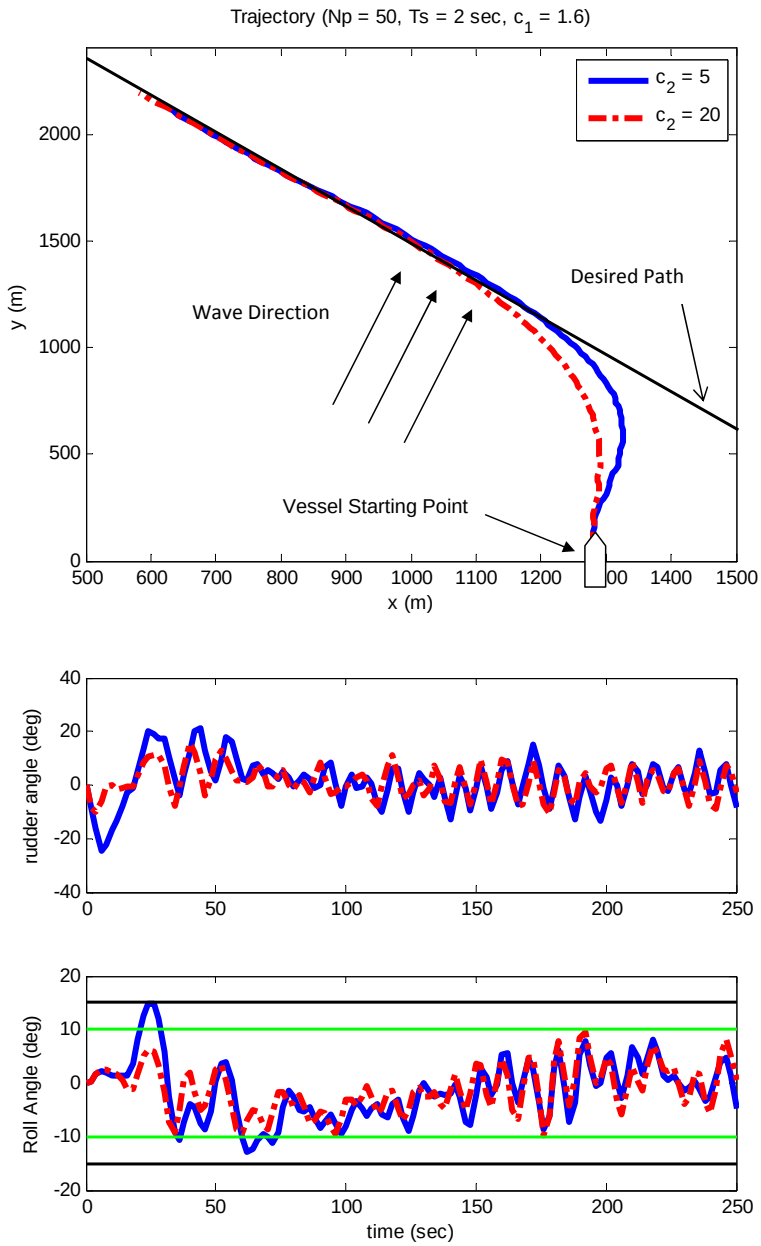

Figure 5.3: Simulation results of the ship response with re-tuned one-input MPC path following controller in wave fields.

roll motion lasting over time should be avoided [53].

The soft-constraint MPC approach transfers the original cost function (4.8) into the following form [77]:

$$J(U_k, \bar{x}_k) = \sum_{j=1}^{N_p} (\bar{x}_{k+j}^T Q \bar{x}_{k+j} + \delta_{k+j-1}^T R \delta_{k+j-1} + \epsilon^T P \epsilon), \tag{5.1}$$

where P is the constant weighting matrix to penalize the constraint violations. Correspondingly, the original state constraints (4.11) become:

$$-\bar{x}_{max} - \epsilon \leq \bar{x}_{k+j} \leq \bar{x}_{max} + \epsilon, \ j = 1, 2, \cdots, N_p. \tag{5.2}$$

The value of the weighting matrix P determines how "soft" (or "hard") the state constraints are. Setting P to zero removes the state constraints while increasing P results in increasingly "hard" constraints. As discussed in [63], tuning the matrix P can be counterintuitive because of the mismatch between the predicted states based on the nominal system and the actual system states. Therefore the matrix P normally does not serve as the performance parameter to shape the system response [77]. In this study, $P = 10$ gives satisfactory performance. If P is too small, say $P \leq 1$, the state violation will be too large because it effectively removes the state constraints, while P is too large, say $P \geq 100$, it introduces constraints that are too "hard" resulting in poor performance, in terms of extremely slow path following convergence. One advantage of the soft-constraint method is the computational efficiency, because just a single quadratic program needs to be solved. Another advantage is that it normally will not induce instability [63].

By the introduction of soft state constraints, the feasibility issue of the MPC optimization is eliminated [63]. However, the roll constraints might be violated. To achieve roll constraint satisfaction, the constraint tightening technique can be employed. Normally, the constraint tightening technique requires the knowledge of the disturbance bound [11, 45]. As an example, in a given sea state, the wave amplitude can be estimated, thus the bound on the roll angle induced by wave disturbances can be estimated. With the knowledge of the disturbance bound, the amount of the state constraints should be tightened can be determined. For example, to make the maximum roll angle less than 10 degree when the maximum roll angle induced by

waves is known to be 5 degrees, the roll constraints can be tightened to 5 degrees. Initially, the tightened soft constraint MPC scheme tries to make the roll angle within 5 degrees. With the wave disturbance entering the system, the roll angle will probably violate the 5 degree roll constraints, which is allowed by the soft constraints. However, the actual roll angle will be still within 10 degrees, the pre-set goal, if proper gains are adopted.

In order to successfully enforce roll constraints in wave fields, the estimation of the maximum wave induced roll angle is needed. The wave induced roll response may be the largest in the beam seas, which is the study focus in this case. The roll angle history in wave fields without rudder control ($\delta = 0$) is shown in Figure 5.4, where the ship forward speed is maintained at 10 m/s and the wave heading angle β is 90 deg. From Figure 5.4, we can see the maximum roll angle is about 5 deg, which is used to tighten the roll constraints.

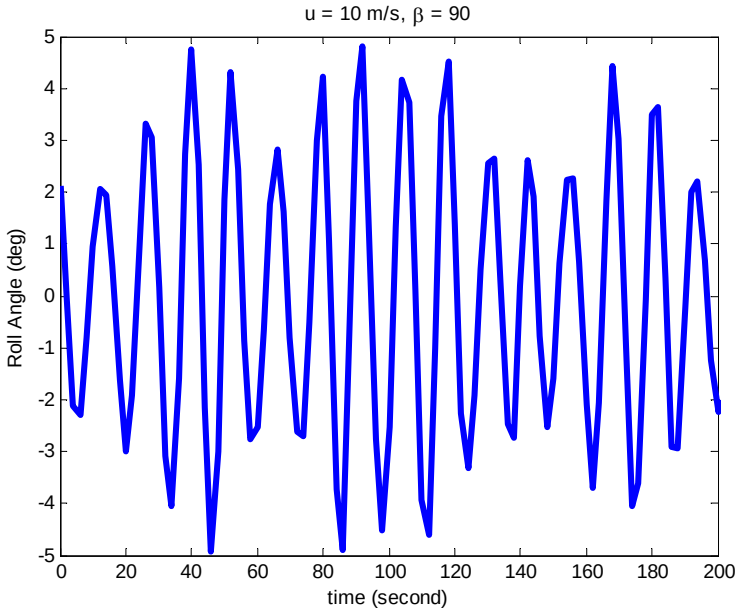

Figure 5.4: Roll angle in wave fields without control.

The simulations of the path following MPC scheme with constraint tightening and softening in wave fields are shown in Figure 5.5. The goals of the maximum roll angles are 15 and 10 degree, respectively, while the nominal roll constraints imposed in MPC

are 10 and 5 degree, respectively, since the estimated wave induced roll angle is about 5 degree. From Figure 5.5, we can see that the 15 and 10 degree roll constraints are actually satisfied although the nominal soft 10 and 5 degree roll constraints are, respectively, violated. The path following convergence speed for the 5 deg soft roll constraints is slightly slower than the 10 deg case.

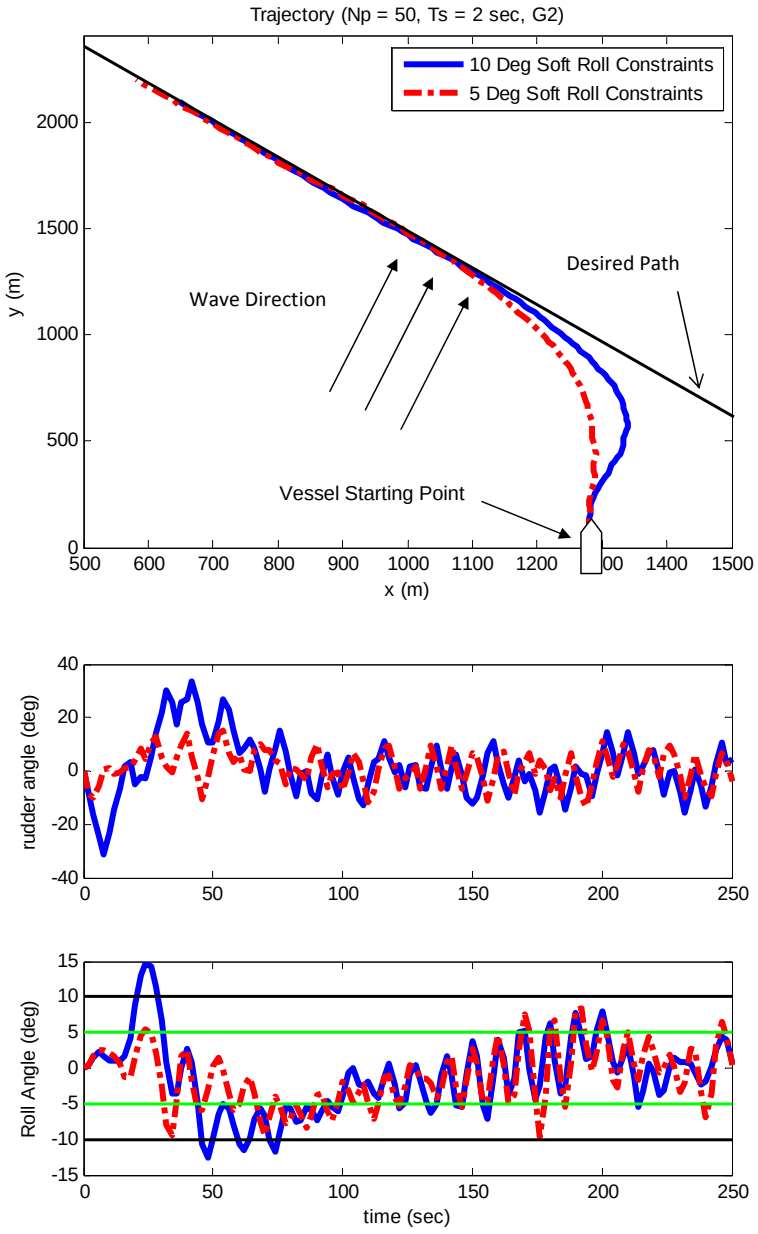

Figure 5.5: Simulation results of the ship response with one-input constraint tightened and softened MPC path following controller in wave fields.

5.3 Summary

By the methods of gain re-tuning and constraint softening and tightening, the path following with roll constraints was achieved in wave fields. For both cases, the roll limits were satisfied at the expense of slight slower path following convergence speed. While the gain re-tuning technique more or less relies on trial-and-error, the constraint softening and tightening strategy supplies a more systematic method to achieve the constraint satisfaction. However, more information about the system, especially the wave disturbance magnitude, is needed to perform successful constraint tightening. With the development of sophisticated robust MPC algorithm, this problem can be attacked from other angles.

CHAPTER 6

Disturbance Compensating MPC Scheme: Development and Applications

This chapter presents a disturbance compensating model predictive control (DC-MPC) algorithm to satisfy state constraints for linear systems with environmental disturbances, which has been motivated by state constraint violation and feasibility issues identified in the evaluation of standard MPC scheme for path following application in wave fields. The proposed algorithm focuses on modifying the standard MPC to satisfy state constraints while achieving good system performance with low additional computational effort. The capability of the novel DC-MPC algorithm is first analyzed theoretically. Then the proposed DC-MPC algorithm is applied to solve the ship heading control problem and its performance is compared with a time varying MPC controller. The simulation results show the constraint satisfaction capability and good performance of the DC-MPC controller. Furthermore, the limitations of proposed DC-MPC scheme are discussed and future research is suggested.

6.1 Motivation

One of the primary reasons for the success of MPC in industrial applications is its capability in enforcing of various types constraints on the process [63]. However, it may happen, because of model mismatches or disturbances, that the constrained optimization problem considered in MPC becomes infeasible at particular time steps. Namely, no solution can be found that satisfies all constraints. As an example, wave disturbances may cause infeasibility of the standard MPC path following controller, which is shown in Chapter 4.

To address the feasibility issues in MPC applications, numerous studies on robust MPC have been pursued and the efforts have led to extensive publications in the literature ([44, 48, 58] and references therein). The typical Robust MPC approaches [11,36,45,62,76] often consider bounded disturbances, assuming that they are confined to a compact set and allowed to take values within the set. However, this assumption may be conservative in the case where the disturbance dynamics are known or can be estimated. Aiming to reduce the controller conservativeness by explicit mitigation of disturbances, [27] estimates the disturbance based on current states and previous states and controls, and compensates for the disturbance to avoid constraint violation and conservativeness.

Inspired by the work of [27], this study proposes a novel disturbance compensating model predictive control (DC-MPC) algorithm to guarantee state constraint satisfaction and successive feasibility for linear systems with environmental disturbances while achieving good system performance with low additional computational effort compared with standard MPC, with an assumption that the disturbance is "measurable".

6.2 Problem Statement

Consider a discrete-time linear time-invariant system with disturbances:

$$x(k+1) = Ax(k) + Bu(k) + w(k), \quad w \in W, \tag{6.1}$$

where $x \in \mathbb{R}^{n_o}$ is the system state, $u \in \mathbb{R}^{n_i}$ is the control and $w \in \mathbb{R}^{n_o}$ is an unknown disturbance taking values in the set W.

The standard MPC considers optimization problem $\mathcal{P}(x(k))$ as follows:

$$\underset{u(\cdot|k)}{min} \sum_{j=1}^{N_p} [x(k+j|k)^T Q x(k+j|k) + u(k+j-1|k)^T R u(k+j-1|k)], \tag{6.2}$$

subject to

$$x(k+j+1|k) = Ax(k+j|k) + Bu(k+j|k); x(k|k) = x(k), j = 0, 1, \cdots, N_p - 1, \tag{6.3}$$

$$Cx(k+j+1|k) \leq D, \ j = 0, 1, \cdots, N_p - 1, \tag{6.4}$$

$$Su(k+j|k) \leq T, \ j = 0, 1, \cdots, N_p - 1, \tag{6.5}$$

where (6.3) is the nominal system dynamic equation used to predict the future states, (6.4) and (6.5) are general state and input constraints, respectively. Q and R are the corresponding weighting matrices and N_p is the predictive horizon. $x(k+j|k)$ and $u(k+j|k)$ are the state and control, respectively, j steps ahead of the current time k as a reference, $x(k)$ is the (measured) state at time k.

If the optimization problem $\mathcal{P}(x(k))$ is feasible, then the optimal solution is given by $\{u'^*(k|k), u'^*(k+1|k), \cdots, u'^*(k+N_p-1|k)\}$. Accordingly, the predicted optimal states are $\{x'^*(k+1|k), x'^*(k+2|k), \cdots, x'^*(k+N_p|k)\}$. For the standard MPC approach, the control action for the system (6.1) is chosen to be the first vector in

the optimal sequence, i.e.,

$$u(k) = u'^{*}(k|k). \tag{6.6}$$

With disturbances ($w \neq 0$), even if the optimization problem $\mathcal{P}(x(k))$ is feasible, the feasibility of $\mathcal{P}(x(k+1))$ can not be guaranteed if the control action for the system (6.1) is given by (6.6). More specifically, $Cx(k+1) \leq D$ can not be guaranteed.

One goal of this study is to ensure that $Cx(k+1) \leq D$ is always satisfied if $Cx(k) \leq D$ is satisfied. The other goal of this study is to make the system response with disturbances as close as possible to the system response without disturbances, since the performance without disturbances is always satisfactory if the MPC controller is properly implemented. Mathematically, we want to make $x(k+1) \rightarrow x^{*}(k+1|k)$.

6.3 Disturbance Compensating Model Predictive Control

If we can accurately estimate the future disturbances, even just in the current time step k, it is possible to improve the system performance by utilizing the additional disturbance information.

The disturbances at time step $k-1$, i.e., $w(k-1)$, can be estimated by the following equation if the state and control are measurable [27]:

$$\hat{w}(k-1) = x(k) - Ax(k-1) - Bu(k-1). \tag{6.7}$$

When the sampling time T_s is small and/or the disturbance changes slowly with time, we can make the following assumption:

Assumption 6.1. The disturbance at time step k, i.e. $w(k)$, can be estimated by:

$$w(k) = \hat{w}(k-1) + \varepsilon, \tag{6.8}$$

where $\varepsilon \in V$ and $V \subset W$.

Remark 6.1. *If the sampling rate is very fast compared with the disturbance changing rate, the disturbance variate ε will be very small and the bound on V will be much tighter than that for W. One important consideration in selecting the sampling rate of the MPC is the available computation recourses. Assumption 6.1 is valid for applications where computational resource is not an issue and fast sampling can be implemented.*

With Assumption 6.1, the following disturbance compensating MPC scheme is proposed:

- **Step 1:** At time step k, calculate the disturbance $\hat{w}(k-1)$ of the previous time step $k-1$ using the equation of (6.7), and measured values of $x(k)$, $x(k-1)$ and $u(k-1)$.

- **Step 2:** Calculate the disturbance compensation control Δu by solving the following low-dimension optimization problem $\mathcal{P}'_{\Delta}(\hat{w}(k-1))$:

$$\min_{\Delta u \in \mathbb{R}^{n_i}} ||CB\Delta u + C\hat{w}(k-1)||, \tag{6.9}$$

subject to

$$CB\Delta u \leq -C\hat{w}(k-1) - E, \tag{6.10}$$

$$S\Delta u \leq T, \tag{6.11}$$

where $E = max(C\varepsilon)$ with $\varepsilon \in V$. Suppose the corresponding optimal solution for $\mathcal{P}'_{\Delta}(\hat{w}(k-1))$ is Δu^*. Particularly, if $\hat{w}(k-1) = 0$, $\Delta u = 0$, which leads to the standard MPC.

- **Step 3:** Solve the optimization problem $\mathcal{P}'(x(k), \Delta u^*)$:

$$\min_{u(\cdot|k)} \sum_{j=1}^{N_p} [x(k+j|k)^T Q x(k+j|k) + u(k+j-1|k)^T R u(k+j-1|k)], \quad (6.12)$$

subject to

$$x(k+j+1|k) = Ax(k+j|k) + Bu(k+j|k); x(k|k) = x(k), j = 0, 1, \cdots, N_p - 1, \quad (6.13)$$

$$Cx(k+j+1|k) \leq D,\ j = 0, 1, \cdots, N_p - 1, \quad (6.14)$$

$$Su(k|k) \leq T - S\Delta u^*, \quad (6.15)$$

$$Su(k+j|k) \leq T,\ j = 1, \cdots, N_p - 1. \quad (6.16)$$

Suppose the solution of $\mathcal{P}'(x(k), \Delta u^*)$ is $\{u^*(k|k), u^*(k+1|k), \cdots, u^*(k+N_p-1|k)\}$ and the corresponding predicted states are $\{x^*(k+1|k), x^*(k+2|k), \cdots, x^*(k+N_p|k)\}$.

- **Step 4:** Implement the following control to the system (6.1):

$$u(k) = u^*(k|k) + \Delta u^*. \quad (6.17)$$

Proposition 6.1. *If the optimization problems $\mathcal{P}'_\Delta(w(k-1))$ and $\mathcal{P}'(x(k), \Delta u^*)$ are both feasible, the state constraint satisfaction, i.e., $Cx(k+1) \leq D$, can always be guaranteed if the control law (6.17) is applied to the linear system (6.1).*

Proof. If the optimization problems $\mathcal{P}'_\Delta(w(k-1))$ and $\mathcal{P}'(x(k), \Delta u^*)$ are feasible, we have the corresponding optimal solutions and the following constraints are satisfied:

$$CB\Delta u^* \leq -Cw(k-1) - E, \quad (6.18)$$

$$Cx^*(k+1|k) \leq D, \tag{6.19}$$

$$Su^*(k|k) \leq T - S\Delta u^*. \tag{6.20}$$

From (6.20), it follows that $S(u^*(k|k) + \Delta u^*) \leq T$, thus the input constraints $Su(k) \leq T$ are satisfied.

By the control (6.17) and Assumption 6.1, the state $x(k+1)$ is given by:

$$\begin{aligned} x(k+1) &= Ax(k) + Bu(k) + w(k) \\ &= Ax(k) + B(u^*(k|k) + \Delta u^*) + w(k) \\ &= x^*(k+1|k) + B\Delta u^* + \hat{w}(k-1) + \varepsilon. \end{aligned} \tag{6.21}$$

Notice that inequality (6.18) and (6.19) are already satisfied. By adding each side of them together, we have

$$CB\Delta u^* + Cx^*(k+1|k) \leq -C\hat{w}(k-1) - E + D, \tag{6.22}$$

which leads to

$$Cx^*(k+1|k) + CB\Delta u^* + C\hat{w}(k-1) + E \leq D. \tag{6.23}$$

Since $E = max(C\varepsilon)$, $C\varepsilon \leq E$, then

$$\begin{aligned} Cx(k+1) &= Cx^*(k+1|k) + CB\Delta u^* + C\hat{w}(k-1) + C\varepsilon \\ &\leq Cx^*(k+1|k) + CB\Delta u^* + C\hat{w}(k-1) + E \\ &\leq D. \end{aligned} \tag{6.24}$$

Therefore, the state constraints $Cx(k+1) \leq D$ are satisfied. □

Remark 6.2. *The computational effort needed for the DC-MPC scheme is*

similar to the standard MPC scheme. In addition to the quadratic programming (QP) problem (which has the same structure as for the standard MPC) solved in Step 3, the DC-MPC scheme also solves an m-dimensional optimization problem in Step 2, where m is the dimension of the control input. Compared with the QP problem in Step 3, which has a dimension of $N_p \times n_i$, such a low-dimension optimization problem does not involve much additional computational cost. As a result, the proposed DC-MPC scheme is much more computational efficient than the robust MPC algorithm discussed in [44, 48, 58].

Remark 6.3. *The minimization of the cost function in $\mathcal{P}'_\Delta(\hat{w}(k-1))$ is redundant for satisfying the state constraints. However, solving $\mathcal{P}'_\Delta(\hat{w}(k-1))$ is meaningful in terms of tracking the system response achieved without disturbances, which is always desired in real applications. Specifically, if $||CB\Delta u + C\hat{w}(k-1)|| = 0$ is satisfied, $x(k+1) = x^*(k+1|k)+\varepsilon$, which means the states of the system with disturbances is made to be almost the same as the desired ones without disturbances. By solving $\mathcal{P}'_\Delta(\hat{w}(k-1))$, the performance of system under disturbances is reinforced to be the desired one achieved without disturbance.*

Remark 6.4. *The feasibility of $\mathcal{P}'_\Delta(\hat{w}(k-1))$ is largely depend on the structure of matrix CB, which indicates the control authority on the constrained states, and the magnitude of the disturbance. If the disturbance is too large or CB is ill-conditioned, the required compensation might exceed the input limits, which results in infeasibility of $\mathcal{P}'_\Delta(\hat{w}(k-1))$. Only if the required compensation satisfies the input constraints, can the feasibility of $\mathcal{P}'_\Delta(\hat{w}(k-1))$ be guaranteed.*

Remark 6.5. *The assumption of the feasibility of $\mathcal{P}'(x(k), \Delta u^*)$, i.e., the initial constraint satisfaction indicates feasibility, might not hold for some systems. Particularly, if one of the constrained states is the direct integral of other state, the feasibility can not be guaranteed even the state constraints are satisfied ini-*

tially. For example, if there are position constraints for a dynamical positioning system, the initial position of the ship in the feasible region can not guarantee the feasibility of $\mathcal{P}'(x(k), \Delta u^*)$. Specifically, when the ship is on the boundary of the feasible region and the ship speed is large and pointing outside the feasible region, $\mathcal{P}'(x(k), \Delta u^*)$ might be infeasible.

Another approach, which might be more straightforward than the DC-MPC scheme, would be to utilize the disturbance information directly in the optimization problem in Step 3, instead of solving an additional optimization problem. Specifically, the following optimization problem $\mathcal{P}''(x(k), \hat{w}(k-1))$ is proposed by:

$$\min_{u(\cdot|k)} \sum_{j=1}^{N_p} [x(k+j|k)^T Q x(k+j|k) + u(k+j-1|k)^T R u(k+j-1|k)], \tag{6.25}$$

subject to

$$x(k+1|k) = Ax(k|k) + Bu(k|k) + w(k), x(k|k) = x(k), \tag{6.26}$$

$$x(k+j+1|k) = Ax(k+j|k) + Bu(k+j|k),\ j = 1, \cdots, N-1, \tag{6.27}$$

$$Cx(k+j+1|k) \leq D,\ j = 0, 1, \cdots, N-1, \tag{6.28}$$

$$Su(k+j|k) \leq T,\ j = 0, 1, \cdots, N-1. \tag{6.29}$$

The first element of the optimal sequence of $\mathcal{P}''(x(k), \hat{w}(k-1))$ is implemented in the system (6.1). This MPC scheme adopts a time-varying linear model to predict the future states, thus it will be refereed as time-varying MPC (TV-MPC) in the sequel.

6.4 DC-MPC Application in Ship Heading Control

6.4.1 Introduction of Ship Heading Control

Ship heading control, or the so-called course-keeping, is the primary task of autopilots. The control objective of ship heading control is to make:

$$\psi \rightarrow \psi_d, \tag{6.30}$$

where ψ_d is the desired ship heading angle and normally is assumed to be constant [23].

For the ship heading control design, the Nomoto Model is by far the most commonly employed one in the literature [24]. The Nomoto Model considers one DoF of ship dynamics, namely the yaw r, and one control input, namely the rudder angle δ. For container ship S175, the corresponding one DoF linear dynamics in continuous-time are given by:

$$\dot{x} = A_c x + B_c \delta, \tag{6.31}$$

where $x = [r, \psi]^T$ and

$$A_c = \begin{bmatrix} -0.1068 & 0 \\ 1 & 0 \end{bmatrix}, \quad B_c = \begin{bmatrix} 0.0026 \\ 0 \end{bmatrix}. \tag{6.32}$$

Normally, the rudder saturation has to be enforced due to the physical limit. Furthermore, to avoid abrupt turns, which may induce unexpected ship motion, a yaw rate limit is considered in the control design. Therefore, the corresponding matrices

C, D, S and T are given by:

$$C = \begin{bmatrix} 1 & 0 \\ -1 & 0 \end{bmatrix}, \quad D = \begin{bmatrix} 0.006 \\ 0.006 \end{bmatrix}, \quad S = \begin{bmatrix} 1 \\ -1 \end{bmatrix}, \quad T = \begin{bmatrix} 35\pi/180 \\ 35\pi/180 \end{bmatrix}. \quad (6.33)$$

The proposed DC-MPC scheme is first implemented in the linear system with sinusoidal and constant disturbances to illustrate the constraint satisfaction capability compared with the standard and TV-MPC scheme. Then the DC-MPC scheme is applied to the original nonlinear system in wave fields for the performance validation.

6.4.2 Simulation Results: Linear System with Constant and Sinusoidal Disturbances

Two kinds of disturbances are considered in this case. One is sinusoidal and the other is constant, which mimic the first-order and second-order wave disturbances. In this particular study, the rudder constraints are $|\delta| \leq 35$ deg and the yaw rate constraints are $|r| \leq 0.006$ rad/sec (0.34 deg/sec).

The standard MPC scheme is first studied by the simulations, which are summarized in Figure 6.1. Figure 6.1 shows that although the standard MPC scheme achieves good performance in calm water in terms of constraint satisfaction and desired heading tracking, the performance of the standard MPC with disturbances is not satisfactory. First, the yaw constraint violations are found with both constant and sinusoidal disturbances. Second, a steady state error exists in the constant disturbance case, while heading angle oscillations are observed with the sinusoidal disturbance.

The TV-MPC and DC-MPC are also implemented with different prediction horizons to study their performance with constant and sinusoidal disturbances. The simulations of the TV-MPC are summarized in Figure 6.2 and Figure 6.3, while those of the DC-MPC shown in Figure 6.4 and Figure 6.5, for constant and sinusoidal dis-

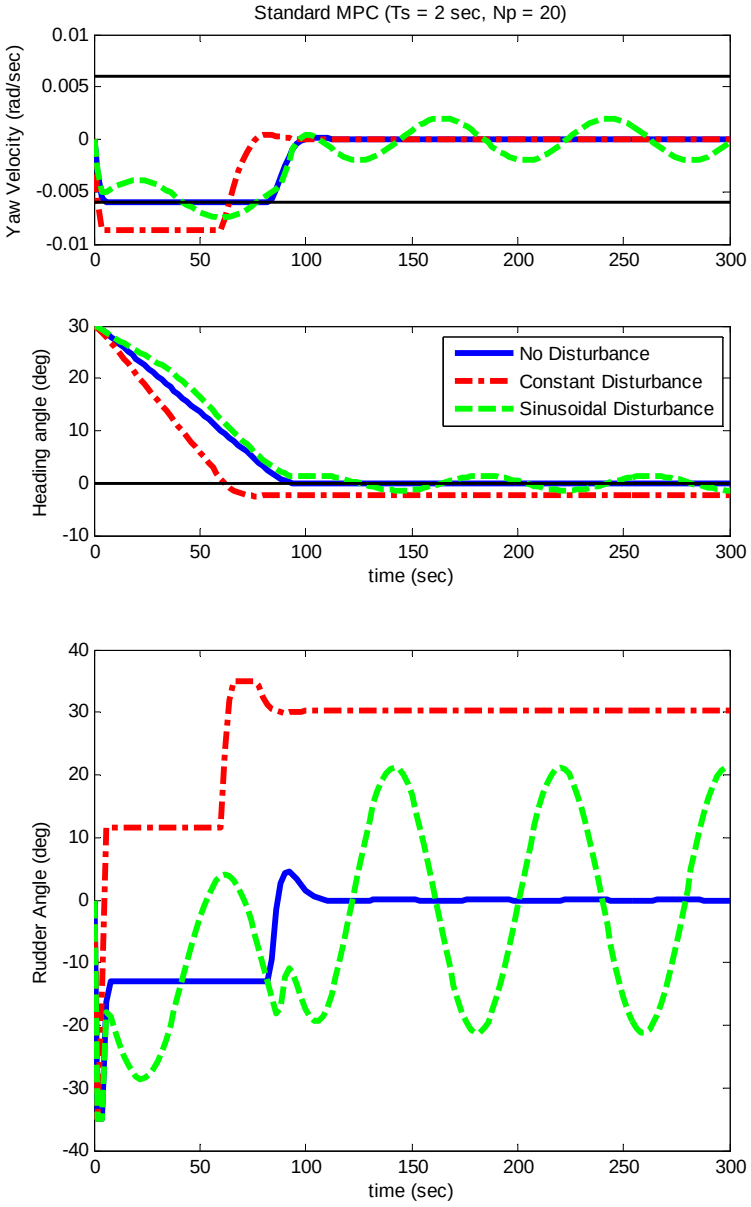

Figure 6.1: Standard MPC ship heading controller simulations with and without disturbances.

turbances, respectively. In these simulations, $Q = \{1000,300\}$, $R = 1$ and E is 0 for constant disturbance and 0.0003 for sinusoidal disturbance.

As shown in Figure 6.2 and Figure 6.3, although the yaw constraints are successfully enforced by the TV-MPC for all prediction horizons, the heading tracking performance is not satisfactory, particular with those having short prediction horizons. The longer prediction horizon results in better performance for both constant

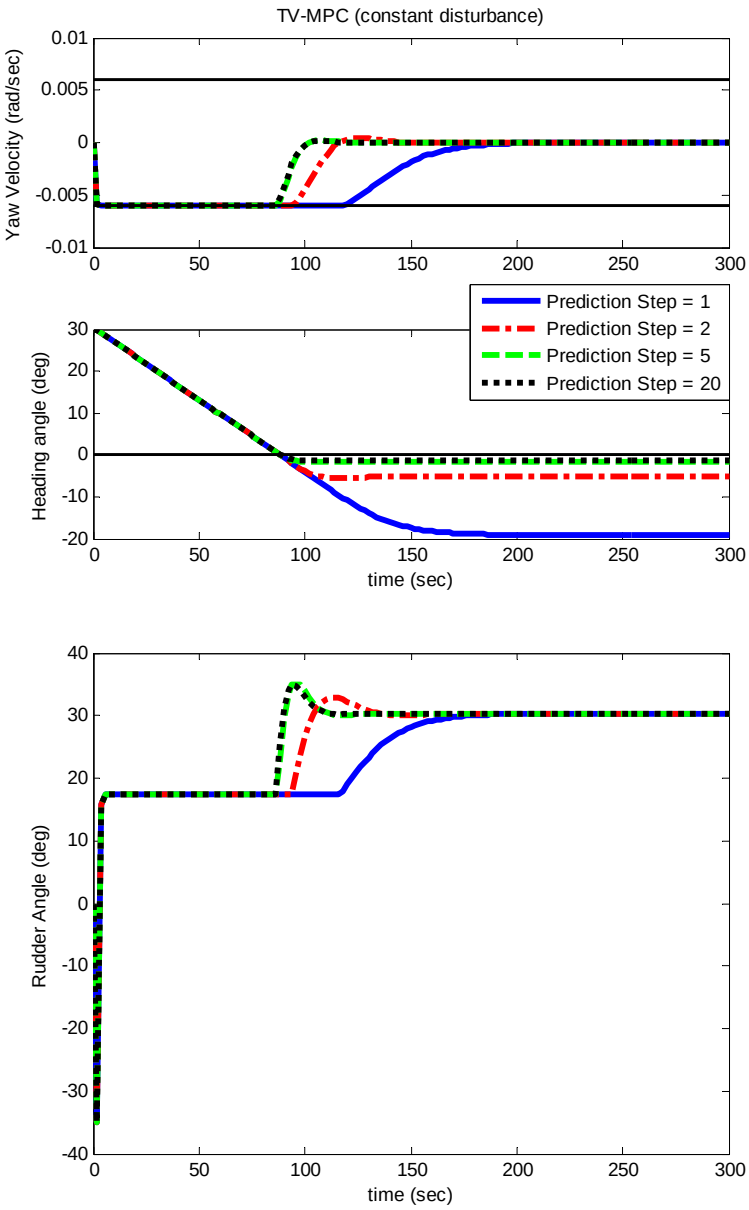

Figure 6.2: Simulations of the TV-MPC ship heading controller with constant disturbances for different prediction horizons.

and sinusoidal disturbances. However, the steady state error can not be completely eliminated.

Figure 6.4 and Figure 6.5 show that the DC-MPC has the capability to satisfy the state (yaw) constraints for all prediction horizons with both constant and sinusoidal disturbances. Furthermore, the DC-MPC scheme can eliminate the steady state error with the constant disturbance for all prediction horizons. It also largely reduces

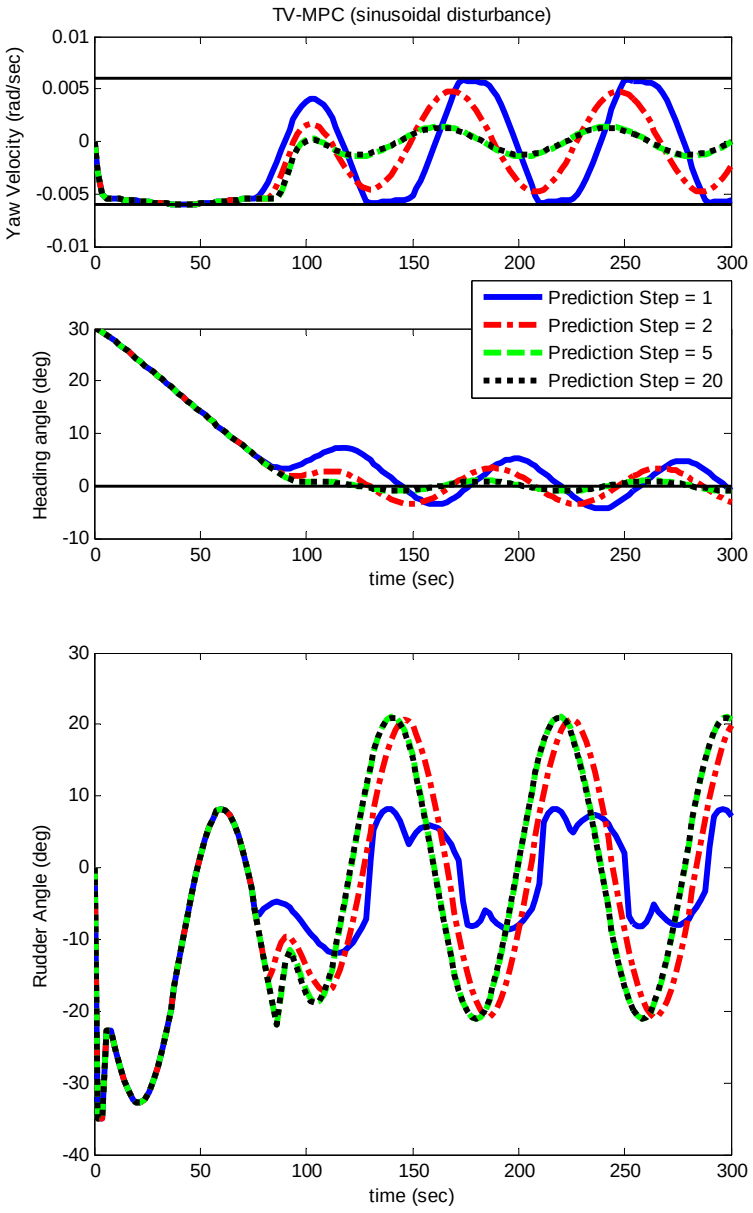

Figure 6.3: Simulations of the TV-MPC ship heading controller with sinusoidal disturbances for different prediction horizons.

the heading angle oscillations with the sinusoidal disturbance compared with the standard MPC and TV-MPC cases. With longer prediction horizons, the DC-MPC scheme achieves better performance in terms of faster heading angle tracking and less heading angle oscillations.

The comparisons of the results of both TV-MPC and DC-MPC schemes with a sinusoidal disturbance are summarized in Figure 6.6. Figure 6.6 shows that the

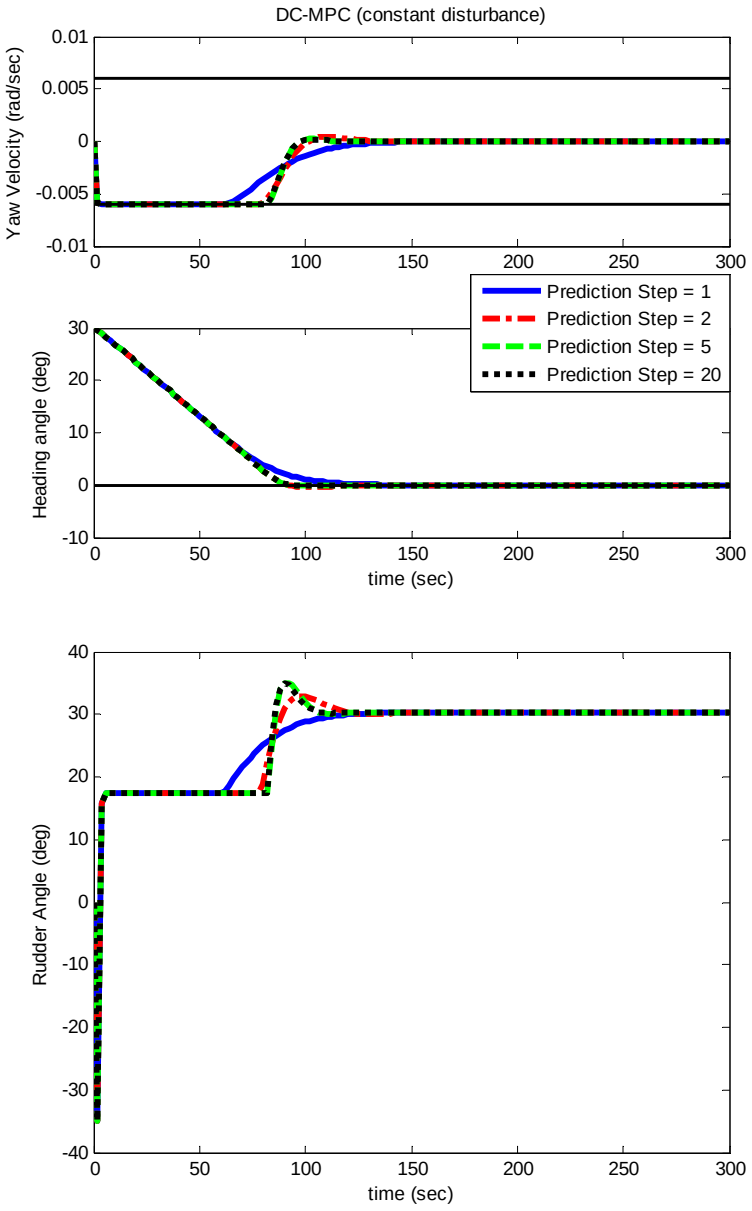

Figure 6.4: Simulations of the DC-MPC ship heading controller with constant disturbances for different prediction horizons.

DC-MPC has less heading angle oscillations than the TV-MPC. The amplitude of heading angle oscillations with the DC-MPC is around 0.2 deg, while that with the TV-MPC is around 0.9 deg. Furthermore, the capability of the DC-MPC scheme to track the system response without disturbances is illustrated (also see Figure 6.4 and Figure 6.5), which is discussed in Remark 6.3.

For the ship control problem with yaw rate limit, the feasibility of $\mathcal{P}'_\Delta(\hat{w}(k -$

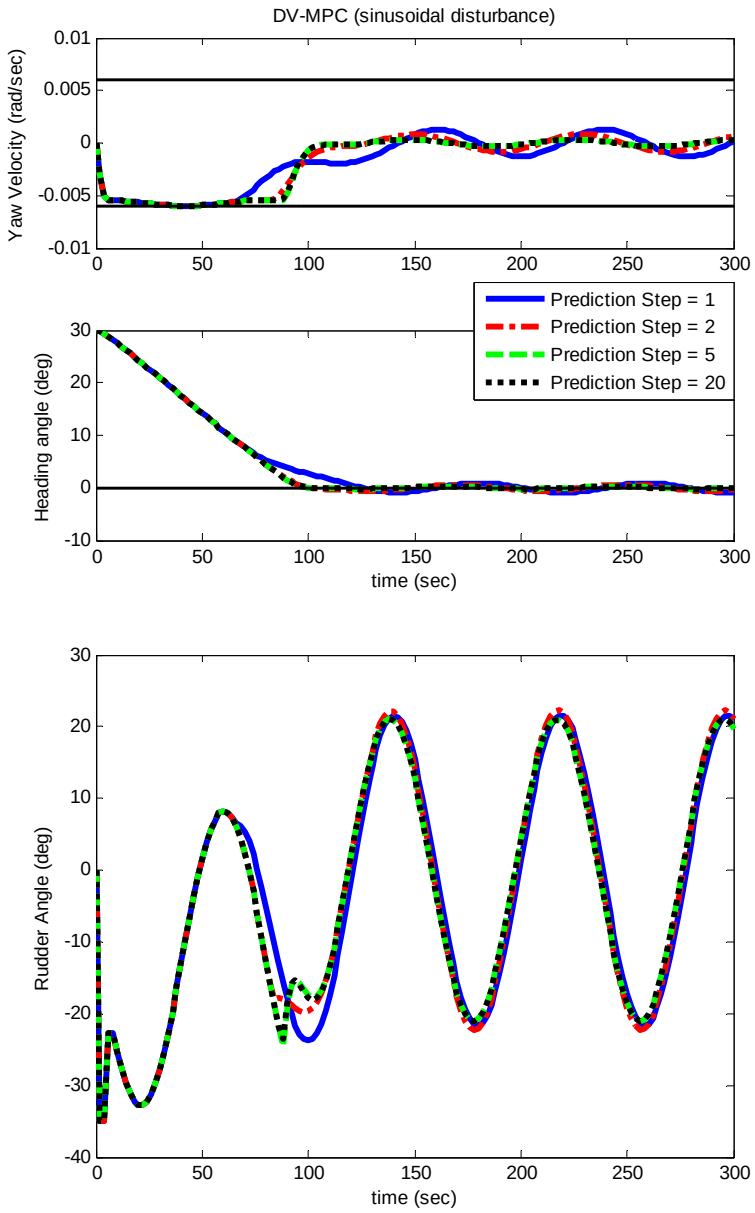

Figure 6.5: Simulations of the DC-MPC ship heading controller with sinusoidal disturbances for different prediction horizons.

1)) is guaranteed if the disturbance is not too large because the rudder input has enough authority on yaw rate and thus CB is well conditioned. The feasibility of $\mathcal{P}'(x(k), \Delta u^*)$ can be guaranteed if the yaw rate constraints are satisfied initially, since the yaw rate is controlled directly by the input and is not the direct integral of other states.

To quantitatively evaluate the controller performance, the comparison of perfor-

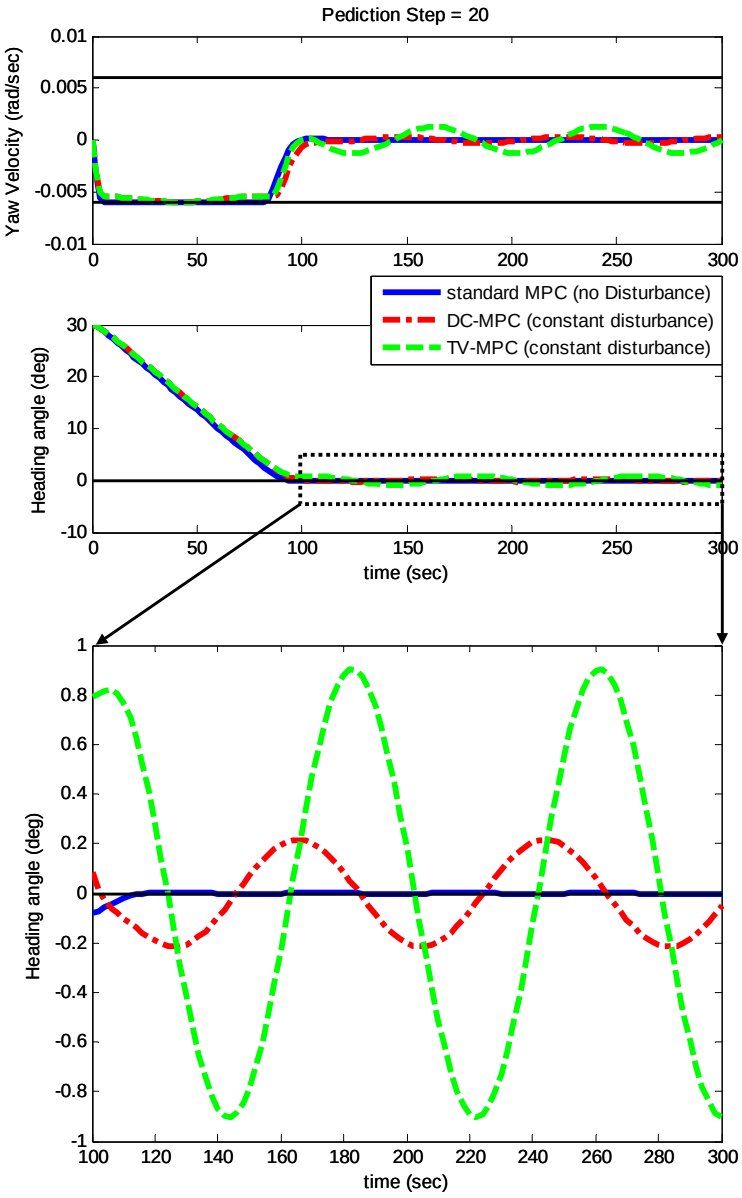

Figure 6.6: Comparisons of the standard MPC, TV-MPC and DC-MPC ship heading controller.

mance indices for the DC-MPC and TV-MPC under disturbances, both constant and sinusoidal, is summarized in Table 6.1. It is shown from Table 6.1 that the DC-MPC scheme has better performance in terms of less steady state and cumulative errors with constant and sinusoidal disturbances, respectively.

The different approaches adopted by the TV-MPC and DC-MPC lead to the performance differences. The TV-MPC scheme minimizes the cost function based on

Table 6.1: Performance index comparisons of DC-MPC and TV-MPC.

	N_p	DC-MPC	TV-MPC
Steady State Error [deg] (Constant Disturbance)	1	0	19.07
	2	0	5.16
	5	0	1.51
	20	0	1.38
$\int_0^{t_{final}} \lvert\psi\rvert dt$ [deg·sec$\times 10^3$] (Sinusoidal Disturbance)	1	1.6502	2.1637
	2	1.5504	1.9154
	5	1.4997	1.6035
	20	1.4987	1.5916

the predictions of the nominal system (considering only the disturbance in one time step), thus the mismatch of the nominal system and real system results in the steady state error (constant disturbance) or state oscillations (sinusoidal disturbance). In contrast, the DC-MPC scheme is trying to track the desired no-disturbance performance (minimize the distance between the actual states and the predicted stated without disturbance), which results in steady state error elimination and state oscillations reduction. The DC-MPC algorithm has the potential to be applied to other motion control problems with environmental disturbances, such as flight, automobile and robotics controls, since in these cases the system response without disturbances is always designed to be desirable.

6.4.3 Simulation Results: Nonlinear System with Wave Disturbances

To further validate its performance, the DC-MPC scheme is evaluated in the numerical test-bed developed in Chapter 2. The simulation results, compared with the standard MPC without yaw constraints, are summarized in Figure 6.7. In the simulations, sea state 5 is used and the initial wave heading β is 0 deg and the final wave heading β is 30 deg. Sampling time $T_s = 1$ sec and the prediction horizon

$N_p = 40$. Figure 6.7 shows that the DC-MPC scheme successfully enforces the yaw rate constraints. The initial course changing speed for the DC-MPC is slower than the standard MPC without yaw constraints. However, the final convergence speeds for both cases are similar.

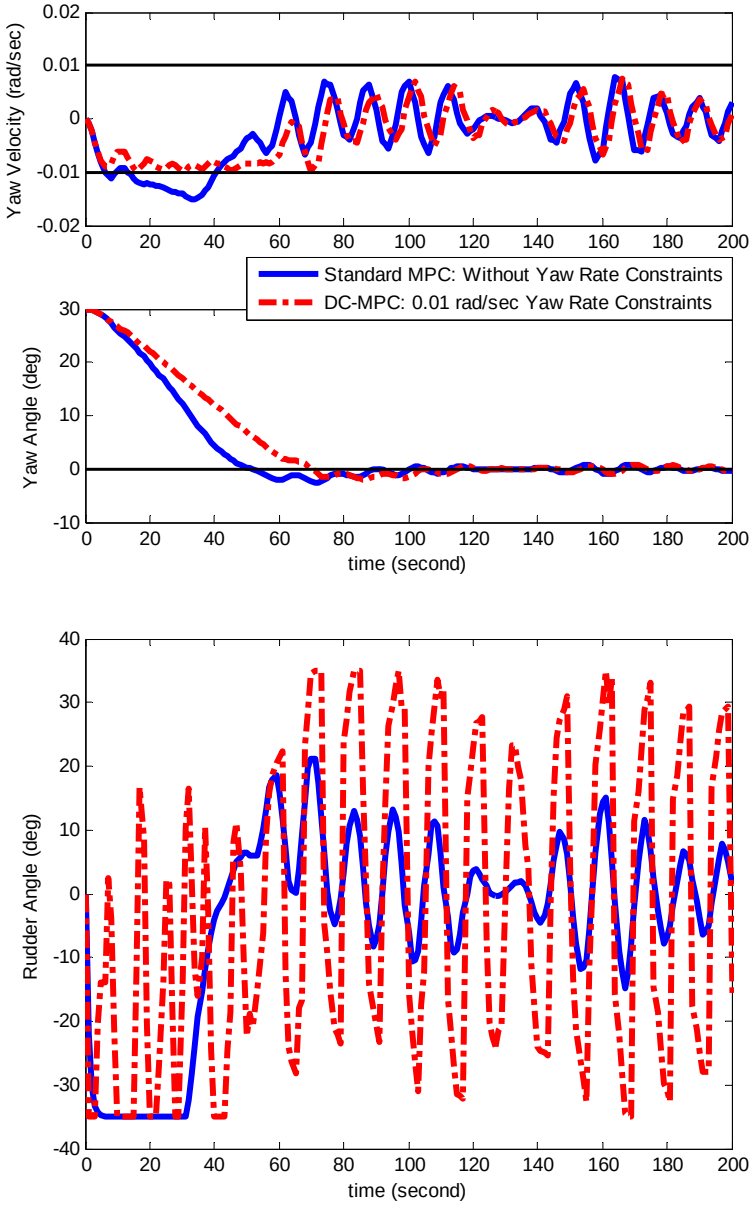

Figure 6.7: Simulations of DC-MPC scheme applied to the nonlinear system in wave fields.

Figure 6.7 shows that the DC-MPC is very useful to satisfy the yaw constraints in the course-changing stage. However, large rudder actions, for compensating the

wave disturbance, are observed in course-keeping stage. In such circumstances, the remedial strategies, such as introducing penalties in rudder angle and rudder angle changing, should be implemented to avoid large rudder actions. These mitigating strategies are under investigation now.

The wave disturbance in the simulation, predicted by linear seakeeping theory (first-order) [5] and empirical equation (second-order) [12] (described in details in Section 2.2 and [39]), is shown in Figure 6.8.

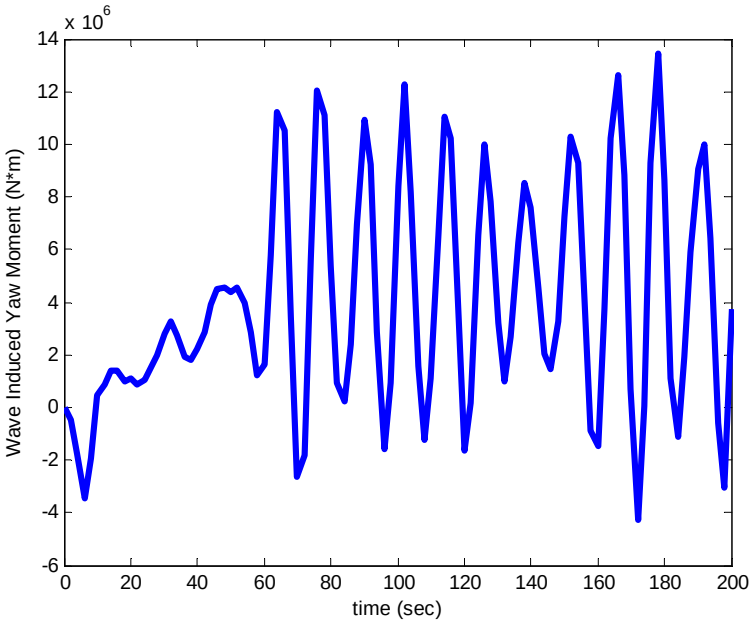

Figure 6.8: Actual wave induced yaw moment.

6.5 Limitation of Disturbance Compensating MPC

The effectiveness of the DC-MPC scheme implementation largely depends on whether the assumptions, which are made to facilitate the rigorous theoretical analysis, can be satisfied or not. One assumption is the disturbance estimation (Assumption 6.1), which needs accurate measurements of system states and control signals. The other assumption is the feasibility of $\mathcal{P}'_\Delta(\hat{w}(k-1))$. As discussed in Remark 6.4, the feasibility of $\mathcal{P}'_\Delta(\hat{w}(k-1))$ can be guaranteed if the control inputs have enough

authority on the constrained states, which is the case of ship heading control studied in Section 6.4. However, if the constrained states are weakly influenced by the control inputs, the feasibility of $\mathcal{P}'_\Delta(w(k-1))$ is vulnerable. In such cases, the matrix CB is normally ill-conditioned.

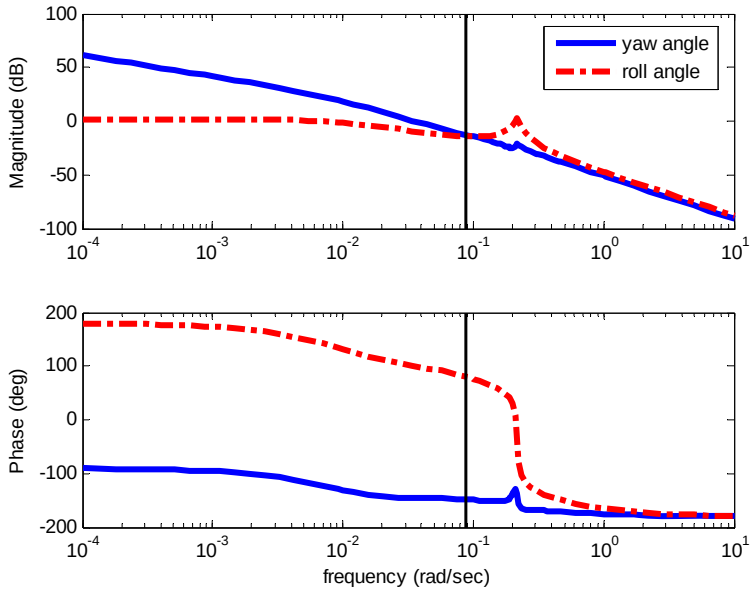

Figure 6.9: Bode plot from rudder angle to yaw angle and roll angle.

For the path following problem with roll constraints for marine surface vessels, the roll angle is a constrained state. However, compared with the significant effect of the rudder on yaw motion, the roll motion is not as easily influenced by the rudder input. A Bode plot from rudder angle to yaw angle and roll angle, as shown in Figure 6.9, shows that the low authority of rudder on roll motion in the low frequency range (the vertical line in Figure 6.9 indicates the highest frequency the rudder action can achieve for S175, namely 5 deg/sec or 0.087 rad/sec). Therefore, the application of the DC-MPC scheme in path following control for the roll constraint satisfaction in wave fields will not be successful. In fact, the disturbance effects on roll motion in wave fields can not be compensated by the limited authority rudder actions.

To address this issue, namely the lack of control authority in constrained states, one possible approach is to predict the disturbance for longer future time. With

enough knowledge of future disturbance, the disturbance can be incorporated into prediction in predicting of the future states to avoid feasibility issue. However, the accurate prediction of future disturbance is normally difficult and deserves future research.

6.6 Summary

The DC-MPC scheme was motivated and developed. An simple disturbance estimation method was first introduced and discussed. The theoretical analysis shows that DC-MPC can satisfy state constraints and achieve good performance if certain assumptions hold. The DC-MPC scheme was applied to the ship heading control with a linear system model and compared with the standard and time-varying MPC. The simulations show that the DC-MPC can mitigate the drawbacks of the standard MPC by satisfying the state constraints, eliminating the state error and reducing the state oscillations. The simulation results also showed the better performance of the DC-MPC over the TV-MPC scheme. Furthermore, the performance of the DC-MPC scheme was validated by simulations of original nonlinear system with wave disturbances. Finally, the limitation of DC-MPC scheme was discussed.

CHAPTER 7

Conclusions and Future Work

This dissertation has addressed the path following of marine surface vessels in wave fields. The control design model, together with the numerical and experimental test-bed for controller evaluation, has been introduced in Chapter 2. The design, robustness analysis and evaluation (both numerical and experimental) of the novel feedback dominance back-stepping for path following without roll constraints have been presented in Chapter 3. The numerical evaluation and modification of the FDBS controller in wave fields have been also included in Chapter 3. The model predictive control approach for path following with roll constraints has been explored in Chapter 4. Both one-input (rudder) and two-input (rudder and propeller) MPC schemes have been developed and analyzed by simulations. Chapter 5 has evaluated the standard MPC path following controller in wave fields, followed by introduction of mitigating strategies to satisfy roll constraints and guarantee feasibility. The theoretical development and application of disturbance compensating MPC scheme have been finally reported in Chapter 6.

7.1 Conclusions

The main work and results are summarized as follows:

- *Developed a numerical test-bed for ship motion controller evaluation in wave fields* - The numerical test-bed introduced in Chapter 2 combines the ship dynamics and both first- and second-order wave effects on vessels. This numerical test-bed, established in MATLAB, is generic and can be widely used in many other ship motion control applications, such as course keeping, roll stabilization and dynamical positioning.

- *Designed a novel robust feedback dominance back-stepping path following controller for marine surface vessels* - The resulting controller, proposed in Chapter 3, is almost linear, with very benign nonlinearities facilitating analysis and evaluation. The performance of the nonlinear controller, in terms of path following, has been analyzed for robustness in the presence of model uncertainties. The simulation results have verified and illustrated the analytic development and the effectiveness of the resulting control against rudder saturation and rate limits, delays in the control execution, as well as measurement noise. Furthermore, the control design has been validated by experimental results conducted in a towing tank using a model ship.

- *Evaluated and modified the novel robust path following controller in wave fields* - Several issues, such as steady state errors and rudder oscillations, have been identified in the evaluation by the numerical test-bed, thereby motivating controller modification and gain re-tuning. Mitigating strategies, i.e., gain re-tuning and gain scheduling, for improving the controller performance has been proposed and numerically evaluated in Chapter 3. The simulation results showed that the performance of the modified controller can be substantially improved in wave fields in terms of steady state error elimination and rudder oscillation reduction.

- *Proposed a model predictive control approach for path following with roll con-*

straints of marine surface vessels - The focus of Chapter 4 was on satisfying all the input (rudder) and state (roll) constraints while achieving satisfactory path following performance. The path following performance of the proposed MPC, both one-input (rudder) and two-input (rudder and propeller), and its sensitivity to the major controller parameters, such as the sampling time, predictive horizon and weighting matrices in the cost-function, have been analyzed by numerical simulations. This study is the first reported MPC application in path following for marine surface vessels.

- *Evaluated and improved MPC path following controller in wave fields* - Roll constraint violation and feasibility issues have been found in the numerical evaluation summarized in Chapter 5, thus motivating the research effort to seek mitigating strategies for state constraint satisfaction and feasibility guarantee. By the methods of gain re-tuning and constraint softening and tightening, the path following with roll constraints has been achieved in wave fields. For both cases, the feasibility of the MPC scheme was guaranteed and the roll constraints were satisfied at the expense of slightly slower path following convergence speed.

- *Developed a disturbance compensating MPC scheme for state constraint satisfaction with disturbances* - Motivated to overcome the constraint violation and feasibility issues of the MPC controller for system with disturbances, a novel DC-MPC algorithm has been proposed in Chapter 6 to guarantee the state constraint satisfaction in the presence of environmental disturbances. The effectiveness of the proposed algorithm was first analyzed theoretically. The state constraint satisfactory of the DC-MPC scheme was validated by numerical simulations, i.e., the applications in ship heading control. The DC-MPC scheme has the potential to be applied to other motion control problems with environmental disturbances, such as flight, automobile and robotics controls.

7.2 Future Work

Although substantial progress has been made on the ship motion control, enormous research opportunities as well as challenges still exist in each frontier of this rapidly evolving field. The work presented in this dissertation can be usefully extended in a number of different aspects.

- *Integrating path following with wave measurement and prediction and optimal path planning*

  This dissertation discussed path following for marine surface vessels when a predetermined path is given. However, the problems of path following and path planning might be coupled in wave fields. Therefore, path following for marine surface vessels should be intergraded with wave measurement and prediction and optimal path planning to improve the vessel performance in wave fields, in terms of minimizing the time for the vessel to reach a target without violating vessel motion constraints.

- *Experimental Validation of the MPC Path Following Controller*

  Although the MPC path following has satisfactory performance in the numerical simulations, further validation on established experimental platform is needed to study real-time implementation issues. Only with the successful experimental validation, could the feasibility of real commercial or military applications of MPC path following controller be claimed.

- *Seakeeping Criteria Development*

  Only using the maximum roll angle as the performance constraint might not always be thorough enough, because roll velocity and acceleration could also induce unpleasant riding experience or cargo damage. However, such guidelines on acceptable level of roll velocity and acceleration are still lacking, although

there are some seakeeping criteria based on statistical measurement, which normally can not be employed in control design.

- *Combining Path Following and Roll Stabilization*

  As discussed in Chapter 6, the rudder action has limited authority in roll motion, which might result in poor performance in wave fields, especially when wave fields is very rough. Therefore exploring the use of other control actuators such as active stabilizing fins and fluid tank to reduce the roll motion will be a rational next step. The coordination of the path following and roll stabilization aiming at improving the overall ship performance also represents an interesting direction that advanced control technology can make substantial impact.

- *Robust MPC Development and Application in Ship Motion Control*

  In Chapter 5, the path following with roll constraints has been achieved in wave fields by the methods of gain re-tuning and constraint softening and tightening. However, the gain re-tuning technique more or less relies on trial-and-error and the constraint softening and tightening strategy needs a good estimation of the wave disturbance. Therefore, robust MPC algorithms, which can attack this problem in a more systematic and sophisticated way, are much needed.

- *Extension from 2D to 3D Path following*

  Finally, it is possible to extend the 2D path following for marine surface vessels to the 3D path following for underwater vehicles, which has attracted a lot of research interest as exploring the ocean resource becomes more and more appealing.

BIBLIOGRAPHY

BIBLIOGRAPHY

[1] M.A. Abkowitz. Lectures on ship hydrodynamics - steering and maneuverability. *Technical Report Hy-5*.

[2] U.S. Marine Administration. http://www.marad.dot.gov/ports_landing_page /marine_transportation_system/mts.htm.

[3] K.J. Astrom and B. Wittenmark. *Computer-Controller Systems: Theory and Design*. Prentice Hall, 1990.

[4] A.E. Baitis. The development and evaluation of a rudder roll stabilization system for the WHEC HAMILTON class. *Technical Report DDDTNSRDC/SPD-0930-02*, 1980.

[5] R.L. Beck and J. Wolfe. Developing a ship motions prediction program using linear theory for a ship maneuvering through a seaway. *Technical Report*, 2007.

[6] M. Blanke, P. Haals, and K.K. Andreasen. Rudder roll damping experience in denmark. *International Proceedings of IFAC Workshop CAMS'89*, 1989.

[7] M. Breivik and T.I. Fossen. Path following for marine surface vessels. *MTTS/IEEE TECHNO-OCEAN*, 4:2282–2289, 2004.

[8] M. Breivik and T.I. Fossen. Path following of straight lines and circles for marine surface vessels. *Proceedings of the 6th IFAC CAMS*, 2004.

[9] M. Breivik and T.I. Fossen. Principles of guidance-based path following in 2D and 3D. *44th IEEE Conference on Decision and Control*, pages 627–634, 2005.

[10] T.W. Chalmers. *The Automatic Stabilisation of Ships*. Chapman and Hall, 1931.

[11] L. Chisci, J.A. Rossiter, and G. Zappa. Systems with persistent disturbances: Predictive control with restrictive constraints. *Automatica*, 37:1019–1028, 2001.

[12] J.C. Daidola. A simulation program for vessel's maneuvering at slow speeds. *Proceedings of Eleventh Ship Technology and Research (star) Symposium*, 1986.

[13] K.S.M. Davidson and L.I. Schiff. Turning and course keeping qualities. *Transactions of Society of Naval Architects Marine Engineers*, 54, 1946.

[14] K.D. Do, Z.P. Jiang, and J. Pan. Underactuated ship global tracking under relaxed conditions. *IEEE Transactions on Automatic Control*, 47:1529–1536, 2002.

[15] K.D. Do, Z.P. Jiang, and J. Pan. Robust adaptive path following of underactuated ships. *Automatica*, 40:929–944, 2004.

[16] K.D. Do and J. Pan. Global tracking control of underactuated ships with off-diagonal terms. *Proceedings of the 42nd IEEE Conference on Decision and Control*, pages 1250–1255, 2003.

[17] K.D. Do and J. Pan. Underactuated ships follow smooth paths with integral actions and without velocity measurements for feedback: theory and experiments. *IEEE transactions on control systems technology*, 14(2):308–322, 2006.

[18] I.S. Dolinskaya, M. Kotinis, M.G. Parsons, and R.L. Smith. Optimal short-range routing of vessels in a seaway. *Accepted by Journal of Ship Research*, 2008.

[19] P. Encarnacao and A. Pascoal. Combined trajectory tracking and path following for marine vehicles. *Proceedings of 9th Mediterranean Conference on Control and Automation*, 2001.

[20] J.W. English and D.A. Wise. Hydrodynamic aspects of dynamic positioning. *RINA*, 1975.

[21] O.M. Faltinsen. *Sea Loads on Ships and Offshore Structures*. Cambridge University Press, 1990.

[22] J. Fang and J. Luo. The ship track keeping with roll reduction using a multiple-states PD controller on the rudder operation. *Marine Technology*, 45:21–27(7), 2008.

[23] T.I. Fossen. *Guidance and Control of Ocean Vehicles*. John Wiley and Sons, Inc., 1994.

[24] T.I. Fossen. *Marine Control Systems*. Marine Cybernetics, 2002.

[25] T.I. Fossen, M. Breivik, and R. Skjetne. Line-of-sight path following of underactuated marine craft. *Proceedings of the Sixth IFAC Conference Maneuvering and Control of Marine Crafts*, pages 244–249, 2003.

[26] H. Frahm. Results of trials of anti-rolling tanks at sea. *Transactions of the Royal Institution of Naval Architects*, 1911.

[27] R. Ghaemi, J. Sun, and I. Kolmanovsky. Computationally efficient model predictive control with explicit disturbance mitigation and constraint enforcement. *45th IEEE Conference on Decision and Control*, 2006.

[28] E.G. Gilbert, I. Kolmanovsky, and K.T. Tan. Discrete-time reference governors and the nonlinear control of systems with state and control constraints. *International Journal of Robust and Nonlinear Control*, 1995.

[29] T. Holzhuter. LQR approach for the high-precision track control of ships. *IEEE Proceedings of Control Theory and Applications*, 144(2):121–127, 1997.

[30] Y. Ikeda. Prediction methods of roll damping of ships and their application to determine optimum stabilisation devices. *Marine Technology, SNAME*, 41(2):89–93, 2004.

[31] Z.P. Jiang. Global tracking control of underactuated ships by Lyapunov's direct method. *Automatica*, 38:301–309, 2002.

[32] C.G. Kallstrom. Autopilot and track-keeping algorithms for high-speed craft. *Control Engineering Practice*, 8(2):185–190, 2000.

[33] C.G. Kallstrom, P. Wessel, and S. Sjolander. Roll reduction by rudder control. *Spring Meeting - STAR Symposium, 3nd IMSDC*, 1988.

[34] M. Krstic, I. Kanellakopoulos, and P.V. Kokotovic. *Nonlinear and Adaptive Control Design*. John Wiley and Sons, Inc., 1995.

[35] L. Lapierre, D. Soetanto, and A. Pascoal. Nonlinear path following with applications to the control of autonomous underwater vehicles. *Proceedings of 42nd IEEE Conference on Decision and Control*, 2:1256–1261, 2003.

[36] Y.I. Lee and B. Kouvaritakis. Robust receding control for systems with uncertain dynamics and input saturation. *Automatica*, 36:1497–1504, 2000.

[37] E. Lefeber, K.Y. Pettersen, and H. Nijmeijer. Tracking control of an underactuated ship. *IEEE Transactions on Control Systems Technology*, 11:52–61, 2003.

[38] E.V. Lewis. *Principles of Naval Architecture*. Society of Naval Architects and Marine Engineers, 1989.

[39] Z. Li, J. Sun, and R.L Beck. Evaluation and modification of a robust path following controller for marine surface vessels in wave fields. *Submitted to Journal of Ship Research*, 2009.

[40] Z. Li, J. Sun, and S. Oh. A robust nonlinear control design for path following of a marine surface vessel. *IFAC Conference on Control Applications in Marine Systems*, 2007.

[41] Z. Li, J. Sun, and S. Oh. Design, analysis and experimental validation of a robust nonlinear path following controller for marine surface vessels. *To appear in Automatica*, 2009.

[42] Z. Li, J. Sun, and S. Oh. Handling roll constraints for path following of marine surface vessels using coordinated rudder and propulsion control. *Accepted by 8th International Conference Maneuvering and Control of Marine Craft (MCMC)*, 2009.

[43] Z. Li, J. Sun, and S. Oh. Path following for marine surface vessels with rudder and roll constraints: an MPC approach. *American Control Conference*, 2009.

[44] D.Q. Mayne, J.B. Rawlings, C.V. Rao, and P.O.M. Scokaert. Constrained model predictive control: stability and optimality. *Automatica*, 36:789–814, 2000.

[45] D.Q. Mayne, M.M. Seron, and S.V. Rakovic. Robust model predictive control of constrained linear systems with bounded disturbances. *Automatica*, 41:1136–1142, 2005.

[46] A. Micaelli and C. Samson. Path following and time varying feedback stabilization of a wheeled mobile robot. *Technical Report. INRIA.*, 1993.

[47] K. Monk. A warship roll criterion. *Transactions of the Royal Institute of Naval Architects*, pages 219–240, 1988.

[48] M. Morari and J.H. Lee. Model predictive control: past, present and future. *Computers and Chemical Engineering*, 23:667–682, 1999.

[49] K. Nomoto, T. Taguchi, K. Honda, and S. Hirano. On the steering qualities of ships. *International Shipbuilding Progress*, 1957.

[50] The Society of Naval Architecture and Marine Engineers. Nomenclature for treating the motion of a submerged body through a fluid. *Technical and Research Bulletin No. 1-5*, 1950.

[51] S. Oh, J. Sun, and Z. Li. Path following control of underactuated marine vessels via dynamic surface control technique. *ASME Dynamic Systems and Control Conference*, 2008.

[52] T. Perez. *Performance Analysis and Constrained Control of Fin and Rudder-Based Roll Stabilizers for Ships*. PhD thesis, School of Electrical Engineering and Computer Science, the University of Newcastle, Australia, 2003.

[53] T. Perez. *Ship Motion Control*. Springer, 2005.

[54] T. Perez, A. Ross, and T.I. Fossen. A 4-DOF SIMULINK model of a coastal patrol vessel for manoeuvring in waves. *7th IFAC Conference on Manoeuvring and Control of Marine Vessels MCMC*, 2006.

[55] T. Perez, C.Y. Tzeng, and G.C. Goodwin. Model predictive rudder roll stabilization control for ships. *Maneuvering and Control of Marine Craft*, 2000.

[56] K.Y. Pettersen and E. Lefeber. Way-point tracking control of ships. *Proceedings of 40th IEEE Conference on Decision and Control*, 2001.

[57] K.Y. Pettersen and H. Nijmeijer. Tracking control of an underactuated surface vessels. *Proceedings of 37th IEEE Conference on Decision and Control*, 1998.

[58] S.J. Qin and T.A. Badgwell. A survey of industrial model predictive control technology. *Control Engineering Practice*, 11:733–764, 2003.

[59] A. Ross. *Nonlinear Manoeuvring Models for Ships: a Lagrangian Approach*. PhD thesis, Department of Engineering Cybernetics, Norwegian University of Science and Technology, 2008.

[60] R. Rysdyk. UAV path following for constant line-of-sight. *Proceeding of the 2nd AIAA*, 2003.

[61] C. Samson. Trajectory tracking for unicycle type and two steering wheels mobile robots. *Proceedings of ICARV*, pages RO–13.1, 1992.

[62] P.O.M. Scokaert and D.Q. Mayne. Min-max feedback model predictive control for constrained linear systems. *IEEE Transactions on Automatic Control*, 43:1136–1142, 1998.

[63] P.O.M. Scokaert and J.B. Rawlings. Feasibility issues in linear model predictive control. *American Institute of Chemical Engineers*, 45:1649–1659, 1999.

[64] F.H. Sellars and J.P. Martin. Selection and evaluation of ship roll stabilization systems. *Marine Technology, SNAME*, 29(2):84–101, 1992.

[65] R. Skjetne and T. I. Fossen. Nonlinear maneuvering and control of ships. *Proceedings of the MTS/IEEE OCEANS*, 2001.

[66] R. Skjetne, T. I. Fossen, and P.V. Kokotovic. Robust output maneuvering for a class of nonlinear systems. *Automatica*, 40:373–383, 2004.

[67] K.H. Son and K. Nomoto. On the coupled motion of steering and rolling of a high speed container ship. *Naval Architect of Ocean Engineering 20*, 1981.

[68] J. van Amerongen and J.C. van Cappelle. Mathematica modeling for rudder roll stabilization. *Proceedings of 6th Ship Control System Symposium SCSS*, 1981.

[69] J. van Amerongen and H.R. van Nauta Lemke. Optimum steering of ships with an adaptive autopilot. *Fifth Ship Control Systems Symposium*, 1978.

[70] J. van Amerongen and H.R. van Nauta Lemke. Criteria of optimum steering of ships. *Symposium on Ship Steering Automatic Control*, 1980.

[71] P.G.M. van der Klught. *Rudder Roll Stabilization*. PhD thesis, Delft University of Technology, The Netherlands, 1987.

[72] J. Velagic, Z. Vukic, and E. Omerdic. Adaptive fuzzy ship autopilot for track-keeping. *IFAC Conference on Maneuvering and Control of Marine Crafts*, 2000.

[73] Z. Vukic, E. Omerdic, and L. Kuljaca. Improved fuzzy autopilot for track-keeping. *IFAC Conference on Control Applications in Marine Systems*, 1998.

[74] A. Wahl and E.D. Gilles. Track-keeping on waterways using model predictive control. *Control Applications in Marine Systems*, 1998.

[75] E. Zafiriou and A.L. Marchal. Stability of SISO quadratic dynamic matrix control with hard output constraints. *American Institute of Chemical Engineers*, 37, 1991.

[76] A. Zheng and M. Morari. Robust stability of constrained model predictive control. *Proceedings of American Control Conference*, pages 379–383, 1993.

[77] A. Zheng and M. Morari. Stability of model predictive control with mixed constraints. *IEEE Transactions on Automatic Control*, 1995.